NTNU

Norwegian University of
Science and Technology

Condition Assessment of Hydro Generator Insulation Using Partial Discharge Measurements

Regina Skattenborg

Master of Energy and Environmental Engineering
Submission date: June 2018
Supervisor: Erling Ildstad, IEL
Co-supervisor: Torstein Grav Aakre, IEL

Norwegian University of Science and Technology
Department of Electric Power Engineering

NORGES TEKNISK-NATURVITENSKAPELIG UNIVERSITET

Hovedoppgave våren 2018

Student:	Regina Skattenborg	reginask@stud.ntnu.no
Supervisor:	Prof. Erling Ildstad	erling.ildstad@elkraft.ntnu.no
Co-supervisor:	Stip. Torstein Grav Aakre	torstein.aakre@ntnu.no

Title:

Condition Assessment of Hydro Generator Insulation Using Partial Discharge Measurements

Tittel:

Tilstandskontroll av isolasjon i vannkraftgeneratorer ved måling av partielle utladninger

The majority of the Norwegian hydropower generators have been in service for more than 40 years, and will soon reach their expected service lifetime. In addition to long times in service, new and tougher usage patterns with rapid starts and stops challenge the insulation beyond its design criteria, resulting in increased uncertainty regarding remaining lifetime estimation. The question addressed is what type of diagnostic tests are needed to obtain relevant data regarding the physical condition of insulation systems containing voids.

The main purpose of this master thesis is to facilitate condition assessment of such generator bars by examining possibilities and limitations regarding partial discharge measurements as a diagnostic tool. The main aim of the work is to clarify how inception voltage, detected number and magnitude of PDs relate to the void size and the discharge mechanisms in the voids.

The thesis is expected to constitute:

- A literature survey, including theoretical models, forming the base for suggested diagnostic methods for testing of the multi-component insulation system of generator bars.
- Design and characterization of samples, materials and methods used, including electric field calculations.

- Characterization and experimental examination of the PD activity in samples of real generator bar insulation as well as specially designed laboratory samples.
- Comparison and evaluation of the experimental results with respect to previous works and existing theoretical models.
- Conclusions regarding the ability of the PD approach and suggestions for further work.

The details of the test program are to be decided in cooperation with the supervisor.

Start:	15. januar 2018
Innlevering:	11. juni 2018

Preface

This Master's Thesis is the concluding work for the MSc program Energy and Environmental Engineering at the Norwegian University of Science and Technology (NTNU) in Trondheim, Norway. The thesis constitutes 30 ECTS-credits, or a work-load of one semester, and has been carried out during the spring semester of 2018.

First and foremost, would like to thank my supervisor, Prof. Erling Ildstad, for all the help and guidance he has given me throughout the work with this thesis. I would also like to express my gratitude to my co-supervisor, Ph.D. Candidate Torstein Grav Aakre, for his help with the experimental and planning part of this thesis work and for always being open for discussions and questions. In addition, I would like to thank Morten Flå for making the test samples for my experiments.

I would also like to thank my partner, Thomas Engrav, for taking the time to read through drafts of the thesis and for always being so supportive of everything I do.

Lastly, I would like to thank my family for their support throughout the years of my studies. This accomplishment would not have been possible without them.

Trondheim, June 2018

Regina Skattenborg

Abstract

More than half of all hydro generator failures are caused by insulation breakdown. Insulation failures inflict serious damage on the generator and represent significant operating costs for utility companies. One of the main reasons for insulation breakdowns is the irreversible degradation caused by internal partial discharges (PD) resulting from voids in the insulation system. Therefore, it is crucial that methods for condition assessment of generator insulation can identify and analyze the partial discharge activity in these voids.

The main purpose of this thesis is to facilitate condition assessment of generator bar insulation by measuring partial discharges resulting from voids in insulating materials. The aim is to clarify how important PD parameters relate to the void size and the discharge mechanisms in the voids. A part of the work also involves comparing the experimental results with the theoretical model of internal partial discharges: the Abc Model. In addition, possibilities and limitations of partial discharge measurements as a diagnostic tool are examined.

The test samples consist of both real generator bar insulation and specially designed laboratory samples containing disk-shaped voids of different diameters. A thin layer of aluminum was applied by vacuum evaporation to the cavity surfaces of one sample group to investigate the effects of increased surface conductivity. Electrical detection of partial discharges was performed using a conventional measuring circuit, and the PD activity was analyzed in the form of inception voltage, as well as the discharge magnitude and discharge frequency at a voltage frequency of 50 Hz.

The inception voltage is found to decrease with increasing void diameter due to lower field enhancement in larger voids. In the case of the laboratory samples, the discharge magnitude is generally increasing with increasing diameter. The discharge magnitude is larger when the void surfaces are conducting since the discharge area then is equal to the void surface area. However, for samples made of aged generator insulation, the discharge magnitude is constant regardless of void diameter. More importantly, it was not possible to conclusively distinguish the PD activity in the voids from the PD activity inherent in the insulation. The discharge frequency tends to increase with increasing void size. This can be explained by the differences in the electric field strength in the different cavities at the specific voltage level, and the occurrence of parallel discharges. Higher void surface conductivity generally leads to lower discharge frequency.

In conclusion, the PD activity is seen to depend on the void size. The theoretical model is successful in describing the PD activity in voids with conducting surfaces, but fails to describe the PD activity in aged generator insulation. PD measurements performed on the laboratory samples can detect the voids and assess the relative void size. However, the voids in aged generator insulation cannot conclusively be detected using the chosen PD approach. This represents an important limitation of the PD method.

Sammendrag

I tilfeller der vannkraftgeneratorer svikter, er mer enn halvparten av hendelsene forårsaket av isolasjonssvikt. Dersom isolasjonen svikter, vil dette gjøre stor skade på generatoren, i tillegg til at det fører til høye kostnader for kraftleverandørene. En av hovedårsakene til isolasjonssvikt er den irreversible degraderingen som skyldes delutladninger (PD) i hulrom i isolasjonssystemet. Det er derfor avgjørende at metoder for tilstandskontroll av generatorisolasjon kan identifisere og analysere PD-aktivitet i slike hulrom.

Hovedhensikten med denne masteroppgaven er å tilrettelegge for tilstandskontroll av statorisolasjon ved å måle delutladninger som forårsakes av hulrom i isolasjonsmaterialer. Målet er å avklare hvordan viktige PD-parametere avhenger av hulromstørrelsen og utladningsmekanismene i hulrommet. En del av arbeidet involverer også å sammenlikne de eksperimentelle resultatene med den teoretiske abc-modellen som beskriver hulromsutladninger. I tillegg vil muligheter og begrensninger ved PD-målinger som et diagnostisk verktøy bli undersøkt.

Prøveobjektene består av både ekte statorisolasjon og spesialdesignet laboratorieobjekter med disk-formede hulrom av ulike diametere. Et tynt lag med aluminium ble ved vakumfordampning påført hulromsoverflatene for en gruppe med prøveobjekter, med hensikt å undersøke konsekvensene av økt overflatekonduktivitet. Elektrisk deteksjon av delutladninger ble utført ved bruk av en konvensjonell målekrets, og PD-aktiviteten ble analysert i form av tennspenning, utladningsstørrelse og utladningsfrekvens ved en spenningsfrekvens på 50 Hz.

Tennspenningen viste seg å synke med økende hulromsdiameter på grunn av lavere feltforsterkning i større hulrom. I tilfellet for laboratorieobjektene, øker generelt utladningsstørrelsen med økende diameter. Utladningene er større når hulromsoverflaten er ledende siden utladningsområdet i dette tilfellet er likt arealet til hulromsoverflaten. For prøveobjektene som består av aldret generatorisolasjon, derimot, viste det seg at utladningsstørrelsen er tilnærmet konstant uavhengig av diameteren på hulrommet. Viktigere er det at det ikke var mulig å entydig skille mellom PD-aktiviteten i hulrommene og PD-aktiviteten som naturlig finnes i isolasjonen. Utladningsfrekvensen har en tendens til å øke med økende hulromsstørrelse. Dette kan forklares med forskjellen i elektrisk feltstyrke i de ulike hulrommene på det spesifikke spenningsnivået, i tillegg til forekomst av parallelle utladninger. Høyere overflateledningsevne fører generelt til lavere utladningsfrekvens.

For å konkludere, har det blitt observert at PD-aktiviteten er avhengig av hulromsstørrelse. Den teoretiske modellen kan vellykket beskrive PD-aktiviteten i hulrom med ledende overflater, men den lykkes ikke med å beskrive PD-aktiviteten i aldret generatorisolasjon. PD-målinger på spesialdesignede laboratorieobjekter kan detektere hulrommene og evaluere den relative hulromsstørrelsen. Hulrom i aldret generatorisolasjon, derimot, kan ikke entydig detekteres ved bruk av den valgte målemetoden. Dette representerer en viktig begrensning ved PD-metoden.

Contents

1 Introduction

1.1 Background

Following the liberalization of the power system, it has become increasingly more important to reduce costs, optimize investments, and maintain an overall high level of reliability of the power system. One of the main operating costs for utility companies is related to generator failures [1]. In addition, the majority of the hydro generators in the Norwegian power system are soon reaching their expected service lifetime [2]. Therefore, it is highly important to make educated decisions on when to refurbish and repair generators. For this to be possible, robust condition assessment methods are needed. These diagnostic methods must be able to detect aging mechanisms, but they must also correctly interpret and assess the condition of the equipment based on the degree of aging and degradation.

One crucial part of the generator is the stator winding insulation. CIGRÉ has conducted a large, worldwide survey to investigate hydro generator failures, and it was concluded that of all generator failures, 57 % were due to breakdowns of the insulation system [1]. In addition, it was found that insulation breakdowns are the single failure type that poses, by far, the greatest damage to the generator [1]. In today's power system, characterized by a rise in intermittent renewable energy, the generator insulation is increasingly exposed to high stresses it was not originally designed for, which significantly reduces the longevity of the generator [2]. Therefore, robust condition assessment of generator insulation is a key element in ensuring a continued high reliability of the hydro generators.

The IEEE (Institute of Electrical and Electronics Engineers) lists several diagnostic tests that are in use on generator stator insulation. These are described in test standards, guides and recommended practices.

1. Insulation resistance and polarization index (IEEE Std 43-2013 [3])
2. AC and DC hipot tests (IEEE Std 56-2016 [4], IEEE Std 95-2002 [5]) and hipot tests for turn insulation (IEEE Std 522-2004 [6])
3. Power factor tip-up test (IEEE Std 286-2000 [7])
4. Partial discharge (PD) tests (online and offline) (IEEE Std 1434-2014 [8])

Electrical PD measurements are one of the main tools used to assess the condition of generator insulation [9, 10, 11]. PD measurements can identify and distinguish different defects by analyzing the phase-resolved partial discharge pattern (PRPDA) [11]. In addition, PD measurements can be used to detect changes in PD activity, which can indicate that a breakdown is imminent [12]. Thus, PD measurements can help make decisions about rewinding of generator bars, which can increase the longevity of the generator and the reliability of the power system.

Internal partial discharges resulting from voids in the insulation system are identified as one of the three most harmful discharge types in AC Machinery [8], and is found to be the root cause of 22 % of insulation failures [1]. Air-filled voids will always be inherent in generator stator insulation due to the impregnation process during manufacturing [13]. The Internal PD activity resulting from these voids is considered harmful because it causes irreversible degradation of the insulation material which, over time, can lead to electrical breakdown of the insulation system [14]. Therefore, identifying and analyzing the PD activity in internal voids is of crucial importance in regards to effective condition assessment of hydro generators.

1.2 Aim and Approach

The thesis work is mainly experimental and deals with analyzing partial discharges resulting from internal voids in insulating materials. The main aim of this thesis is to investigate and clarify how important PD parameters relate to the void size and the discharge mechanisms in the voids. The results will also be discussed in light of existing theoretical models. In addition, limitations and possibilities regarding partial discharge measurements as a diagnostic tool will be investigated.

To reduce the number of unknown parameters, specially made laboratory samples with embedded voids of different sizes have been designed. This makes it possible to exclusively analyze the PD activity in one single void. The embedded voids are air-filled and disk-shaped with diameters ranging from 1 mm to 20 mm.

A total of four different sample types have been tested in this thesis work. Two of the sample types are made of polycarbonate, of which half of the samples have conducting void surfaces for the purpose of investigating what effects increased void surface conductivity has on the PD activity. In an effort to extend the analysis to voids in actual generator insulation, two sample types made of generator insulation material have been tested: samicatherm (specially made laboratory samples) and mica mat (actual aged generator insulation).

The main PD parameters which will be analyzed in this thesis are:

- The inception voltage
- The discharge magnitude

- The discharge frequency

1.3 Structure of Thesis

Chapter 1 includes a brief introduction to the thesis. Chapter 2 presents the theory regarding partial discharges that is needed to analyze the measurements. Then, in Chapter 3, the experimental method is presented. Chapter 4 contains the results from the theoretical model of partial discharges as well as the results from electric field strength simulations and the experimental results. Next, the results are discussed in Chapter 5 with a focus on discharge mechanisms that govern the PD activity. Finally, conclusions are being drawn and suggestions for further work are presented in Chapter 6. Appendices which support the work and present detailed explanations of the chosen experimental methods, as well as detailed results, are placed at the end of this thesis.

2 Theory

Since the author's own specialization project [15] is concerned with the same topic as this thesis, the theoretical background is very similar. The following chapter is therefore partly based on the literature study that was conducted as a part of the specialization project. Information taken from works that are not the author's own, is, of course, properly acknowledged and cited accordingly.

2.1 Stator Bar Insulation for Generators

A commonly used stator bar insulation is mica mixed with epoxy resin. The mica tape is wound around the generator bar as illustrated in Figure 2.1. The figure also shows the other components that are necessary to suppress corona discharges both between the bar and the stator slots and between the individual copper strands.

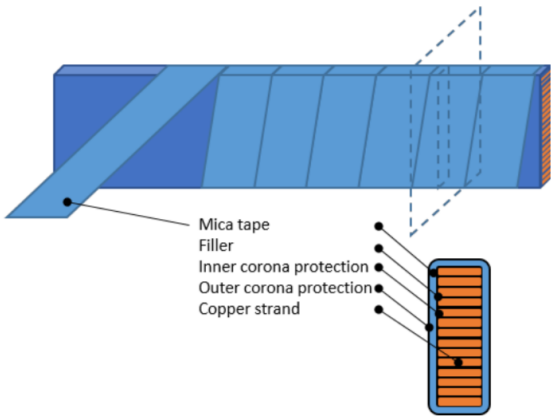

Figure 2.1: The components of the main part of a generator bar [13].

Mica is an inorganic substance which occurs naturally in the form of for example aluminum silicates [16]. Mica has very good electric properties and mixed with a resin, it can also withstand the high operating temperatures the bars experience [16]. The problem with solid insulation is the possibility of formation of cavities/voids. This is particularly a problem with organic matter, which can easily be degraded by partial discharges. In a mica-epoxy insulation, the mica can handle the stresses the insulation is under, but the epoxy resin is susceptible to damage by partial discharges. PD activity has been shown both by experiments in

the field and in the laboratory to be an important indicator for the breakdown of insulation systems [17].

2.2 Partial Discharges

According to the international standard, IEC 60270, a partial discharge (PD) is defined as a

> "localized electrical discharge that only partially bridges the insulation between conductors which can or can not occur adjacent to a conductor" [18]

In other words, partial discharges are spark-overs in only a certain part of the insulation system. They are initiated when the local, electrical field strength exceeds the dielectric strength of the material/gas and a start electron is available. Partial Discharges are an important aging mechanism in many types of high voltage equipment. They cause chemical and physical erosion, which after a while can lead to more severe breakdown mechanisms like electrical treeing, and eventually cause a breakdown of the insulation system [19]. Therefore, partial discharges are considered to reduce the lifetime of the insulation [20].

Partial discharges in insulation systems can be divided into three different types [21]:

1. Discharges in gases or at gas-insulation interfaces
2. Discharges in liquids and at liquid-insulation interfaces
3. Discharges in solids

In solid mica-epoxy generator rod insulation, the most prominent discharge type is discharges in gases or at gas-insulation interfaces. Impurities and inhomogeneities, for example, delaminations inherent in the insulation, gas-filled cavities, sharp points and inclusion of particles give areas with reduced dielectric strength and thus these areas are highly susceptible to partial discharge activity [19].

2.2.1 Characteristic Parameters

Apparent Charge

The real charge that is transferred during a discharge is impossible to measure, but there has been found a quantitative link between this charge and an induced charge (apparent charge), which on the other hand is measurable [21]. This parameter is therefore used as a measure for the discharge magnitude. The quantitative link between the real charge and the apparent charge is important for the ability to interpret partial discharge measurements.

The apparent charge is defined as:

> "the charge which has to be transferred to the test object from the external circuit in order to restore the voltage across the test object after a partial discharge" [16]

Inception Voltage and Extinction Voltage

The inception voltage, U_i, (also denoted PDIV - Partial Discharge Inception Voltage) is the lowest voltage level at which there are observed repetitive partial discharges when the voltage is increased from a lower value [18].

The extinction voltage, U_e, (also denoted PDEV - Partial Discharge Extinction Voltage) is the applied voltage at which discharges cease to occur when the voltage is gradually reduced from a higher value [18]. The term "cease to occur" will in practice mean that the magnitude of the partial discharge is lower than a specified minimum level - the threshold value. The extinction voltage will not necessarily be the same as the inception voltage. When discharges once have started, it is possible to reduce the voltage without the discharges stopping due to different memory effects which will be discussed in a later section.

Discharge Frequency

The discharge frequency, or the repetition rate, is the total number of PD pulses (above a chosen threshold value) during a given time interval, divided by the duration of this interval [18]. The parameter is often denoted by n. For the analysis of the discharges in this thesis, it is desirable to define the time interval as one half-period of the applied voltage.

2.3 Internal Partial Discharges

Internal partial discharges are discharges occurring in small, enclosed cavities in the insulation of a high voltage apparatus. According to A CIGRÉ survey of hydro generator failures [1], internal discharges are one of the main root causes for insulation damage: in 22 % of all incidents related to insulation, internal discharges were the cause of the incident. Therefore, it is of great importance to work to understand the mechanisms of internal discharges, how to avoid them from occurring, and how the potential damage can be reduced.

2.3.1 Sufficient Conditions for Partial Discharges

There are two conditions that have to be met for a partial discharge to occur [22]: First, the local electric stress must exceed the breakdown strength of the gas/material. Generator rods in medium voltage generators typically have an insulation thickness of 3 mm. With a phase to ground voltage of 6.4 kV, the electric stress is more than 2 kV/mm. The insulation has a higher dielectric strength than this, but gaseous voids in the insulation have a lower dielectric strength. Here, the electric field will also be higher than in the insulation. For example, the electric field in an air-filled cavity perpendicular to the applied electric field is [16]:

$$E_{cavity} = \varepsilon_r \cdot E_{ins} \tag{2.1}$$

where ε_r is the relative permittivity of the insulation material. A material made of mica and

epoxy resin has a relative permittivity of about 4 [23]. This means that the electric field in gas-filled cavities is about four times higher than in the rest of the insulation and the field can therefore easily exceed the dielectric strength of the gas. If the cavity is spherical, the maximum field enhancement is 1.5 compared to the background field, and the expression is as follows [16]:

$$E_{cavity} = \frac{3\varepsilon_r}{1+2\varepsilon_r} \cdot E_{ins} \tag{2.2}$$

Secondly, for discharges to occur, there must be a start electron available. Assuming the only discharge mechanism present is the common streaming mechanism, start electrons can originate from volume generation or surface emission [21]. Volume generation includes ionizing radiation i.e. cosmic or radioactive radiation [24] and electrons being detached from negative ions due to the external electrical field [21]. Surface emission of electrons is the emission of electrons from traps in the surface walls of the voids [22].

Which process or processes that are dominating the production of electrons depend on factors like the condition of the surface walls and the specific insulation material [24]. For example, in a cavity bounded by a conducting surface, emission from the surface is dominating the production of start electrons [21]. On the other hand, in the case of voids molded in epoxy, is has been found that the volume processes is the most active process [24].

2.3.2 Degradation of Insulation Due to Partial Discharges

The aging process of the insulation due to internal discharges proceeds as illustrated in Figure 2.2. First, the surface conductivity increases before the surface starts to erode. Possible processes that govern the erosion are presented in a paper by T. Tanaka and can be summarized as shown in Figure 2.3 [25] . The erosion leads to a decrease of the insulation thickness and an increase in surface roughness. Then, the formation of localized crystals takes place which enhances the local electric field in these areas which is then causing PDs to intensify at the crystal tips [14]. This causes pit formation and the start of electric tree growth which, as the tree grows, can lead to the breakdown of the insulation [14].

2.3.3 Streamer Propagation of Discharges in Voids

The streamer process is the major discharge mechanism in voids [22]. There are different discharge types in voids enclosed by resin, but a streamer discharge produces a signal strong enough to detect [24]. Streamer discharges also cause damage which can lead to more serious sparks and electrical breakdown [21]. This complex discharge type is defined as a self-channeling ionization phenomenon that is propagating through a gas [26, 24]. For the streamer process to start, the local electric field must be higher than a specific threshold value that varies depending on the properties of the gas, the geometry of the void, the field enhancement of the void, etc. The result is a critical criterion for the inception of an electron

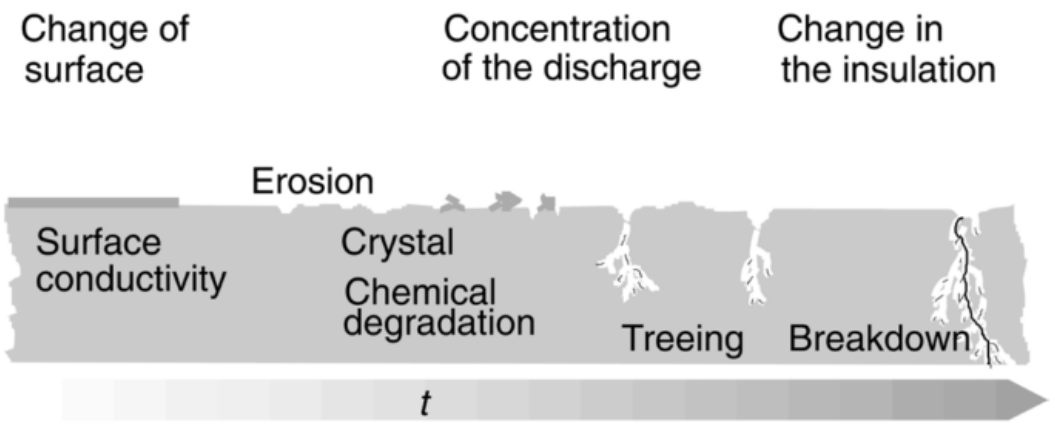

Figure 2.2: The different stages of insulation damage due to internal PD [14].

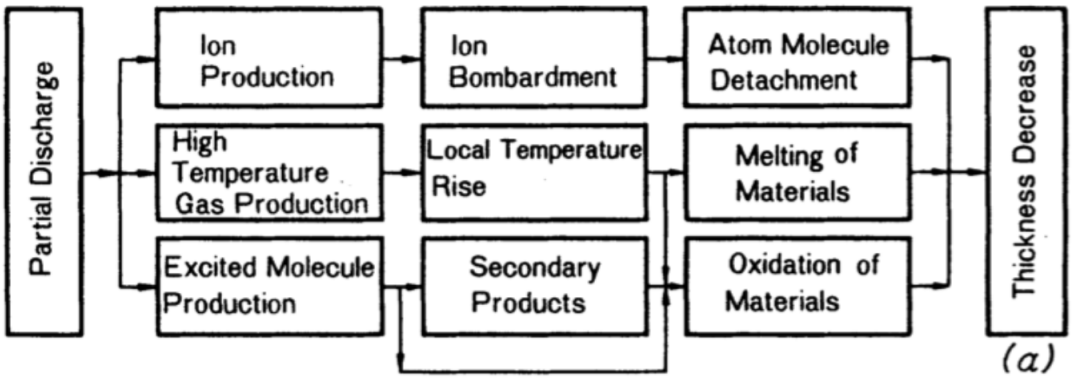

Figure 2.3: Possible processes that cause erosion of the insulation due to internal partial discharges [25].

avalanche [24].

$$fE_0 > E_{streamer} = \left(\frac{E}{p}\right)_{er} p\left[1+\frac{B}{(2pa)^n}\right] \tag{2.3}$$

For air, the parameters $\left(\frac{E}{p}\right)_{er} = 25.2\ \mathrm{VPa^{-1}M^{-1}}$, $B = 8.6\ \mathrm{m^{0.5}Pa^{0.5}}$ and $n = 1/2$ characterize the ionization process, whereas the parameter f represents the field enhancement of the electric field in the void compared to the rest of the bulk insulation. For a disk-shaped cavity, the field enhancement is given by Equation 2.1. In addition to the electric field criterion being fulfilled, a start electron is needed for the ionization process to unfold. Possible electron generation processes are presented in section 2.3.1.

The streamer process can be explained by four stages as seen in Figure 2.4.

From a conducting surface, the streamer initiates and propagates in the direction of the electrical field. Then when it reaches the other "electrode" - the insulation, it propagates laterally along the surface until it reaches the maximum possible extension [21]. How far the discharge extends depends on the defect geometry and the discharge structure [21].

If the electron avalanche starts at an insulating surface, the discharge develops into two discharges - one that propagates laterally along the surface, and another which propagates

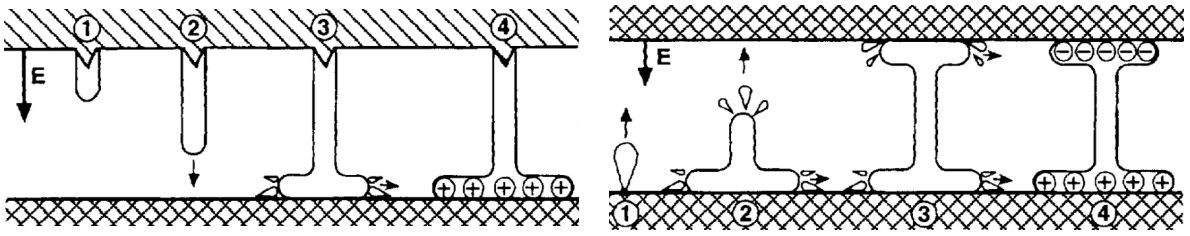

(a) (b)

Figure 2.4: Illustrations of the four stages of streamer propagation [21]: (a) Starting on a conducting surface, ending on an insulating surface, (b) Starting and ending on an insulating surface.

parallel to the direction of the field. When the latter part of the discharge reaches the opposite insulating surface, the rest of the discharge progresses in the same way as for a discharge starting at a conducting surface.

2.3.4 Memory Effect and Statistical Nature of Partial Discharges

The electric field in a cavity is not only decided by the electric field caused by the applied voltage. A second contribution is the field caused by the deposited charge from previous discharges [24]. These deposited charges can either act in the direction of the background field or oppose it. Therefore, they can delay the next discharge and thus affect at which phase of the applied voltage a discharge occurs. The charges left in the cavity after the discharge not only affect the field, but they also serve as a source for new initial electrons [22, 21, 24]. These two effects cause the subsequent discharges to be dependent on previous discharges, resulting in a memory effect [21].

The deposited charge can also be transported away from the site depending on the properties of the surfaces. This can be described by a decay of charge and an associated time constant [21]. The process of decaying charge happens by ion drift through the gas and conduction along the surface of the void in case of a conducting surface [24].

The availability of electrons governs the statistical time lag of the discharges. During PD activity, there is a balance between the production of start electrons by earlier discharges and the decay of available electrons. In addition, there is the randomness of electron generation by volume and surface processes.

The statistical time lag and the memory effect of previous discharges affect the discharge characteristics substantially; the PD magnitude, the number of discharges per voltage period and the phase angle at which the discharges occur are all affected. This manifests itself in the phase-resolved partial discharge pattern which is being extensively used to interpret discharges for diagnostic of insulation systems.

2.3.5 PRPDA - Phase-Resolved Partial Discharge Analysis

The PRPD pattern of discharges can be considered the fingerprint of the corresponding discharge type [22]. One such pattern (of void discharges) is shown in Figure 2.5. Each dot

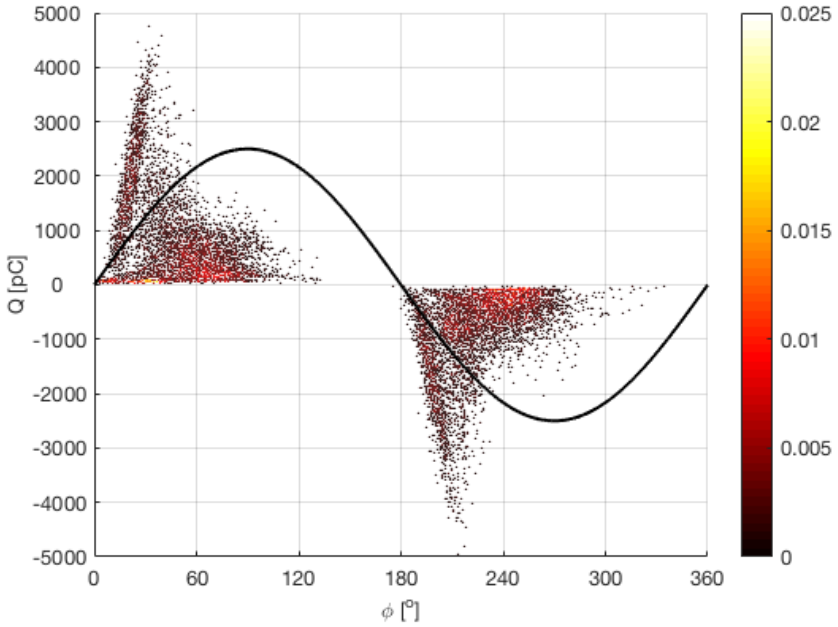

Figure 2.5: The PRPD pattern of internal discharge activity measured on a artificial disc-shaped cavity in poly carbonate at 9.6 kV, 50 Hz for 1 minute. Along the x-axis there is the phase angle, whereas the apparent charge is shown along the y-axis. The color shows the intensity of the discharges (PDs per voltage period).

represents one discharge which is characterized by its magnitude and at which phase value of the applied voltage it occurs. The AC voltage shape is also shown for reference. The intensity of the discharges is illustrated by a heat map.

Internal discharges exhibit symmetric characteristics: There is a symmetry between the two half phases of the voltage cycle when it comes to both the number of discharges and the maximum amplitude [11].

The spread in magnitude and phase of the discharges is partly due to the statistical nature of PDs. If there are an abundance of start electrons, the discharge will happen as soon as the electric stress exceeds the breakdown strength of the cavity, thus this corresponds to the smallest charge transfer possible during a discharge. If, however, there are few or no electrons present, the moment the discharge happens is dependent on when and if (and where) an electron appears in the cavity. During this condition, the discharges will have a shifted phase and a larger charge than the minimum charge transfer since the discharge can be delayed until the electric stress is higher [22]. The effect of this manifests itself in the PRPD pattern.

However, the characteristics of the PRPD pattern can be understood by the construction of a model for internal partial discharges. One such model, the extensively used abc model will be presented in detail in the next section.

2.3.6 Detection of Partial Discharges

The principle for measuring PD by electrical methods relies on measuring a voltage pulse from an external circuit which is proportional to the apparent charge of the partial discharge. A diagram of a detection circuit as seen in Figure 2.6 illustrates the concept of electrical detection of partial discharges. The exact detection circuit and the acquisition system that is being used in this project will be explained in detail in the Methods section.

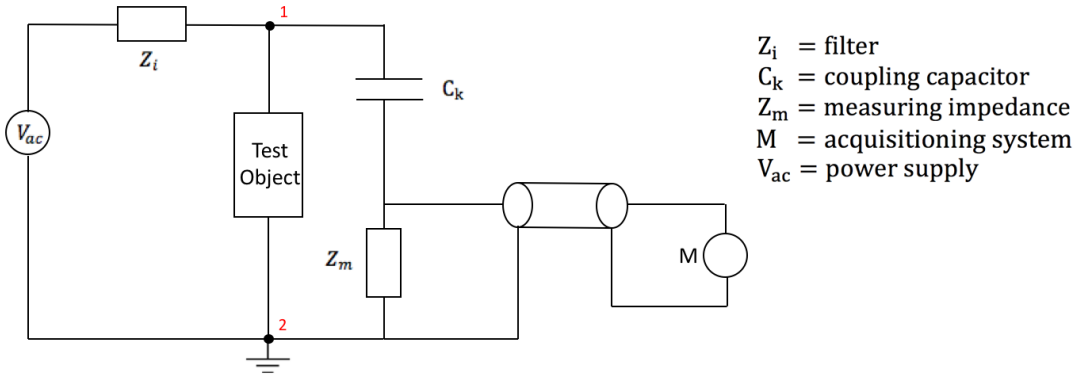

Figure 2.6: A simplified classic detection circuit for electrical detection of partial discharges. It consists of a power supply, a filter which reduces noise from the source, a coupling capacitor which is providing the current pulse needed to restore the voltage drop across the test object during a PD event, a measuring impedance and a measuring system. The measuring impedance is here placed at the ground terminal of the test object to achieve better sensitivity compared to other configurations [27].

During a discharge, the voltage drops slightly across the test object. To restore this voltage, a rapid current pulse is provided by a coupling capacitor, C_k - a low inductive element with a high capacitance up to several nF. The measuring impedance is a passive element - either a pure resistor or often a parallel R-L-C circuit [16]. In the case of the latter, the current pulse is transformed into an amplified damped oscillatory voltage signal [17]. The purpose of this element is to transform the sharp current pulse to a voltage signal which can then be processed by the acquisition system or measuring system.

Calibration

The shape of the oscillatory voltage signal depends on the impedance of the measuring device, the coupling capacitor and the capacitance of the test object [16]. Therefore, the apparent charge, q_a, has to be calibrated in a detection circuit. This is being done by injecting a known charge across the terminals of the test object. Based on the known target value and the reading on the measuring system, a divider factor or the scale factor is then calculated:

$$q_a = q_0 \frac{R_i}{R_0} \tag{2.4}$$

Where the ratio R_i / R_0 is the scale factor and q_0 is the calibrating charge injected into the terminals of the test object.

Sensitivity of Measurements and Challenges Concerning the Ambiguity of Apparent Charge

To achieve a satisfactory sensitivity for detection of partial discharges, the coupling capacitor should have a higher capacitance than the test object, C_t. How the capacitance affects the sensitivity of detection of discharges is described by [27]:

$$\frac{q_a}{q} = \frac{C_k}{C_t + C_k} \tag{2.5}$$

The larger C_k, the greater the ratio of apparent charge to the real charge and thus higher sensitivity is achieved.

It is important to be aware of the fact that the apparent charge is not strictly decided by the capacitance of the coupling capacitor and the test object. The apparent charge is also dependent on where in the test object the charge is, the geometry of the object, and the thickness of the insulation [27]. Stator bars in machines of a higher rated voltage have a thicker insulation, causing a reduction in the ratio of the apparent charge to the real charge [27]. Thus a higher sensitivity is necessary as the insulation increases. A larger test object will also lead to poorer sensitivity due to both a larger capacitance and to effects like attenuation and distortion of signals from the discharges during propagation [17].

2.4 Breakdown Strength of Gases

The breakdown strength of a gas in a homogeneous field is a function of the product of the pressure of the gas and the distance between the electrodes of the cavity [16], and is governed by Paschen's law. The corresponding Paschen curve for air is shown in Figure 2.7. For air at 1 bar and 20 °C in a homogeneous field between two metal plates, the empirical expression for the Paschen curve has been found to be [28]:

$$V_B = 6.72\sqrt{pd} + 24.4 \cdot pd \text{ [kV]} \tag{2.6}$$

Where pd is in bar·cm and the constants are related to the ionization of the gas (not dimensionless). The numerical expression for the breakdown voltage is only valid for values of pd to the right of the minimum in the Paschen curve.

2.5 Dielectric Polarization

In a dielectric, dipoles will oppose the external applied electrical field. This can be described as a relationship between the electric flux density, D, and the electric field, E [16]:

$$D = \varepsilon_0 \varepsilon_r E \tag{2.7}$$

Where $\varepsilon_0 = 8.85 \cdot 10^{-12}$ F/m is the permittivity of vacuum and ε_r is the relative permittivity

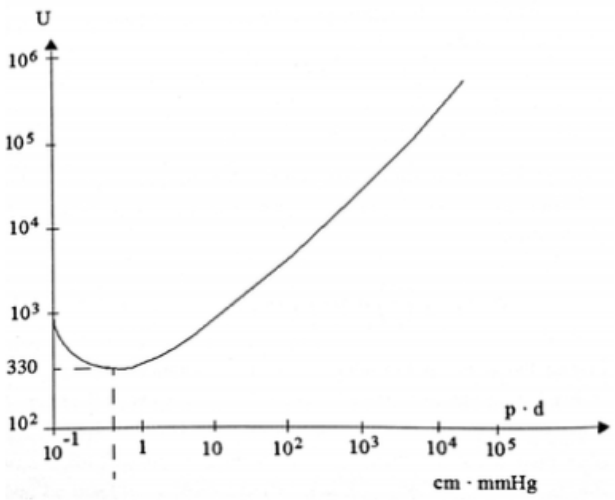

Figure 2.7: The Paschen curve for air [16].

of the dielectric which describes the reduction of the electric field caused by the alignment of dipoles in the dielectric compared to the situation with vacuum [29]. For gases, $\varepsilon_r \approx 1$ whereas for solid or liquid dielectrics $\varepsilon_r \geq 2.1$ [16].

There are different mechanisms which cause polarization in a dielectric. Some of these mechanisms act momentarily, whereas others are slower (relaxation mechanisms) and contribute to losses as well as causing ε_r to be frequency dependent [16]. An alternating field forces the dipoles to switch direction according to the change of direction of the electric field. If the frequency is low, the polarization can keep up with the switching, but as the frequency increases, the slow polarization mechanisms cannot keep up with the external field - reducing the polarization of the dielectric. Consequently, the relative permittivity is reduced at higher frequencies [16].

Mathematically this can be described by a complex permittivity:

$$\underline{\varepsilon}_r^* = \varepsilon_r' - j\varepsilon_r'' \tag{2.8}$$

where both the real and imaginary part are frequency dependent and the absolute value of $\underline{\varepsilon}_r^*$ describes the relative permittivity for the material. Usually, $|\varepsilon_r| = |\varepsilon_r'|$ since $|\varepsilon_r''| \ll |\varepsilon_r'|$ [16].

2.6 Modeling of Partial Discharges - The A-B-C Model

Discharges in gaseous cavities bounded by solid dielectrics can be considered one of the most harmful type of partial discharges [30] because of the irreversible deterioration of the insulation. Therefore, there has been a lot of research in the past century focusing on understanding and modeling discharges in gaseous cavities. This work started in 1932 with Gemant and Philippoff researching cavity discharges that caused high losses in mass-impregnated cables [31]. This model consisted of a spark gap in series with a capacitance and a protection

resistor. The circuit was applied an AC voltage and the number of discharges per half-cycle and the voltage across the spark gap was measured. The original circuit was then in the 1950s modified to enable calculation of the charge transfer in the sample. This included representing the bulk dielectric around the cavity as an added capacitance in parallel with the spark gap and the capacitance of the cavity as reported by F. H. Kreuger [32]. This resulted in the capacitive equivalent circuit that today is known as the abc model (see Figure 2.8).

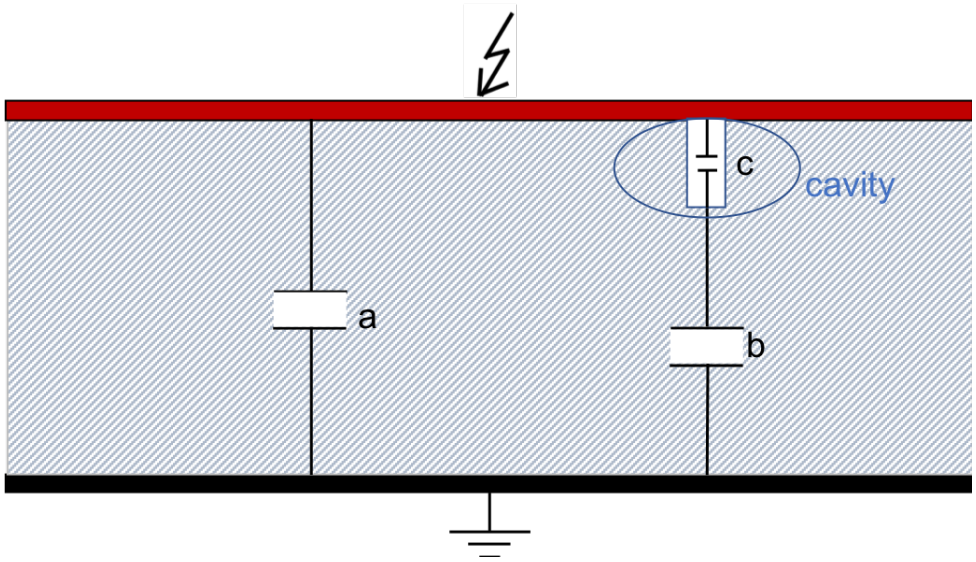

Figure 2.8: The acb model for modeling of partial discharges. c is the capacitance of the void (here a cylindrical void bordering the electrode), the b is the capacitance in series with the defect and a is the capacitance of the rest of the object.

The abc model is a simple equivalent where the insulation system is assumed purely capacitive. The capacitance of the cavity is denoted c, the capacitance in series with c is denoted b, whereas the rest of the object is represented by the capacitance a.

Today, the model is still widely used to model partial discharges in cavities as it is a useful tool for analyzing measurable quantities which can be detected by electrical measurements of partial discharges [16]. Furthermore, PD measurements that comply with the IEC 60270 standard are based on the quantity apparent charge, q_a [18]. This quantity can easily be calculated from the abc model which has contributed to the popularity and extensive use of the model.

The model is based on some important assumptions. First, it is assumed that the cavity and the bulk dielectric around can be modeled as a network of capacitors. Secondly, there is only one cavity in the insulation where discharges occur. Lastly, the model assumes that the current in the external test circuit is zero during the short duration (in the ns range) of a discharge. During a discharge, the equivalent circuit then becomes as shown in Figure 2.9.

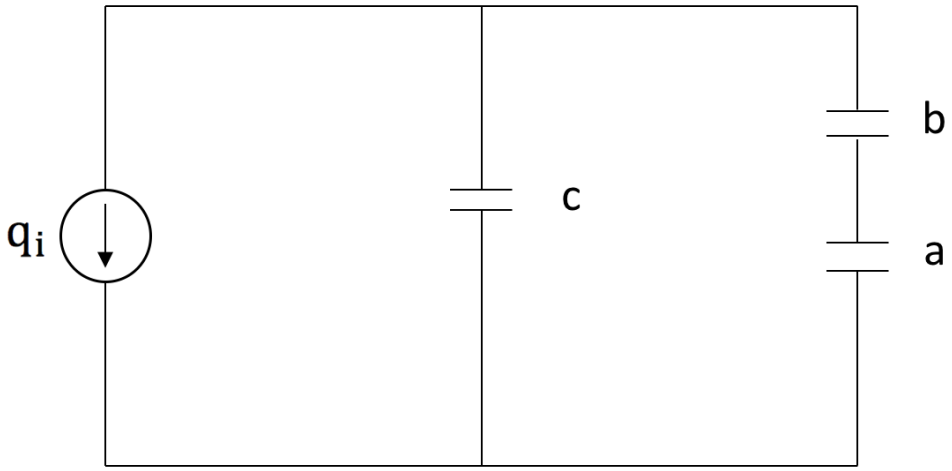

Figure 2.9: Abc-equivalent during a PD event.

2.6.1 The Capacitances in the A-B-C Model

When assuming that the capacitances in the abc model are ideal parallel plate capacitors, spreading of electrical field lines (fringe effects) outside the region limited by the two electrodes is ignored. The capacitances can then be calculated by the following formula [29]:

$$C = \frac{Q}{V} = \frac{\varepsilon_0 \varepsilon_r S}{d} \tag{2.9}$$

Where S is the surface area of the equipotential surfaces that bound the specific capacitance, and d is the distance between the surfaces. The cavity surfaces are also assumed to consist of two parallel equipotential surfaces.

When detecting partial discharges, the capacitance of the test object is effectively the total capacitance in parallel with the coupling capacitance and the measuring impedance as seen from the terminals “1” and “2” in Figure 2.6. This means that the test object, the electrode arrangement and the air around – the entire area where energy is stored contributes to the total capacitance.

With the test setups used in this project (see Figure 3.8), simulations have shown that the electric field is not only concentrated to the region between the common area of the electrodes (meaning the area of the smallest electrode); there are significant fringe effects. Actually, the amount of energy that is stored in the test setup in general (the epoxy around the electrodes, the air, etc.) was shown to be in the same range as the energy that is stored in the actual insulation sample. This energy contributes to the capacitance in the form of stray capacitance.

Taking stray capacitance into consideration has lead the author to develop a modified abc model; the abcd model (see Figure 2.10). In this model, the capacitance a only represents the region of the sample that is limited by the common area of the electrodes. All the electric energy that is stored elsewhere than in this region, is represented as a bulk stray capacitance, d. The stray capacitance can also be included in the capacitance $a^* = a + d$ as an effective

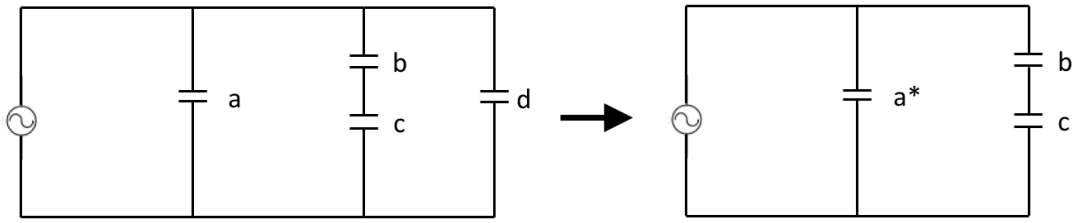

Figure 2.10: The abcd model. The stray capacitance is modeled in parallel with the capacitances of the original abc model. The model can effectively be represented by an a*bc model where the stray capacitance is included in the effective capacitance a^*.

capacitance a^* of the a*bc model. The capacitances b and c are unchanged from the original model. The total capacitance as seen from the terminals of the test setup is then given by Equation 2.10.

$$C_{tot} = a + \frac{bc}{b+c} + d = a^* + \frac{bc}{b+c} \tag{2.10}$$

Where a, b and c are calculated according to Equation 2.9, and C_{tot} is found by measuring the stored energy in the test setup and using the relationship between energy and capacitance [29]:

$$C = \frac{2W_e}{V^2} \tag{2.11}$$

Where W_e is the total stored energy and V is the applied voltage. The stray capacitance can then easily be found from Equation 2.10.

2.6.2 Apparent Charge

When a discharge happens in the cavity, the capacitance c is short-circuited and the voltage across the cavity is reduced from an initial value U_{s0} (ignition voltage), which is given by Pascehn's law (Equation 2.6) to a remanent voltage U_{r0}. The voltage drop across the cavity is thus:

$$\Delta U = U_{s0} - U_{r0} \tag{2.12}$$

The voltage drop that occurs during a discharge causes a small voltage drop across the capacitance a [16]:

$$\Delta u_a = \frac{b}{a+b} \cdot \Delta U \tag{2.13}$$

A transient current from the external circuit will restore the voltage drop across a. Based on this, the charge this current represents can be found [16]. The resulting parameter is the apparent charge:

$$q_a = \Delta u_a \cdot \left(a + \frac{bc}{b+c} \right) \tag{2.14}$$

This parameter is being used to represent the discharge magnitude. This is the parameter which the IEC60270 standard is based on. As can be seen from the formula, the apparent charge can be calculated once the capacitances and the voltage drop across the cavity are known. In real insulation systems, the relations a ≫ c and c > b hold and the expression for the apparent charge can be simplified:

$$q_a = b \cdot \Delta U \tag{2.15}$$

However, for laboratory experiments conducted on artificial samples or only a part of the insulation system, this approximation must be used critically.

2.6.3 Applying AC Voltage

When applying AC voltage across the sample, the voltage across the cavity (if there is no discharge) will according to the abc model be:

$$u_{c0}(t) = \frac{b}{b+c} \sqrt{2} U \sin \omega t \tag{2.16}$$

When the voltage across the cavity exceeds the breakdown strength of the gas (and a start electron is available), a discharge occurs. The voltage across the cavity will then instantly fall from the ignition voltage to the remanent voltage. After the discharge, the voltage across the cavity varies in the same way as before the discharge. The voltage across the cavity varies then as shown in Figure 2.11. In the figure, two different voltage levels are shown. When the voltage increases above the inception voltage, the number of discharges per half-cycle of the voltage increases. The discharges are concentrated around the rising and falling parts of the voltage cycle as can also be seen in the PRPD pattern in Figure 2.5.

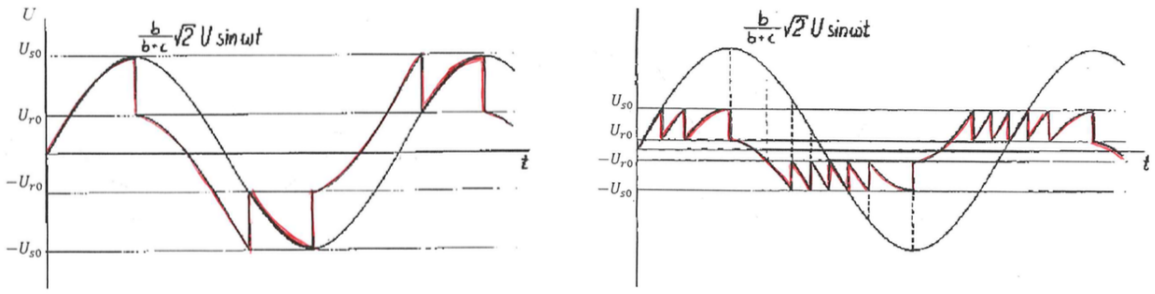

(a) Just after PDIV is reached.

(b) Higher voltage than PDIV.

Figure 2.11: The voltage across the cavity under the application of AC voltage. Figure 2.11a shows the voltage across the cavity right after PDIV is reached, whereas Figure 2.11b shows the voltage at a higher voltage level when there are more discharges occurring.

The relationship between the inception voltage and the ignition voltage is:

$$U_i = \frac{b+c}{b} \cdot \frac{U_{s0}}{\sqrt{2}} \tag{2.17}$$

According to [16], the number of discharges per half-cycle can be found by using Equation 2.18. If the formula does not give an integer, then the number must be rounded down to the closest integer. This theoretical value assumes that the entire surface area is active during a discharge so that there are no parallel discharges.

$$n = \frac{2\left(\frac{b}{b+c}\sqrt{2}U - U_{r0}\right)}{U_{s0} - U_{r0}} \tag{2.18}$$

2.6.4 Dissipated Energy

The overall goal of partial discharge measurements is to say something about the damage that is being inflicted on the insulation system and eventually to be able to say something about the condition of the insulation. The dissipated energy during a discharge can be used as a measure of the potential damage caused by a partial discharge. The dissipated energy from one discharge is found by the following formula [16]:

$$\Delta W = \sqrt{2}U_e \cdot q_a \tag{2.19}$$

Where U_e is the extinction voltage. As can be seen, the dissipated energy is proportional to the apparent charge. This justifies the use of apparent charge as a measure of the discharge magnitude.

However, when the approximation in Equation 2.15 does not hold (as is the case with the samples used in this project), a factor k has to be included in the formula for the dissipated energy. In addition, when the remanent voltage is negligible, the extinction voltage is one half of the inception voltage [16], and the dissipated energy from one discharge is then:

$$\Delta W = \frac{\sqrt{2}}{2}U_i \cdot kq_a \tag{2.20}$$

where $k = (a^* + b)\frac{1}{a^* \frac{bc}{b+c}}$.

To find the dissipated energy over a certain time period, the dissipated energy from all discharges during this period has to be added up. The theoretical dissipated energy per second, or the dissipated power, for a voltage frequency of $f = 50$ Hz is then:

$$\Delta W = \frac{\sqrt{2}}{2}U_i \cdot kq_a \cdot 2n \cdot f \tag{2.21}$$

where U_i is found according to Equation 2.17, the apparent charge of each discharge is equal to the maximum apparent charge according to Equation 2.14, and the number of discharges per voltage half-cycle, n, is found by Equation 2.18.

3 Methods

This chapter goes through the design and the preparations of the test samples, the design of the test setups, the technicalities of the PD measurements, and the post-processing and presentation of PD data. It also includes a section of how a computer simulation of the test setup was made to facilitate numerical electric field calculations.

3.1 Preparation of Test Samples

The test samples used in this project are all made up of three 1.0 mm thick sheets of the same material with a circular hole in the middle layer. Sandwiched between the other two whole layers, this results in an embedded air-filled disk-shaped cavity. The aim of this project is to clarify how important PD parameters relate to the cavity size and therefore five different cavity diameters have been chosen for PD measurements. The diameters range from 1 mm to 20 mm (see Table 3.1). The diameter of the void is consistently used as a measure of void size throughout this project. An illustration of the cross-section of the specimens is shown in Figure 3.1.

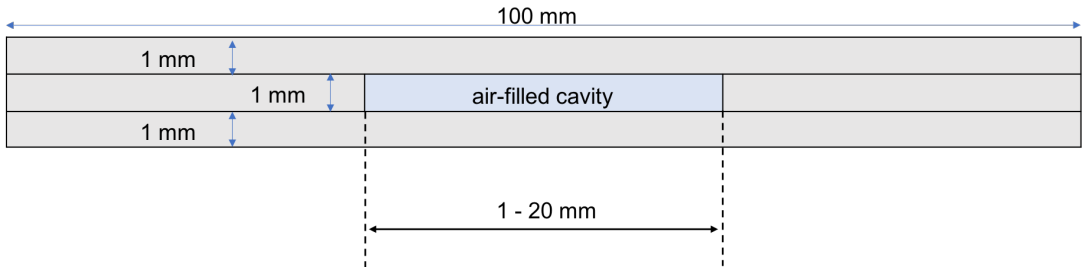

Figure 3.1: A cross-section of the center of the test object. The cavity is cylindrical and has a height of 1 mm and a diameter of either 1, 3, 5, 10 or 20 mm. The samples are 100 mm x 100 mm except from the mica mat samples which are 50 mm x 100 mm. The thickness of the plates is exaggerated to show detail.

Table 3.1: The diameter of the cavities.

Cavity Diameters				
1 mm	3 mm	5 mm	10 mm	20 mm

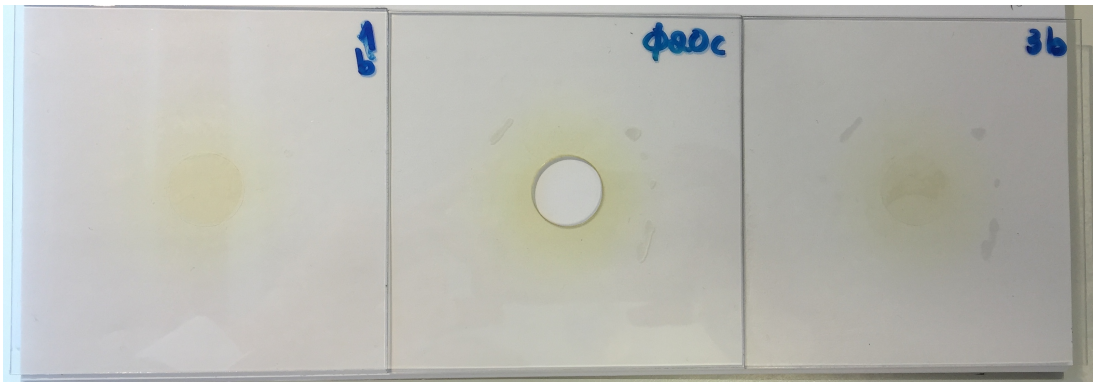

Figure 3.2: Three sheets of polycarbonate which make up one sample when stacked on top of each other. These photos are taken after the samples had underwent PD testing, and some discoloration can therefore be observed.

There are four different kinds of sample materials that have been used in this thesis work. For every kind, one sample for every cavity size was made.

1. Polycarbonate (plexiglas sheets)
2. Polycarbonate (plexiglas sheets) with conducting cavity surfaces
3. Samicatherm (new mica insulation tape)
4. Mica Mat (aged generator bar insulation)

3.1.1 Polycarbonate

The polycarbonate sheets are made of the product Lexan 9030 [33]. Polycarbonate is an insulating material which, because of its high dielectric strength, is PD free (no PD above the threshold value set for the experiments) at the voltage levels which the PD measurements are conducted.

The polycarbonate sheets were cut into smaller 100 mm x 100 mm squares and cavities were made by drilling through the plates. This was done by help from the workshop. One of the polycarbonate samples (with the 20 mm cavity) is shown in Figure 3.2.

Aluminum Application

The widely known abc model represents an insulation system containing a void as a network of capacitances. Therefore, an implicit assumption is that the void surfaces (normal to the applied field - the top and bottom of the disk void) behave like equipotential surfaces or, in other words, the void surfaces are conducting. This thesis will therefore investigate what effects conducting void surfaces have on the discharge activity in the voids and if the discharge activity in these voids can be described accurately by the theoretical model.

For this purpose, a layer of aluminum was applied to the top and bottom sample sheets. An illustration of the cross-section of the sample where the aluminum is indicated is found

in Figure 3.3. The area of the aluminum corresponds to the respective cavity surface area: $\pi\frac{d^2}{4}$, where d is the diameter as shown in Table 3.1. The choice of making the area of the aluminum equal to the void surface area is based on a discussion of several factors. The full reasoning behind this choice is found in Appendix A.

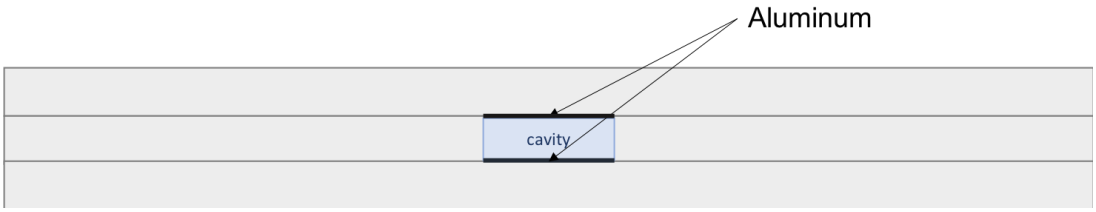

Figure 3.3: The top and bottom surface of the cavity are covered in a thin layer of aluminum (colored black in the illustration). The two side walls still consist of the insulating polycarbonate material.

The aluminum coating was applied to the surfaces of the cavity using a vacuum evaporator. A schematic of the vacuum evaporator is shown in Figure 3.4. The reason for choosing this application method over for example using aluminum paint or tape, is the superior end result: thin and even coating. This ensures that the field is homogeneous, that the height of the cavity is not reduced, and that the field enhancement at the edge of the aluminum is limited.

The specimen to which the coating was applied was placed in a bell jar which was then evacuated to achieve vacuum. By running a 40 A current through a wire basket source with an aluminum pellet placed in the spiral of the wire, the aluminum evaporates (or sublimes) and aluminum atoms are spread spherically in all directions from the source. Since the material they hit has a much lower temperature than the aluminum, the aluminum will condense and form a thin, even layer of solid aluminum on the specimens. See appendix B for a detailed description of the procedure.

3.1.2 Samicatherm

Samicatherm 366.28-02 from VonRoll is one of the materials used as insulation of hydro generator stator bars. The material consists of calcine mica paper, woven glass fabric and epoxy resin (binder) [34]. The sheets are made of 7 layers of samicatherm tape, resulting in 1.0 mm thick sheets. The sheets were made by Stip. Torstein Grav Aakre. Then, the final samples of samicatherm were made by pressing three of these sheets together with a hole through the middle sheet (diameters according to Table 3.1). One of the samples (with a 20 mm void) is shown in Figure 3.5.

3.1.3 Mica Mat

The final material that has been tested, is the actual insulation from generator bars. The generator entered service in 1976 and was taken out of service in 2011 after operating for 35

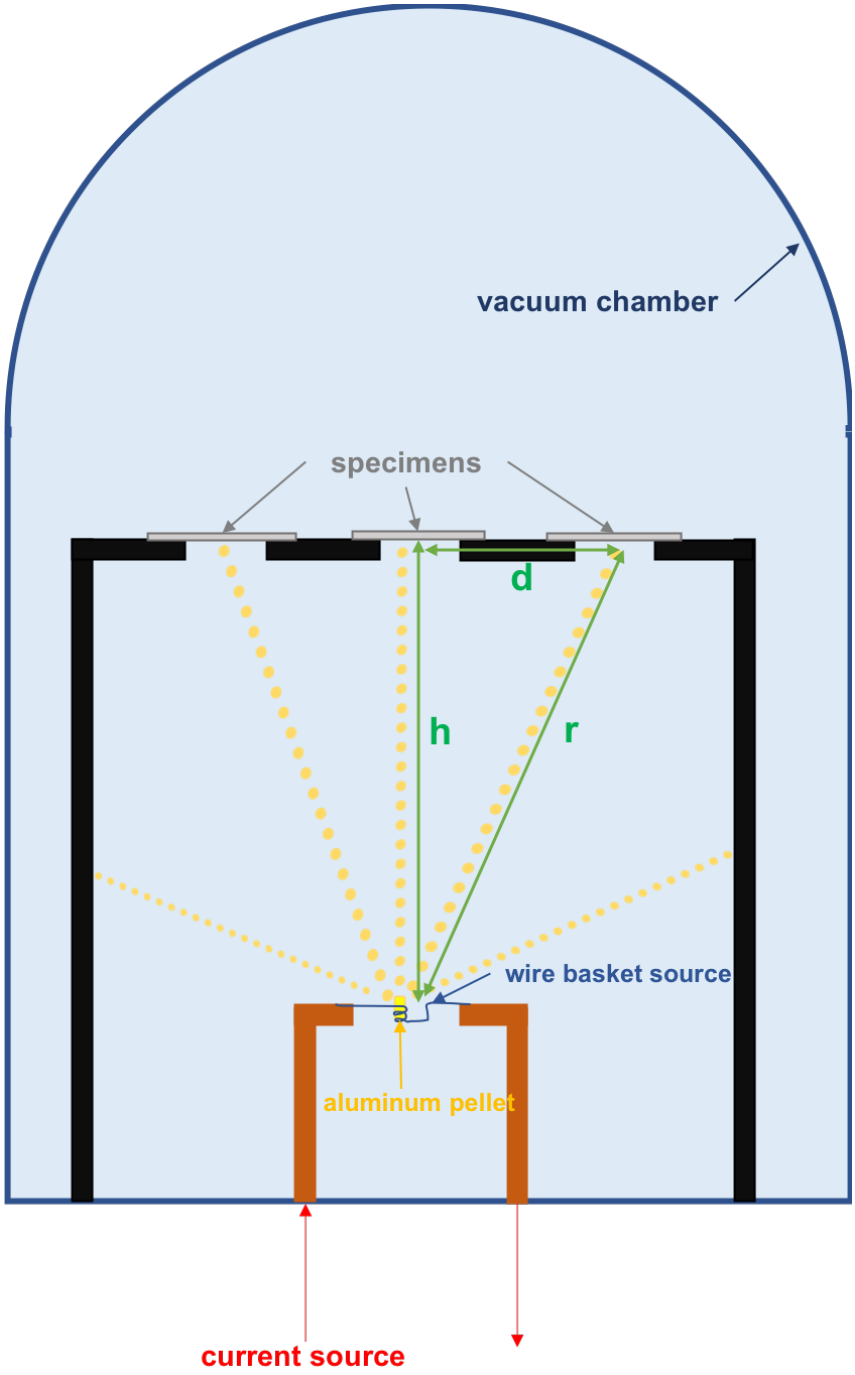

Figure 3.4: Illustration of the vacuum chamber (bell-jar) with the aluminum pellet positioned under the stand with the specimens. The yellow beams illustrate the aluminum spreading from the source and condensing at the first surface it hits.

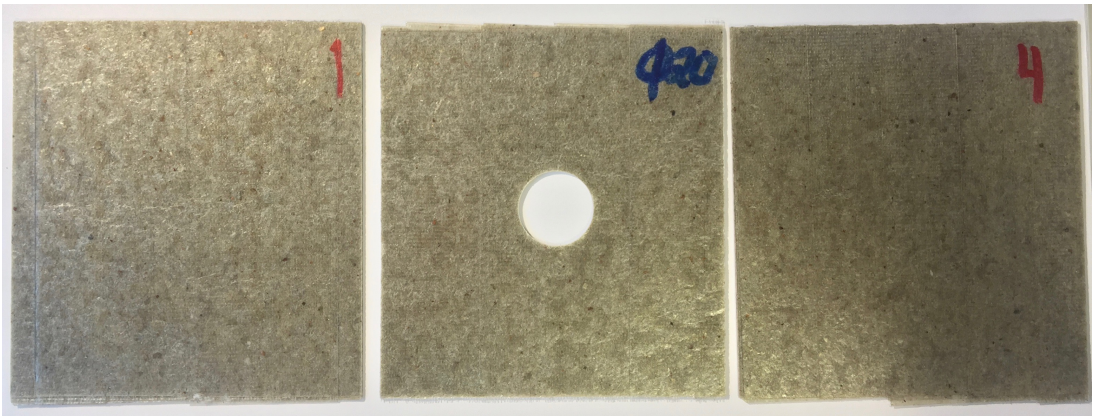

Figure 3.5: The sheets of one of the samicatherm samples (with a 20 mm cavity). The sample is created by stacking these sheets on top of each other. Sheet 1 under Ø20, and sheet 4 on top of Ø20.

years. The insulation is made up of mica mat tape consisting of mica paper reinforced with glass fiber and bonded with an epoxy resin. The total thickness of the insulation is 3.0 mm.

The insulation samples used in this project are cut from a part of the generator bar which has been situated close to the high voltage terminal of the generator and on the bottom half of the windings. The insulation samples were detached from the rest of the bar with help from the workshop. In Figure 3.6 one of the samples is shown.

After performing reference measurements on the mica mat samples (without a cavity), the insulation was delaminated into three layers with a thickness of about 1 mm each. Then, holes were punched through the middle layers - creating voids in the same way as for the other materials

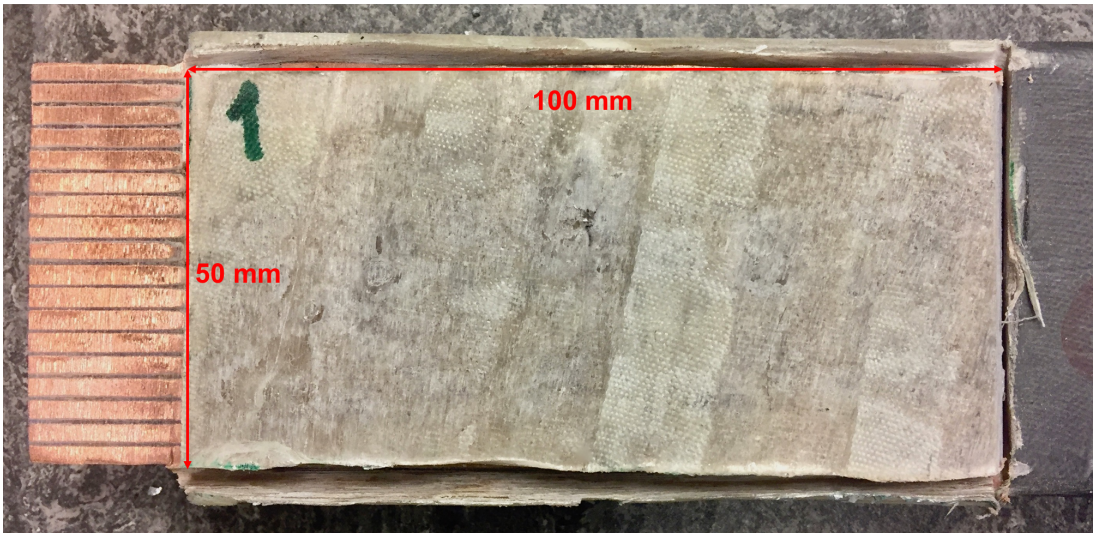

Figure 3.6: One of the samples cut out from the generator bar. The dimensions of the samples are 100 x 50 mm and they have a thickness of 3.0 mm.

3.1.4 Relative Permittivity of Samples

The relative permittivity of the samples for frequencies ranging from 0.1 mHz to 1 kHz was measured using IDAX 206 Insulation Diagnostic Analyzer, 200 V, AC. The measuring device measures the real and imaginary capacitance as a function of frequency. A guard is used to confine the electric field to the defined area and to remove leakage currents from the measured current. Knowing the measured capacitance and the geometry of the test object, the relative permittivity can then be calculated from Equation 2.9. See Appendix C for a detailed explanation of the measurements.

3.1.5 Summary of Test Samples

Table 3.2 shows a summary of the four different types of test samples.

Table 3.2: Summary of the four different types of test samples used in this project. 1 mm cavity was only tested once and the results showed that the discharges were not possible to detect. Therefore, 3 mm became the smallest void diameter that was tested with the remaining samples.

Material	Thickness of specimen	Cavity diameters [mm]
Polycarbonate	3 x 1 mm	1, 3, 5, 10, 20
Polycarbonate w/ aluminum	3 x 1 mm	3, 5, 10, 20
Samicatherm	3 x 1 mm	3, 5, 10, 20
Mica Mat	3 x 1 mm	3, 5, 10, 20

3.2 Development of Electrode Configurations

The two test setups that were developed for PD measurements in this project are shown in Figure 3.7. The reason for changing the electrode arrangement from setup 3.7a to setup 3.7b when testing on mica mat is that the width of the mica mat samples is only 50 mm. Therefore, it is possible that the field would be high enough to cause surface discharges, or even surface breakdowns, where the sample stops had the larger electrode been used.

A schematic of the test setups in Figure 3.7 can be seen in Figure 3.8. The high voltage electrode is a cylindrical copper electrode (diameter = 30 mm) which has rounded corners to reduce the local electric field (the fillet radius is 0.4 mm (measured)). The electrode is also molded in epoxy to further reduce the electric field enhancement. The ground electrode is a cylindrical brass electrode with a diameter of 90 mm. In the case of the setup in Figure 3.7b, the ground electrode is similar to the HV electrode.

The goal with these test setups is to achieve a satisfactory suppression of noise and disturbances. Internal discharges in the void are the discharges that are being analyzed in this project, and it is therefore important to try preventing any disturbances which may make

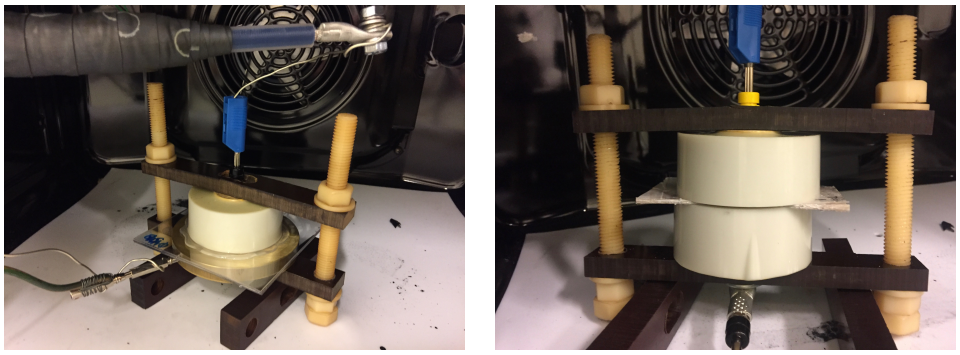

(a) (b)

Figure 3.7: The different test setups used in this project. Figure 3.7a: The setup used for measuring on polycarbonate and samicatherm samples. Figure 3.7b: The setup used for testing on mica mat samples. A clamp was made to press the electrodes and the samples together to avoid air-gaps.

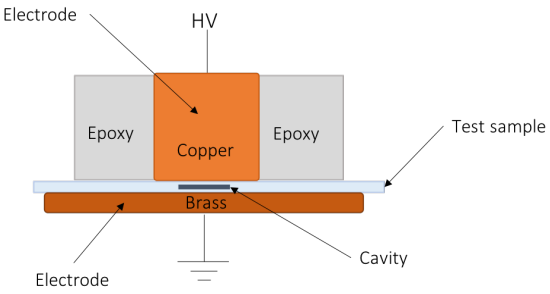

(a) The test setup for measuring PD in polycarbonate and samicatherm.

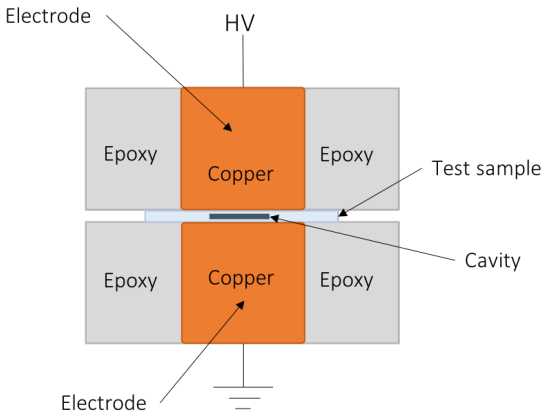

(b) The test setup for measuring PD in mica mat.

Figure 3.8: Cross-sections of the two experimental setups used in this thesis work. In Figure 3.8a, The high voltage electrode is smaller than the ground electrode, while the test setup in Figure 3.8b also uses the small electrode the ground electrode. The stored energy is not the same in these two setups and therefore they have to be treated separately when calculating the capacitance.

the detection of such internal discharges more difficult. Possible sources of disturbances include:

- Surface discharges near the edge of the electrodes
- Discharges between the sheets of the test samples
- Discharges between the electrodes and the samples
- Corona - discharges in air

To mitigate these issues, several measures were taken. In general, any air gaps or bubbles in, on or near the test samples had to be reduced/eliminated, otherwise discharges can occur in unwanted places.

Insulating silicone grease was applied underneath the HV electrode to prevent surface discharges at the edge of the electrode. The epoxy mold alone does not reduce the field enough to prevent discharges from happening. Since the corners of the brass electrode are well outside the area of high electric field (which is concentrated between the common area of the two electrodes), there is not a risk of surface discharges happening at the edge of the brass electrode. Silicone grease was therefore not added between the brass electrode and the sample. Unnecessary use of silicone grease would just introduce new possible sources of error/disturbances (air bubbles, etc.), so as long as the test setup is PD free without silicone grease on the ground electrode, this is the preferable solution. Of course, in setup 3.8b silicone grease was applied to the smaller ground electrode for the same reasons silicone grease was applied to the HV electrode.

To reduce the chance of discharges between the sheets of the samples, new, clean samples were used. When repeating an experiment, the sample sheets were cleaned using isopropanol to remove residues of dirt, oil and particles before performing new tests.

To further prevent discharges between the sample sheets and between the sample and the electrodes, it was deemed necessary to use a clamp to press the setup together and eliminate any air gaps and also to squeeze out any small air bubbles in the silicone grease. Finally, sharp protrusions in areas of high electric field had to be avoided to prevent corona from happening.

3.3 Partial Discharge Measurements

The PD measurements in this projects are based on an electrical detection method which is described in section 2.3.6. The measuring circuit, the acquisition system and the voltage signal controller are the same as the ones that were used in the author's specialization project [15]. The calibration is also performed the same way. Therefore, the following three sections are based on the corresponding sections in the specialization project and some information is taken directly from the project report. Other information used in these sections (which is not the author's own work) is, of course, acknowledged and cited.

For a comprehensible list of the equipment used throughout the work with this thesis, see appendix D.

3.3.1 Measuring Circuit

The measuring circuit (Figure 3.9) consists of a regular measuring system as described in the standard IEC60270 with a noise filter, a coupling capacitor, and a coupling device (measuring impedance).

The low pass filter reduces noise from the voltage source. The coupling capacitor, which has a capacitance of 3.4 nC, provides the current pulses, and restores the voltage when a PD event occurs. The coupling device (measuring impedance) is a passive element designed to

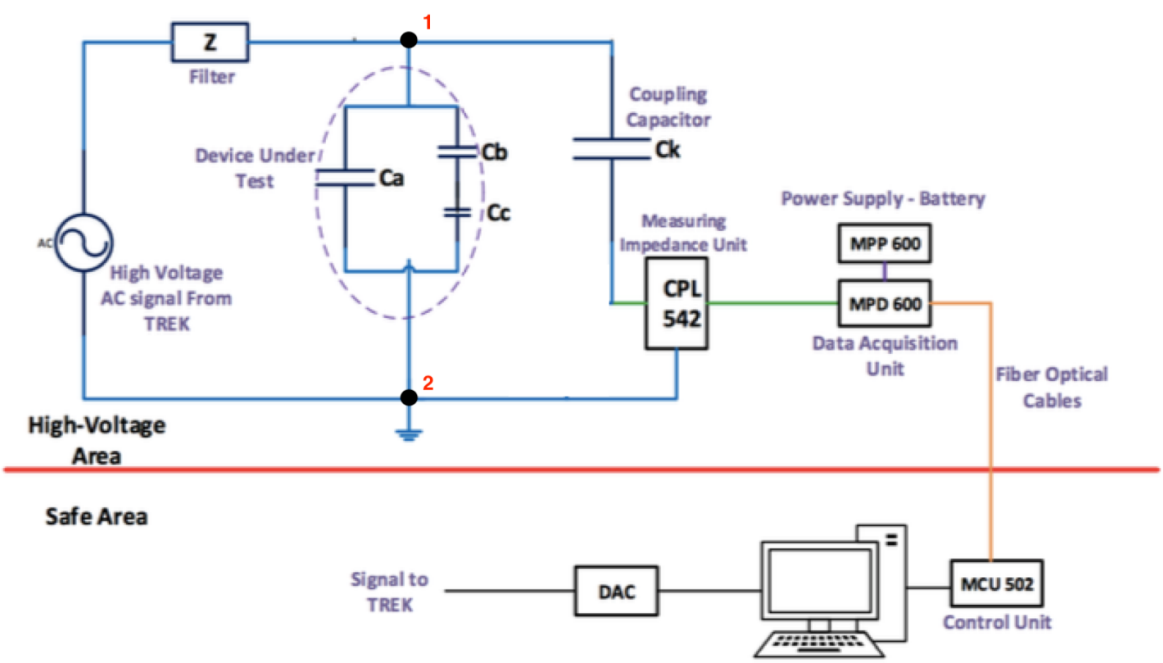

Figure 3.9: The measuring circuit which is used for PD measurements. The illustration was made by the author as a part of the specialization project and is reused here with some minor modifications. The test object (and the entire test setup) is connected between terminal 1 and 2.

prepare the sharp current pulse from the coupling capacitor for processing by the data acquisition system. From the measuring impedance, a voltage signal is sent to the acquisitioning unit which is converting the voltage signal to a digital signal, which then goes through an optical cable, via the control unit, to a computer with OMICRON software.

With a coupling capacitor of 3.4 nC and a test setup with a capacitance of 12-18 pF (see Table 4.2), the capacitance of the test object is less than 0.5 % of that of the coupling capacitor which, according to Equation 2.5, results in good sensitivity.

3.3.2 Data Acquisition System and Voltage Signal Controller

The data acquisition system used in this project (MPD 600) is a product of OMICRON. This software is based on analyzing partial discharges by the means of phase-resolved partial discharge analysis (PRPDA). A screenshot of the computer interface of OMICRON and an explanation of essential settings can be found in Appendix E.

A pre-made LabVIEW program made by PhD-stip. Torstein Grav Aakre was used to control the voltage signal, i.e. the voltage magnitude and the voltage frequency.

3.3.3 Calibration

Before starting the experiments, both the charge and the voltage must be calibrated. The charge is calibrated using a calibrating device hooked up to the high voltage part of the test object and ground. A rapid signal of a known charge is injected into the test object and the

calibration factor is calculated by OMICRON based on the set-point charge and the detected charge. Again, it should be noted that this is the apparent charge q_a and not the real charge q [27]. The charge calibration is dependent on the capacitances of the measuring circuit. Therefore, it is necessary to repeat the calibration before the introduction of every new test object.

The voltage is calibrated using a voltage probe, and based on the measured voltage and the voltage detected by OMICRON, a divider factor is calculated. A new voltage calibration is only necessary if the coupling capacitor or the coupling device is changed, and thus it is not necessary to repeat when changing test object.

3.3.4 Development of Test Program

The PD parameters that need to be extracted from the PD measurements in this project are the inception voltage, the maximum apparent charge and the number of discharges per voltage half-cycle. These are the PD parameters which will be analyzed and compared with the theoretical model. With this in mind, suitable test programs were developed and the resulting test programs (Figure 3.10 and 3.11) comprise an easy and consistent way to extract these parameters. The conditions for all of the measurements performed as a part of this project are 20 °C (room temperature) and 1 atm. The voltage frequency is consistently set to 50 Hz.

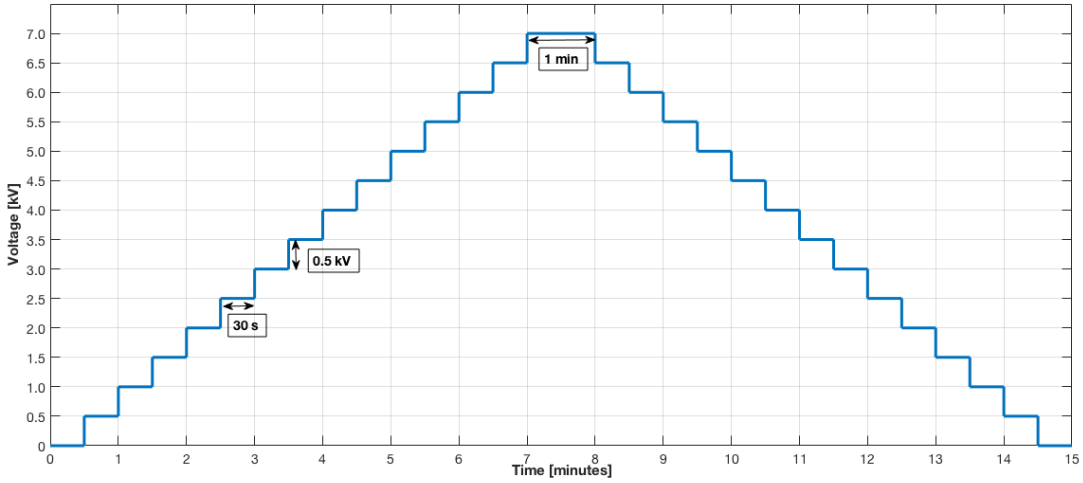

Figure 3.10: Test program for specimens with conducting cavity surfaces. The program is a PDIV/PDEV test where the voltage is increased in steps of 0.5 kV until the max test voltage (7.0 kV) is reached. Then the voltage is decreased from the test voltage to zero voltage in steps of 0.5 kV. No pre-stressing is performed.

Figure 3.10 shows the program used for the samples with conducting void surfaces (polycarbonate with aluminum), whereas Figure 3.11 shows the program used for the samples with insulating surfaces i.e. the rest of the sample types. Only the samples with insulating cavity walls are pre-stressed, or conditioned, before starting the PDIV/PDEV test. This is done as an attempt to achieve the same reference state for all the samples before starting the PD measurements. That way, analyzing and comparing the results from the PDIV/PDEV

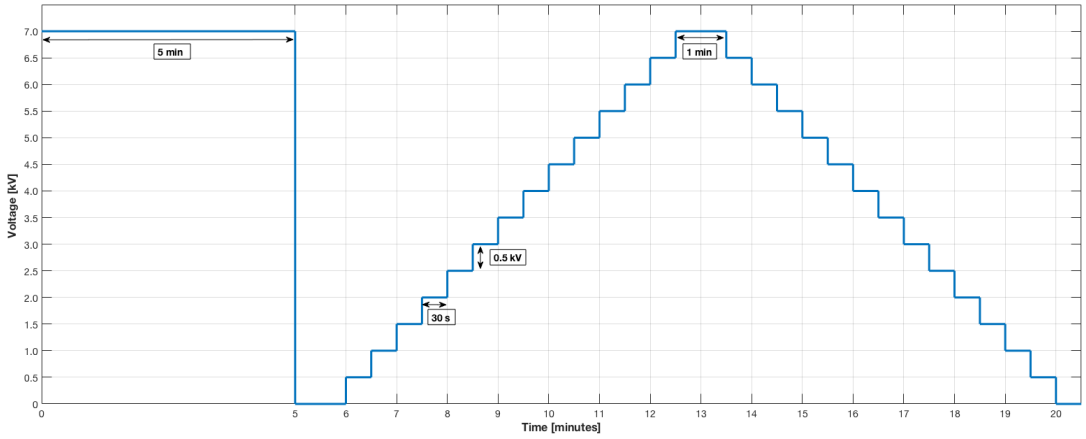

Figure 3.11: Test program for specimens with insulating void surfaces. A five minute pre-stressing at test voltage 7.0 kV is performed before starting the PDIV/PDEV test which is identical to the PDIV/PDEV test performed on specimens with conducting cavity surfaces (3.10).

tests is done on the basis of the same reference state. For the samples with cavity surfaces covered in aluminum, the conditions of the cavity, i.e. the capacitances and the conductivity of void etc., are known. Conditioning in the form of applying electrical stress to reach a "steady state" is thus not needed. Therefore, the program for these specimens starts directly with a PDIV/PDEV test.

The pre-stressing is performed at a voltage level of 7.0 kV (RMS [1]). The duration of the pre-stressing is the same duration as suggested in the IEC 60034-27:2006 standard for off-line PD measurements on stator winding insulation of rotating electrical machines [35]. For the PDIV/PDEV test, the test voltage is increased in steps of 0.5 kV and kept constant for 30 seconds at each voltage level. Then, the voltage is kept constant at test voltage, 7.0 kV, for 1 min before the voltage is decreased again in steps of 0.5 kV with 30 seconds at each voltage level. The reasoning behind the choices of using 7.0 kV as the test voltage, 0.5 kV as the voltage steps and 30 s/1 min as the time duration at each voltage level, is thoroughly explained in Appendix F.

Reference Measurements

First, reference measurements (on samples without voids) were performed to be able to compare the measurements with voids to measurements on samples without voids. This is useful since there might be active PD sources inherently in the samples (especially the mica mat samples), and the test setup might not be completely free for disturbances/noise.

In the case of the polycarbonate and samicatherm samples, tests were performed at three sheets of the material without a cavity. In the case of the mica mat samples, however, the reference measurements were done directly on the 3.0 mm thick insulation sample (without a void).

[1] RMS (Root Mean Square): For a sine wave the RMS value is: $V_{rms} = \frac{V_{max}}{\sqrt{2}}$. All voltages mentioned are RMS values if not otherwise stated.

3.4 Post Processing of Data

While running the experiments, a stream file is recorded in OMICRON. This file includes each and every PD event during the time of recording. Every PD event is saved with its corresponding time of occurrence, the apparent charge of the discharge, and the phase value of the voltage at which the discharge is occurring. This makes it possible to replay the whole sequence of PD events and thus essentially replay the entire experiment.

The stream file, or snippets of it, can be exported to MATLAB for further processing of experimental data (see appendix G and Figure G.2 - G.5 for the scrips that import the files from OMICRON).

3.4.1 PRPDA

The PRPD plots shown in the Results section of this report are made in MATLAB (see script in Figure G.6). The PD data is recorded during *30 seconds of PD measurement at an applied voltage of 7.0 kV, 50 Hz.*

3.4.2 PDIV and PDEV

The PDIV and PDEV can, in most cases, be determined visually by examining the PD activity at the voltage levels of the PDIV/PDEV test program. The PDIV is the lowest voltage level at which reoccurring discharges are observed when the voltage is increased from a lower value. However, in some cases, the discharges are observed in "bursts" - periods of discharges interrupted by shorter or longer periods (which can range from just a fraction of a second to several seconds or minutes) of no PD activity. The bursts can indicate that the voltage is very close to the inception voltage, but to ensure consistency in how the PDIV is determined, requirements have been established to ensure that the PDIV and the PDEV are determined equally for all test samples:

PDIV
The lowest voltage level at which there is minimum one partial discharge per voltage half-cycle with an apparent charge larger than the threshold value of 30 pC. The number of discharges per half-cycle is measured as an average during the final 20 seconds of the total measuring time of 30 seconds at the voltage level in question.

PDEV
The highest voltage level (when decreasing the voltage from the test voltage of 7.0 kV) at which there are no discharges above the threshold level of 30 pC. This is measured during the final 20 seconds of measuring at the voltage level in question.

The PDIV and PDEV are decided with an uncertainty equal to the voltage step: 0.5 kV. If the PDIV is determined to be 6.0 kV, the actual value is somewhere between 5.5 kV and

6.0 kV. Correspondingly, if the PDEV is determined to be 5.0 kV, the actual value is somewhere between 5.5 kV and 5.0 kV.

3.4.3 Discharge Magnitude

All the stream files that are being used to extract the discharge magnitude, or the apparent charge, q_a, are recorded during *30 seconds of PD measurement at an applied voltage of 7.0 kV, 50 Hz*. To even out some of the effects of this statistic variation is has been decided to use *the mean of the ten largest discharges recorded during the measuring period of 30 seconds*. This was found for positive and negative discharges separately and then the mean of the absolute value of these two has been used as the measure of the discharge magnitude.

3.4.4 Discharge Frequency

The discharge frequency [PDs/half-cycle] is calculated based on an average over a measuring period of *30 seconds at 7.0 kV, 50 Hz*. 30 seconds correspond to 1500 voltage cycles. Again, the average discharge frequency of the positive and negative discharges were found separately before using the mean of these two values as the measure of the discharge frequency.

3.5 Electric Field Calculations

To increase the understanding of the discharge mechanisms in the void, a numerical simulation of the test setups was made. This COMSOL Multiphysics model simulates the electric field distribution in the test setups; most importantly, the field distribution if the cavities. The model is 2D axis symmetric with the same dimensions and material properties as the actual test samples and test setups. The specifics of this model are explained in detail in Appendix H. The electric field distribution in the cavities will be important when explaining some of the results from the PD measurements.

The simulation model has also been used to calculate the capacitance of the test setups. First, the total stored energy of the test setups was found by integrating the energy density over the enitre volume of the simulation model. Then the capacitance was found by using Equation 2.11.

4 Results

This chapter includes the following:

1. The results of the theoretical a^*bc model.
2. Results from the numerical simulations of the electric field distribution in the voids.
3. The results from the partial discharge measurements.

4.1 Theoretical Model

The following will be presented in this section: the relative permittivity of the samples, the capacitances of the a*bc model, and the theoretical inception voltage, discharge magnitude, and discharge frequency.

4.1.1 Relative Permittivity of Samples

The measurements that are performed in this thesis work are performed at a voltage frequency of 50 Hz, and a summary of the relative permittivity of the sample materials at 50 Hz is shown in Table 4.1. The relative permittivity for polycarbonate, samicatherm and mica mat as a function of frequency is shown in Figure C.1.

Table 4.1: The relative permittivity of the sample materials at 50 Hz.

	Relative permittivity, ε_r, at 50 Hz
Polycarbonate	3.4
Samicatherm	4.2
Mica mat	3.6

4.1.2 Capacitances of the Abcd Model

The total capacitance, C_{tot}, of the test setup with a polycarbonate sample (without a cavity - b and c can be ignored) was measured using IDAX (see section 3.1.4) and simulated by COMSOL (see section 3.5). The capacitance of the test setup with samples made of mica mat and samicatherm is only found by simulation due to time restrictions.

The results are seen in Table 4.2 and show that the measured and simulated capacitance are consistent. This demonstrates that the simulation model is a good representation of the actual test setup.

The results also show that the capacitance of the mica mat sample is lower than the capacitance of polycarbonate and samicatherm. This is because the stored energy in the test setup that is used for the mica mat samples (Figure 3.8b) is lower than the stored energy the test setup used for polycarbonate and samicatherm (Figure 3.8a).

Table 4.2: The measured and simulated total capacitance of the test setups.

	Total Capacitance, C_{tot} [pF]	
Test Sample	Measured (IDAX)	Simulated (COMSOL)
Polycarbonate	15.5	15.4
Samicatherm	-	17.7
Mica mat	-	12.2

The capacitance a of the abcd model can easily be calculated according to Equation 2.9 based on the known dimensions of the electrode surface area, S, the thickness of the samples, and the relative permittivity ot the samples (Table 4.1). Then, from Equation 2.10, the stray capacitance, d, can be calculated. The resulting capacitances are shown in Table 4.3.

Table 4.3: The capacitance a and d in the abcd model based on the measured and simulated total capacitance of the test setup. No cavity is present, so capacitances b and c are ignored.

	Capacitances of the abcd model [pF]		
Test Sample	a	d (electrode arrangement 1)	d (electrode arrangement 2)
Polycarbonate	7.1	8.4	-
Samicatherm	8.8	8.9	-
Mica mat	7.5	-	4.7

Simulations confirm that the stray capacitance is not affected by the introduction of a cavity in the test sample (introducing b and c in the a^*bc model) and therefore, the values for d that are presented in Table 4.3 are representative for the total stray capacitance regardless of the presence of a cavity in the sample. For a complete table of the capacitances of the abcd model for all five cavity sizes, see Appendix I.

4.1.3 Estimation of Parameters

Inception Voltage

The formula for the inception voltage (Equation 2.17), includes the ignition voltage (or breakdown voltage of the cavity, U_{s0}), the capacitance of the cavity, c, and the capacitance of the bulk insulation in series with the cavity, b.

Since the cavity is ventilated due to the sample being split into three sheets, the pressure in the cavity is assumed to be equal to atmospheric pressure. According to Equation 2.6, the breakdown voltage of the cavity is then:

$$V_B = U_{s0} = 4.6\,\text{kV}$$

The streamer inception criterion (Equation 2.3) gives the same result. Since the height of the cavity is constant, and the relative permittivity of the surrounding material does not affect the breakdown voltage of the cavity, the theoretical breakdown voltage remains constant for the different materials and cavity diameters. Having found the breakdown voltage of the cavity, the inception voltage can then be calculated by Equation 2.17 and the results are found in Table 4.4. The inception voltage is found to increase with decreasing relative permittivity of the sample and varies from 4.8 kV to 5.2 kV.

Table 4.4: The theoretical inception voltage (PDIV) of the three sample types used in this project.

	Inception voltage [kV]
Polycarbonate	5.2
Samicatherm	4.8
Mica mat	5.1

Discharge Magnitude

The theoretical expression for the apparent charge (Equation 2.14), includes the ignition voltage and the remanent voltage, and the capacitances of the a*bc model. At this point, there is not enough information about the characteristics of the discharge mechanisms in the void to make an educated estimate of the remanent voltage. Therefore, the remanent voltage will be assumed negligible.

The apparent charge of the partial discharges for the different materials as a function of cavity diameter is shown together with the experimental results in section 4.3. However, the values for the specific cavity diameters used in this project are summarized in Table 4.5.

Table 4.5: The apparent charge, q_a, resulting from a partial discharge in cavities of different sizes, in the three different sample materials used in this thesis work.

	Apparent Charge, q_a [nC]				
Diameter of cavity	1 mm	3 mm	5 mm	10 mm	20 mm
Polycarbonate	0.054	0.49	1.3	5.3	18
Samicatherm	0.067	0.60	1.6	6.2	20
Mica mat	0.057	0.51	1.4	5.4	18

The theoretical apparent charge increases approximately with the square of the void diameter. Due to the higher relative permittivity, the apparent charge of the partial discharges

in the samicatherm samples is generally higher than that of polycarbonate and mica mat.

See appendix I for a discussion about the validity of the assumptions behind the approximation in Equation 2.15 and why, in this thesis, the exact formula for apparent charge according to Equation 2.14 has been used.

Discharge Frequency

The theoretical number of discharges assumes that there is only one cavity in the sample that produces discharges, and that there are no parallel discharges in this cavity (since the entire discharge area is active during each discharge). In this case, at the test voltage of 7.0 kV, the theoretical discharge frequency according to Equation 2.18, is 2 discharges per voltage half cycle.

The number varies between 2.58 and 2.91, but they all have to be rounded down to the closest integer. The theoretical value will be compared with the experimental results in section 4.3.

4.2 Numerical Simulations

The following sections include a presentation of:

- The electric field distribution in the different cavities at test voltage 7.0 kV.
- The effect of the two different test setups on the field distribution in the cavities.
- How the electric field strength in the cavities is affected by applying aluminum to the cavity surfaces (i.e. effectively introducing two floating potentials).

The aim with the numerical field simulations is to present a more realistic picture of the electric field distribution in the voids and then build the foundation for a discussion about the relationship between the local electric field and the breakdown strength of the cavity as a function of void diameter.

The material that is used in the simulations presented in these sections is polycarbonate with a relative permittivity of 3.4. The results of the simulations of samicatherm and mica mat exhibit the same characteristics as polycarbonate, but the exact values are different because of the difference in relative permittivity. See Appendix J for the maximum, average and minimum electrical field strength of the voids embedded in samicatherm and mica mat.

4.2.1 Electric Field Distribution in the Cavities

The surface plots of the electric field in the cavities are shown in Figure 4.1.

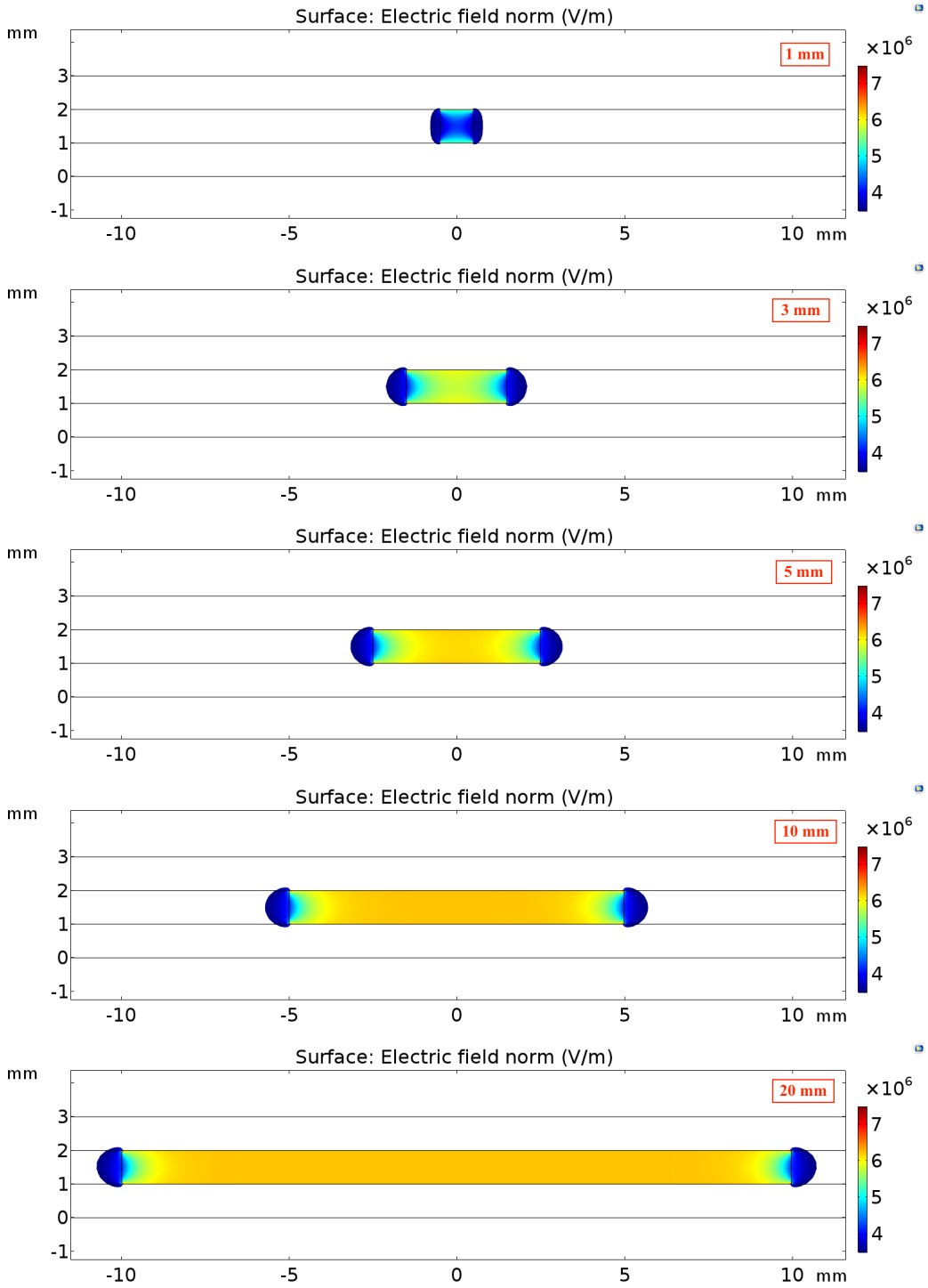

Figure 4.1: The electric field distribution in the cavities in polycarbonate at a voltage of $\sqrt{2} \cdot 7.0$kV (the reason for the choosing the peak value of the AC voltage is explained in Appendix H). The cavity diameters are indicated in the top right corner of the respective figures. The presented electric field is limited to a minimum 3.5 kV/mm and a maximum of 7.5 kV/mm to increase the color range in areas of interest.

An important initial observation resulting from the simulations is the fact that the electric field in the cavities is not homogeneous. The electric field is higher in the center of the cavity and lower at the edges except in the corners of the cavity where there is a strong field enhancement (see Figure 4.2). The surface plots also indicate that that field is generally higher

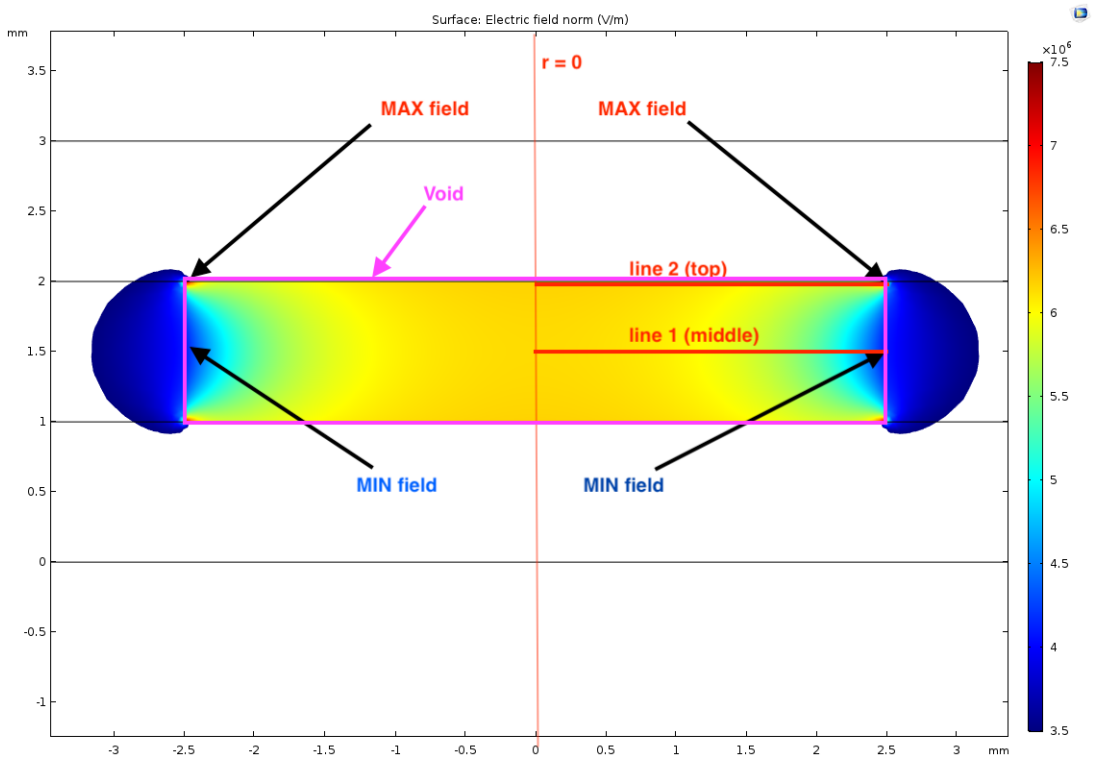

Figure 4.2: Detailed picture of the electric field in the 5 mm cavity. The locations of the maximum field and the minimum field are indicated. These locations are the same for all the cavity diameters. Line 1 (middle) and line 2 (top) represent the line segments along which the electrical field is shown in Figure 4.3 and Figure 4.7. The void boundary is indicated in pink.

the larger the diameter of the cavity.

Figure 4.3 shows the norm of the electric field along two straight line segments in the voids, "line 1 (middle)" and "line 2 (top)" as indicated in Figure 4.2.

This graph confirms what the surface plots indicated: At the top of the cavity (dashed lines), the field increases sharply towards the perimeter of the cavity, while the field in the middle of the cavity (solid lines) decreases towards the perimeter.

Maximum, Average and Minimum Field in the Cavities

Figure 4.4 shows the maximum, average and minimum electric field strength in the cavities as a function of cavity diameter. The figure clearly shows that the field enhancement in a disk-shaped cavity increases with increasing cavity diameter. More accurately, the maximum field increases by 13 % when increasing the diameter from 1 mm to 3 mm, whereas the trend flattens out when the cavity diameter is larger than 3 mm. The field increases only by 3 % when increasing the void diameter from 3 mm to 20 mm. This indicates that there is a significant difference in the field enhancement in cavities where $r \approx h$ compared to cavities where $r \gg h$.

According to Equation 2.1, the theoretical electric field enhancement in a disk-shaped cavity does not depend on the diameter of the cavity and is constantly equal to the relative permittivity of the material. However, this equation is based on the assumption of a homo-

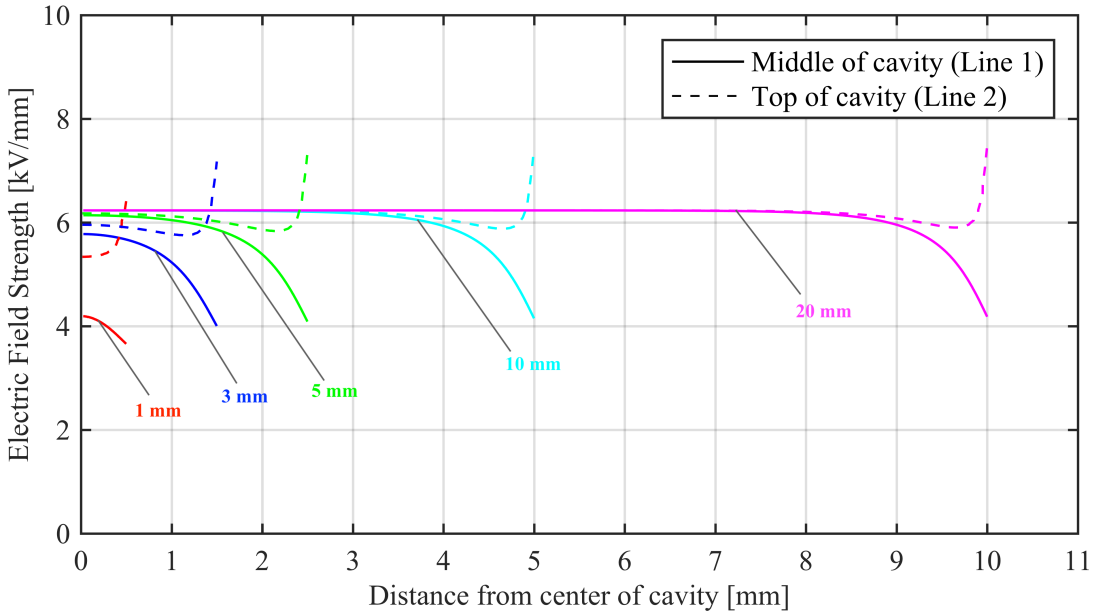

Figure 4.3: The electric field distribution in the cavities. For each cavity, the electric field is plotted along two line segments in the cavity. Solid lines represent the electric field along a line segment starting in the center of the cavity and ending the edge of the cavity ("line 1 (middle)" in Figure 4.2). Dashed lines represent the electric field along a line segment starting at top of the cavity and ending in the top corner of the cavity ("line 2 (top)" in Figure 4.2)

geneous electric field in the cavity and no fringe effects. Since neither of these assumptions hold, it is not surprising that the theoretical field enhancement in the cavities is not representative for the actual electric field.

The average field enhancement f of the 1 mm cavity is 1.9 and 2.7 for the 20 mm cavity. This shows that the field enhancement of the larger cavities is closer to the theoretical field enhancement of $\epsilon_r = 3.4$, whereas the field enhancement in the 1 mm cavity is lower and actually more similar to the theoretical field enhancement of a spherical cavity (Equation 2.2).

4.2.2 Choice of Electrode Configuration and the Effects on the Electric Field

Figure 4.5 shows the electric field distribution in the two different test setups for the same test sample. The electric field distribution in the void is found to be unaffected by the difference in electrode configuration: The average and the minimum field are identical whereas the max field only differs by 1.2 %. Therefore, the two setups are considered equal in the terms of resulting field distribution in the cavities. However, the electric field around the edges of the electrode is higher for the configuration in Figure 4.5a and therefore the risk of surface discharges is higher with this setup.

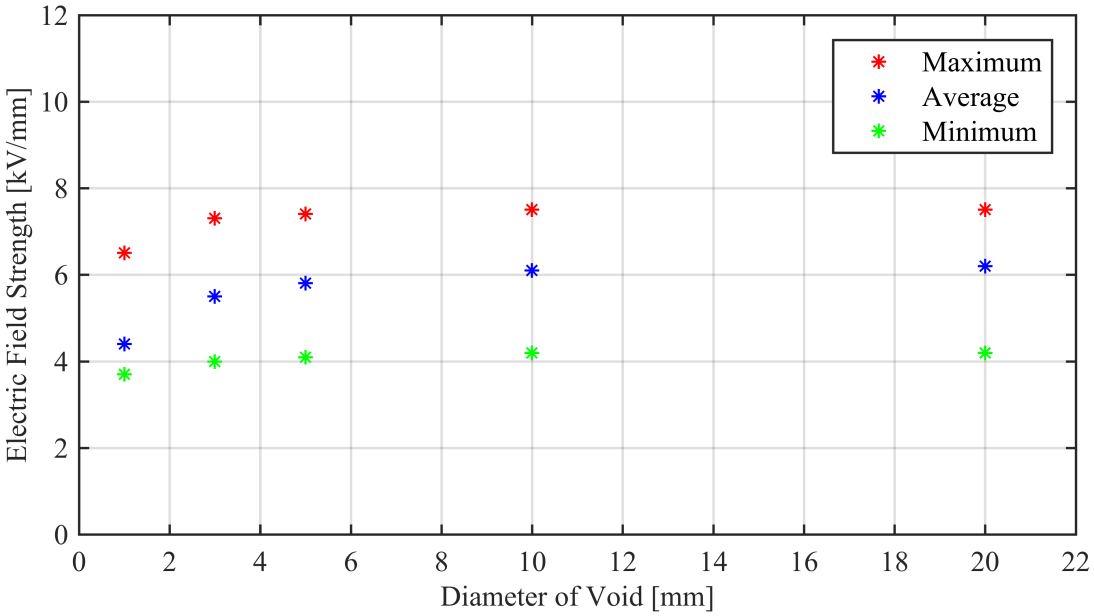

Figure 4.4: The maximum, average and minimum field strength in cavities with insulating surfaces plotted for the different cavity diameters.

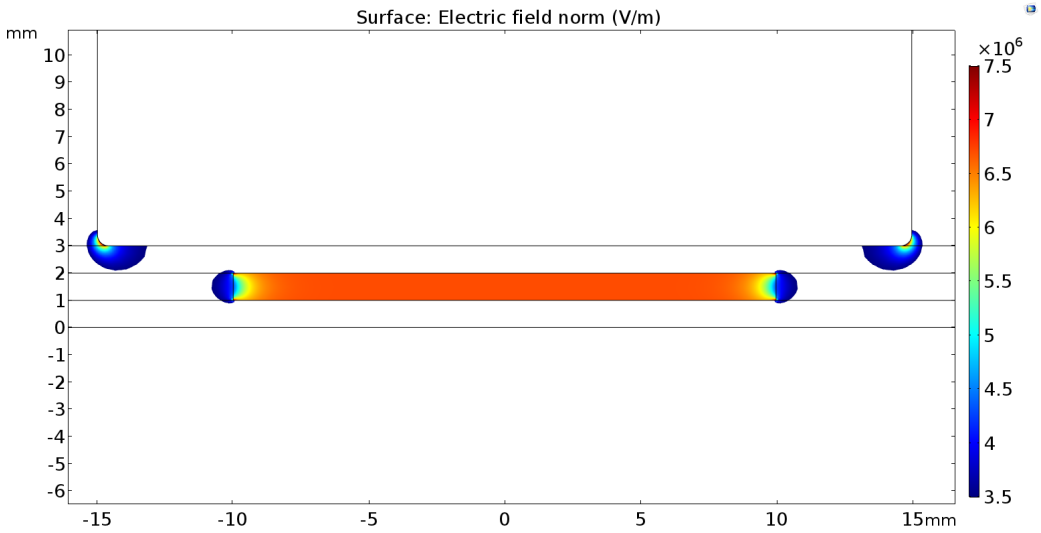

(a) Electrode arrangement 1

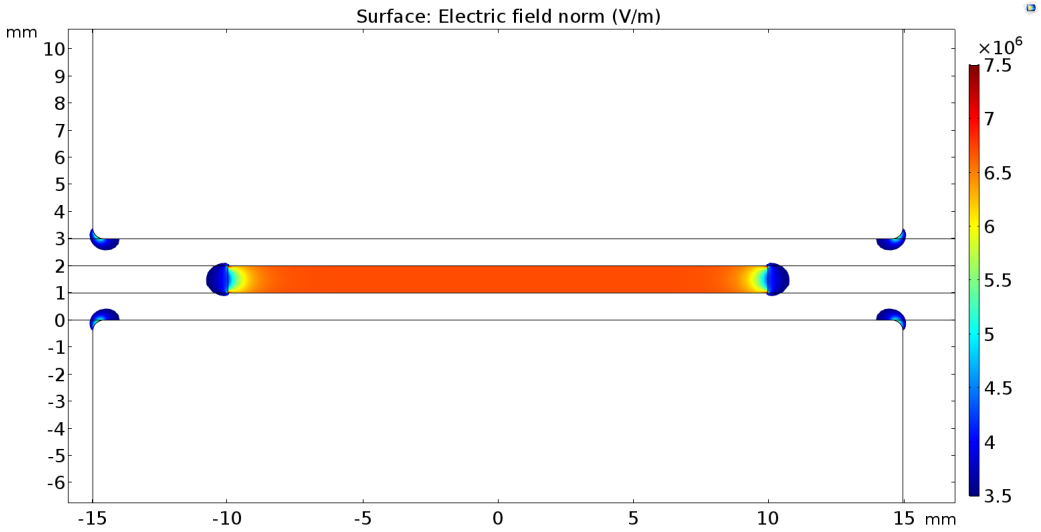

(b) Electrode arrangement 2

Figure 4.5: The electric field distribution in the test setup for the two different electrode arrangements. Note that the field distribution in the cavity is not affected by the change of electrodes.

4.2.3 Conducting Cavity Surfaces and the Effects on the Electric Field

Next, the effect of applying aluminum to the surfaces of the cavity will be presented. Assuming that the applied layer of aluminum behaves like an ideal conducting surface with an infinite conductivity, one can simulate the applied aluminum as a floating potential in COMSOL.

Figure 4.6 shows the simulations of the electric field strength when including two floating potentials (aluminum on both surfaces of the cavity) and Figure 4.7 shows the electric field strength in the cavities along the two line segments "line 1 (middle)" and "Line 2 (top)". Figure 4.8 shows the maximum, average and minimum electric field strength of the voids as a function of void diameter.

If comparing Figure 4.6 with Figure 4.1, it is evident that the homogeneity of the electric field in the voids is higher when the surfaces are conducting. The results also show that the maximum field enhancement in the voids is about 1.3 to 2.4 times higher than in the case of insulating surfaces (Figure 4.4). However, the average field and the minimum field are less affected by the introduction of conducting voids: the average field in the voids with conducting surfaces is between 5-10 % lower, and the minimum field is 1-15 % higher, than the field in the voids with insulating surfaces.

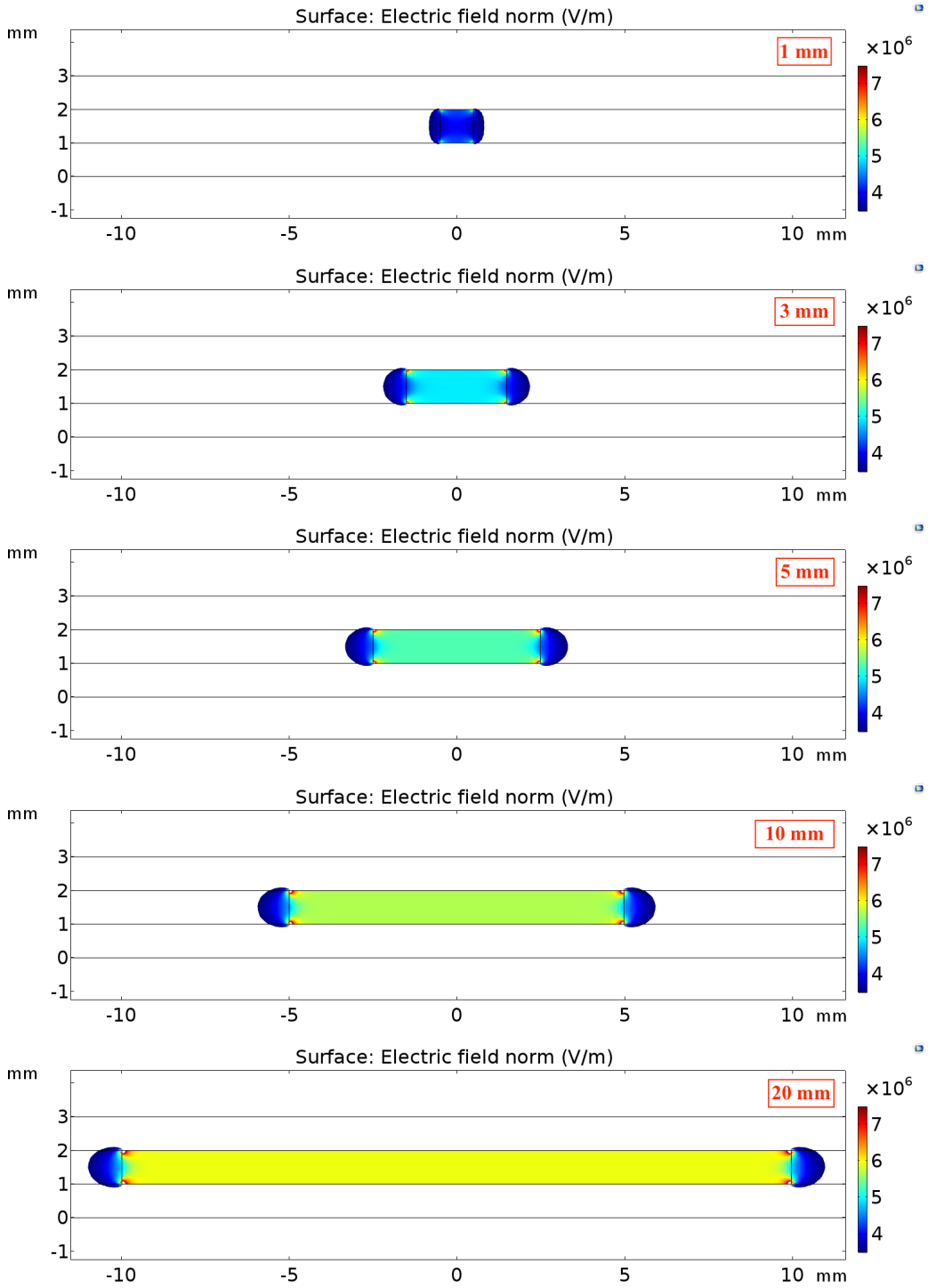

Figure 4.6: The electric field distribution in the test setup when the cavity surfaces are covered in aluminum. Applied voltage: $\sqrt{2} \cdot 7.0$kV. The presented electric field is limited to a minimum 3.5 kV/mm and a maximum of 7.5 kV/mm to increase the color range in areas of interest.

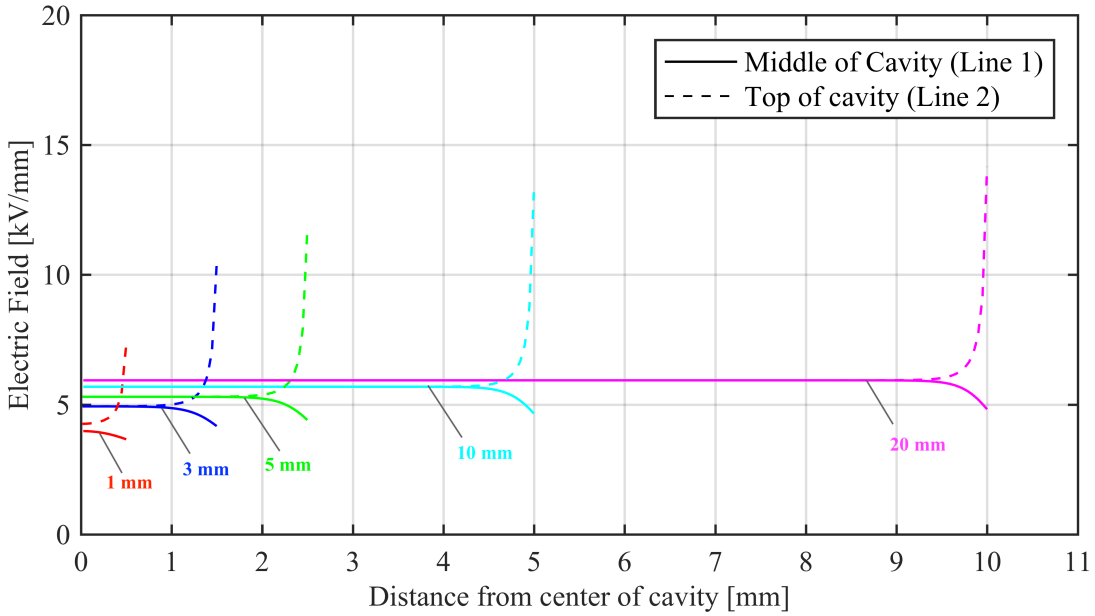

Figure 4.7: The electric field distribution in the cavities with conducting surfaces. Solid lines represent the electric field along "line 1 (middle)" (see Figure 4.2). Dashed lines represent the electric field along "line 2 (top)" (see Figure 4.2)

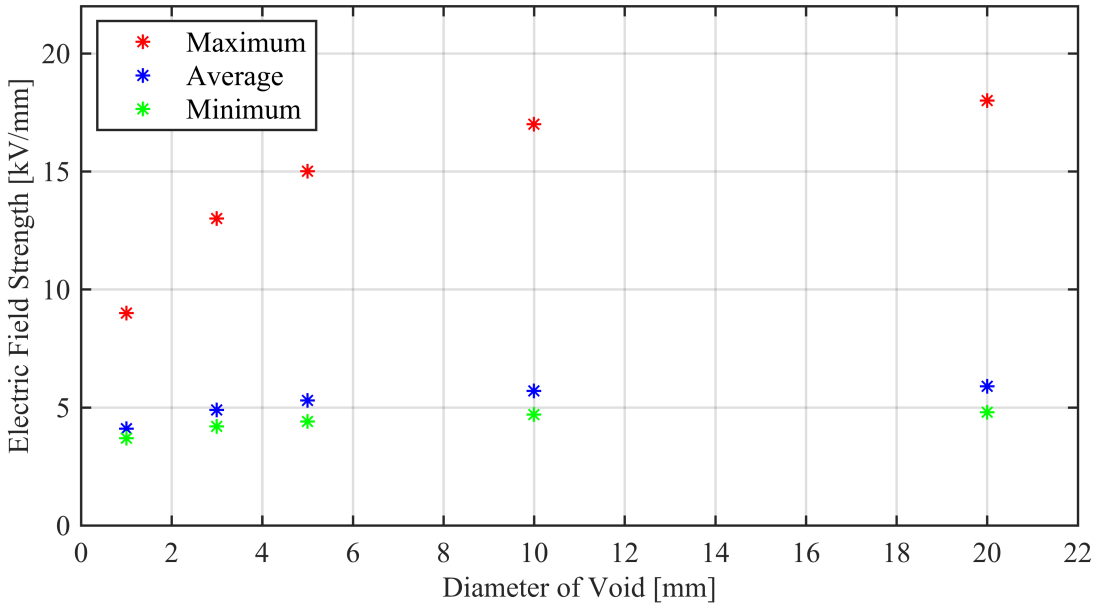

Figure 4.8: The maximum, average and minimum electric field strength in the cavities with conducting cavity surfaces plotted for the different cavity diameters.

4.3 PD Measurements

In this section, the experimental results from PD measurements will be presented. The results from the theoretical model as presented in section 4.1 are also shown together with the experimental results to build a basis for a comparison and evaluation of the results with respect to the theoretical model. The reader is referred back to section 3.4 for a detailed

explanation of how the results that will be presented in this section are obtained and processed.

First, the PRPD plots for the different sample types are presented. Then, the inception voltages and the extinction voltages are presented. Lastly, the information from the PRPD plots is extracted and analyzed in terms of the maximum discharge magnitude and the discharge frequency.

The theoretical analysis of the discharge activity in the voids as well as the simulations are performed on void diameters: 1 mm, 3 mm, 5 mm, 10 mm and 20 mm. The experimental results, however, are shown for void diameters: 3 mm, 5 mm, 10 mm and 20 mm, not the 1 mm cavity. The reason for this is that the 1 mm void proved to have an inception voltage that is higher than the maximum test voltage (9.6 kV), and therefore, there are no discharges to analyze in this void at the test voltage of 7.0 kV.

4.3.1 PRPDA

Figure 4.9 shows the PRPD patterns of the partial discharges from the voids in the polycarbonate samples (with and without aluminum), whereas Figure 4.10 shows the PRPD patterns of the partial discharges from the different voids in samicatherm and mica mat. The applied voltage is 7.0 kV. The inception voltage of the 5 mm samicatherm sample was higher than 7.0 kV and the PRPD pattern is therefore empty.

The PRPD patterns clearly show that the recorded discharges are internal discharges in that the PDs are more or less symmetrical and appear on the increasing part of the voltage on the first half-cycle and on the decreasing part of the voltage on the second half-cycle.

There are some clear differences in the PD pattern between the samples with and without aluminum that become evident by directly examining the PRPD patterns. Most importantly, the discharge magnitude is generally larger in the case of the aluminum covered samples, and the discharge magnitude is generally increasing with increasing diameter for both sample types.

Figure 4.10 indicates that number of discharges is higher for mica mat than for samicatherm based on the color intensity. Interestingly, the discharge magnitude of the PDs from voids in mica mat does not seem to increase with increasing diameter. For PDs from voids in samicatherm, the discharge magnitude is clearly increasing (disregarding the 5 mm cavity).

4.3.2 Inception Voltage and Extinction Voltage

The inception voltage and the extinction voltage of the polycarbonate samples with and without aluminum-covered cavity surfaces are shown in Figure 4.11.

One trend becomes clear from these graphs; the PDIV and PDEV are generally decreasing the larger the diameter of the cavity. The PDIV of the 3 mm cavity is 33 % higher than the PDIV of the 20 mm cavity for the polycarbonate samples. When it comes to the samples with

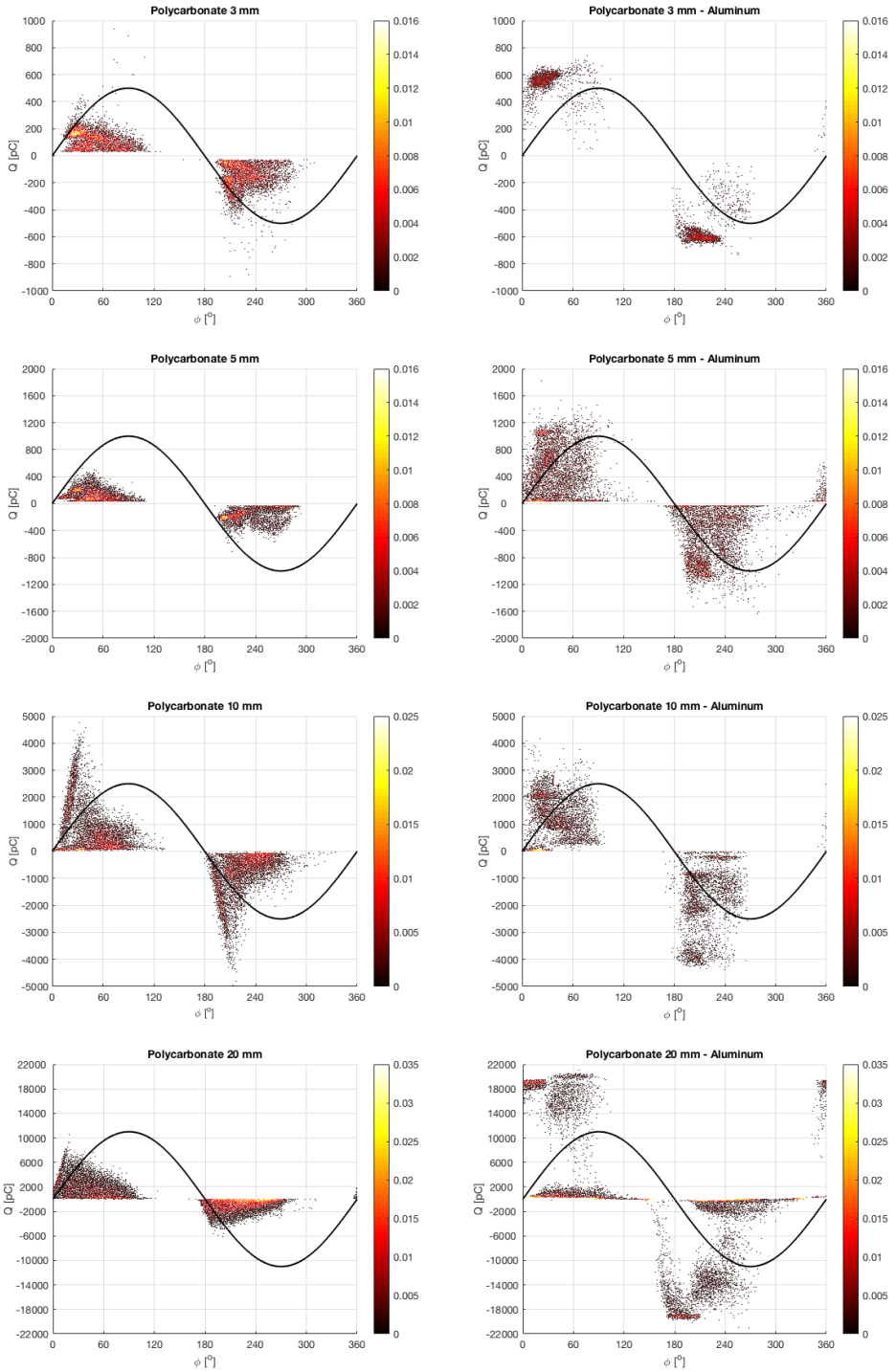

Figure 4.9: The PRPD patterns for polycarbonate (left column) and polycarbonate with aluminum (right column). The cavity diameters are increasing vertically and shown in order: 3, 5, 10, 20 mm. The patterns are acquired during 30 seconds of recordings at 7.0 kV, 50 Hz. The color bar to the right of the PRPD plots shows the intensity of the discharges in number of discharges per period of the applied voltage. The axes are linear. Note that the scale of the y-axis is different for the different cavity diameters.

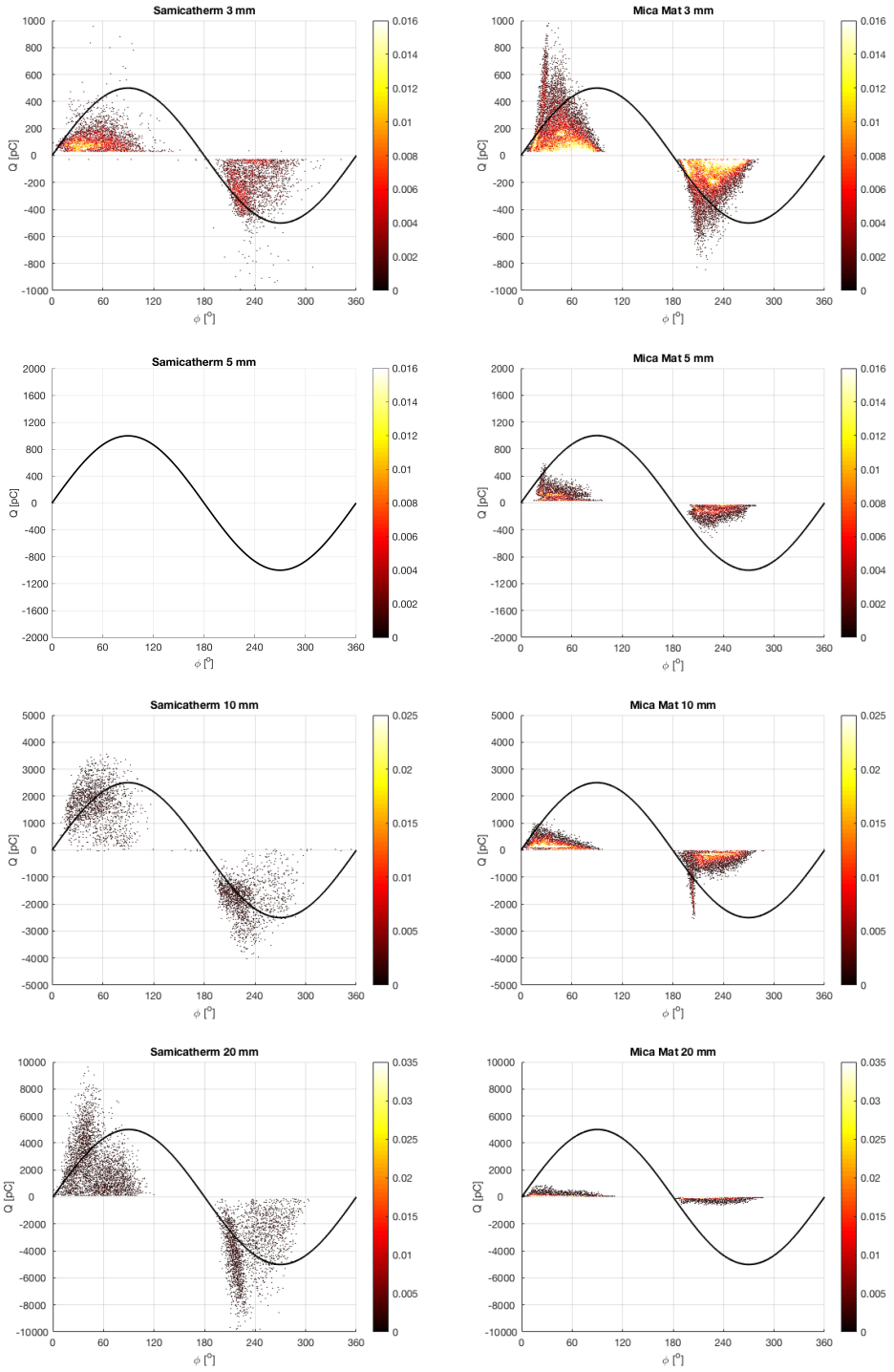

Figure 4.10: The PRPD patterns for samicatherm (left column) and mica mat (right column). The cavity diameters of 3, 5, 10 and 20 mm are increasing vertically. The patterns are acquired during 30 seconds of recordings at 7.0 kV, 50 Hz. The color bar to the right of the PRPD plots shows the intensity of the discharges in number of discharges per period of the applied voltage. The axes are linear. Note that the scale of the y-axis is different for the different cavity diameters. The samicatherm sample with a 5 mm void, had an inception voltage that was higher than 7.0 kV and consequently, the PRPD pattern at 7.0 kV is empty.

aluminum-covered cavity surfaces, the 3 mm cavity has an 18 % higher PDIV than the 20 mm cavity.

The polycarbonate sample with conducting surfaces is closest to the theoretical model of an insulation system with an embedded void. Therefore, it is expected that the theoretical model should match the experimental results for this sample type. And for the two largest voids, the 10 and 20 mm voids, the theoretical model is successful in predicting the inception voltage. The measured PDIV is 5.5 kV, but as explained in section 3.4, this means that the PDIV is somewhere between 5.0 kV and 5.5 kV. This matches the theoretical value of 5.2 kV. However, the theoretical model is not successful in reflecting how the inception voltage increases with decreasing void diameter.

The inception voltage and the extinction voltage of the samicatherm and mica mat samples are shown in Figure 4.12.

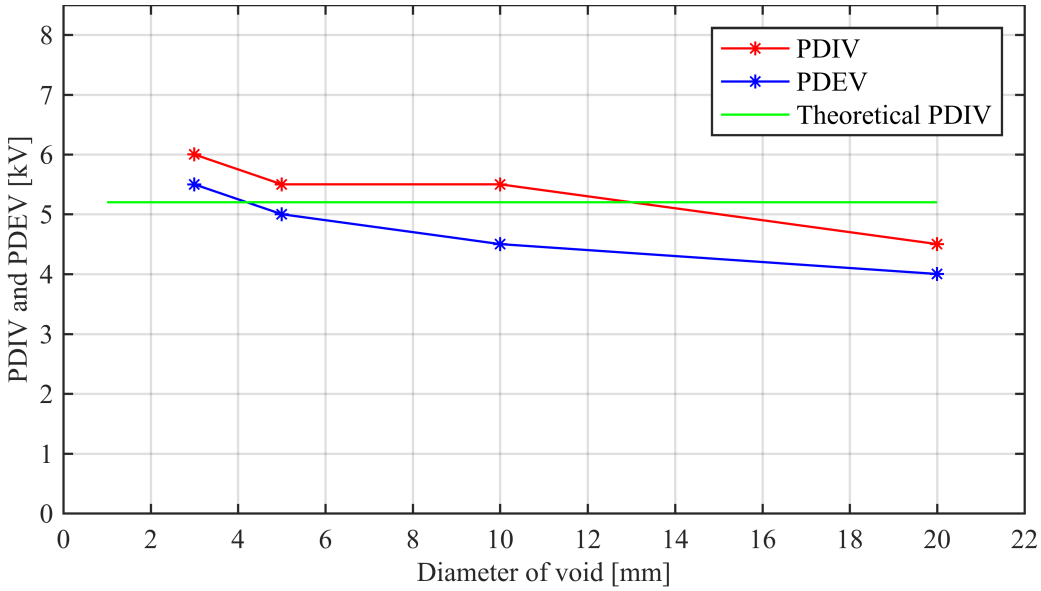

(a) Polycarbonate with insulating cavity surfaces

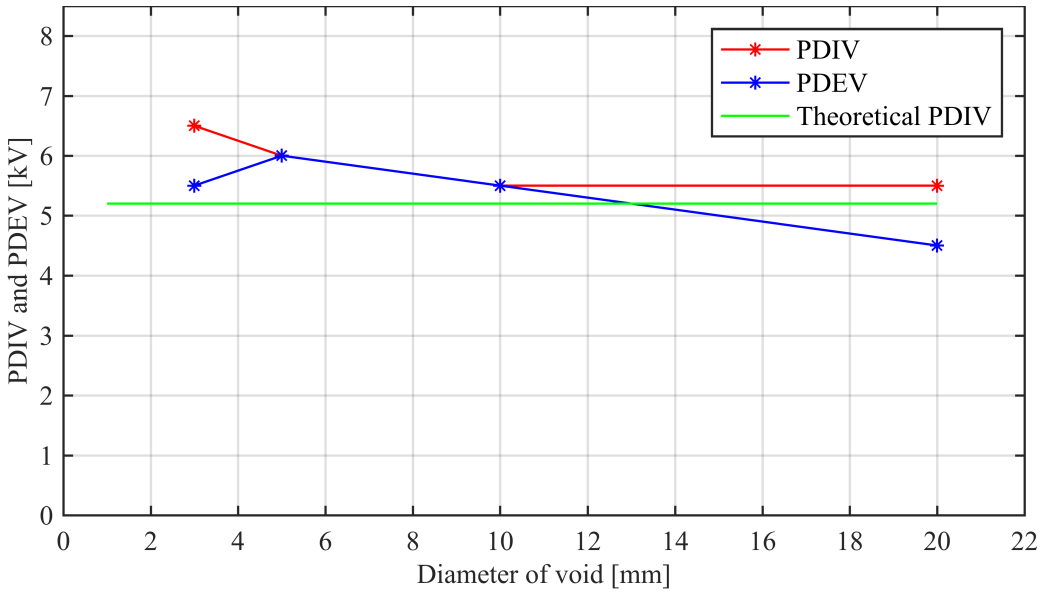

(b) Polycarbonate with conducting cavity surfaces

Figure 4.11: The inception voltage and the extinction voltage of the polycarbonate samples as a function of cavity diameter. The theoretical value is shown in the green graph which is constant at 5.2 kV.

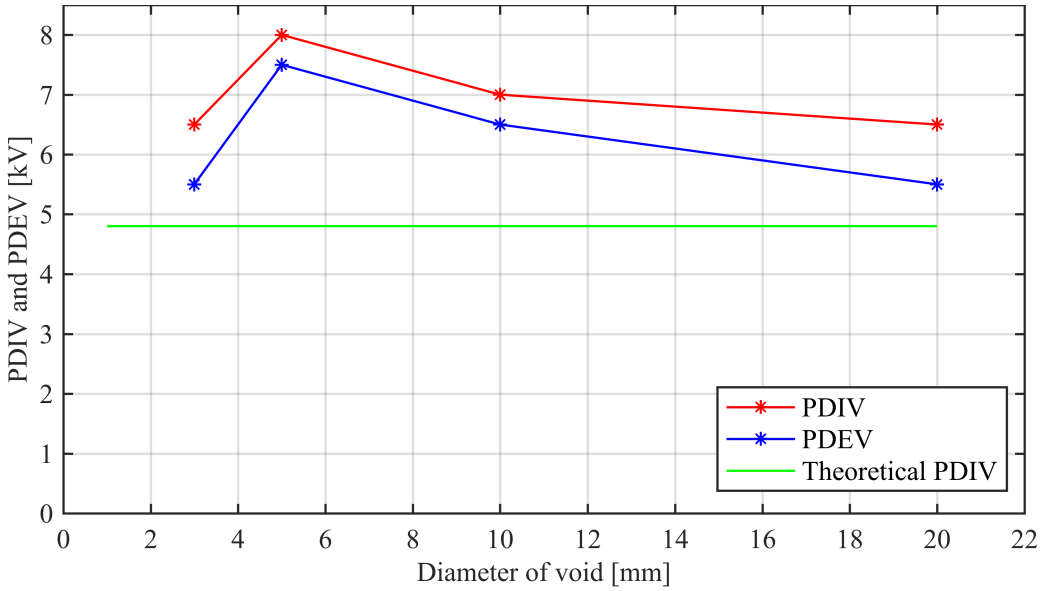

(a) Samicatherm

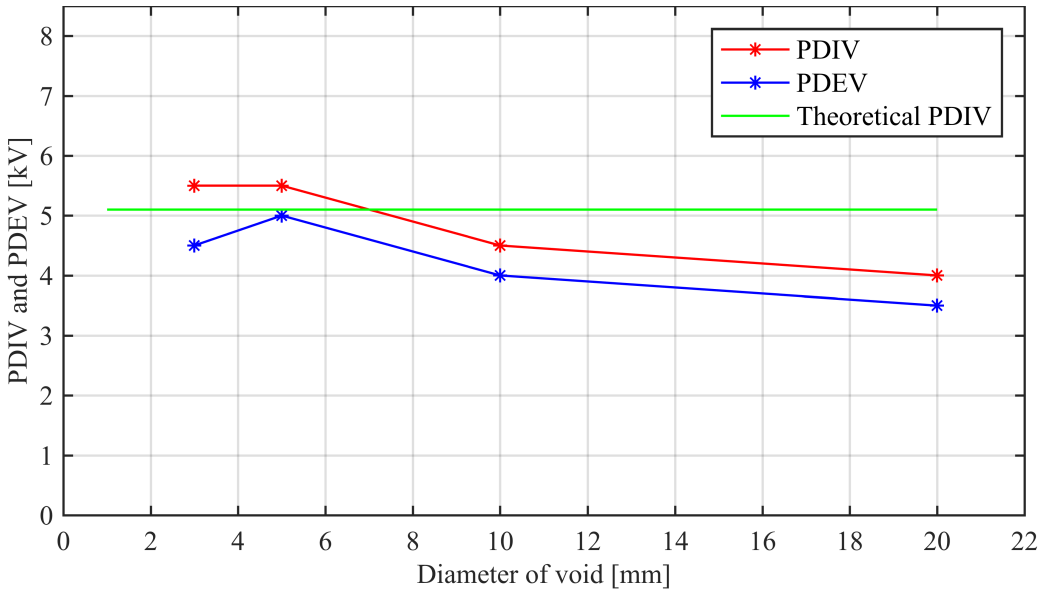

(b) Mica mat

Figure 4.12: The inception voltage and the extinction voltage of the samicatherm and the mica mat samples as a function of cavity diameter. The theoretical value is shown in the green graph which is constant at 4.8 kV for samicatherm and 5.1 kV for mica mat.

The graphs show that the PDIV of the aged mica mat samples is lower than the PDIV of the samicatherm samples even though theoretically, the PDIV for voids in mica mat is slightly higher than for voids in samicatherm.

The decreasing trend of PDIV as observed for the polycarbonate samples, is also prominent for the mica mat samples. The 3 mm and 5 mm cavities have an inception voltage of 5.5 kV which is consistent with the theoretical value. Then, the 10 mm cavity has an inception voltage of 4.5 kV (18 % lower than the 3 mm and 5 mm cavities and 12 % lower than the theoretical value) and the 20 mm cavity has an even lower inception voltage of 4.0 kV (27 % lower than the 3 and 5 mm cavities and 22 % lower than the theoretical value).

The same trend is not seen with the samicatherm samples. The 3 mm cavity and the 20 mm cavity have the same PDIV of 6.5 kV and a PDEV of 5.5 kV, while the 5 mm cavity and the 10 mm cavity have a higher PDIV and PDEV. The PDIV of the 5 mm void is not only higher than the PDIV of the 3 mm sample, it is also higher than the test voltage[1].

4.3.3 Discharge Magnitude

The maximum discharge magnitude (the apparent charge) of the discharges in polycarbonate-embedded voids is shown in Figure 4.13.

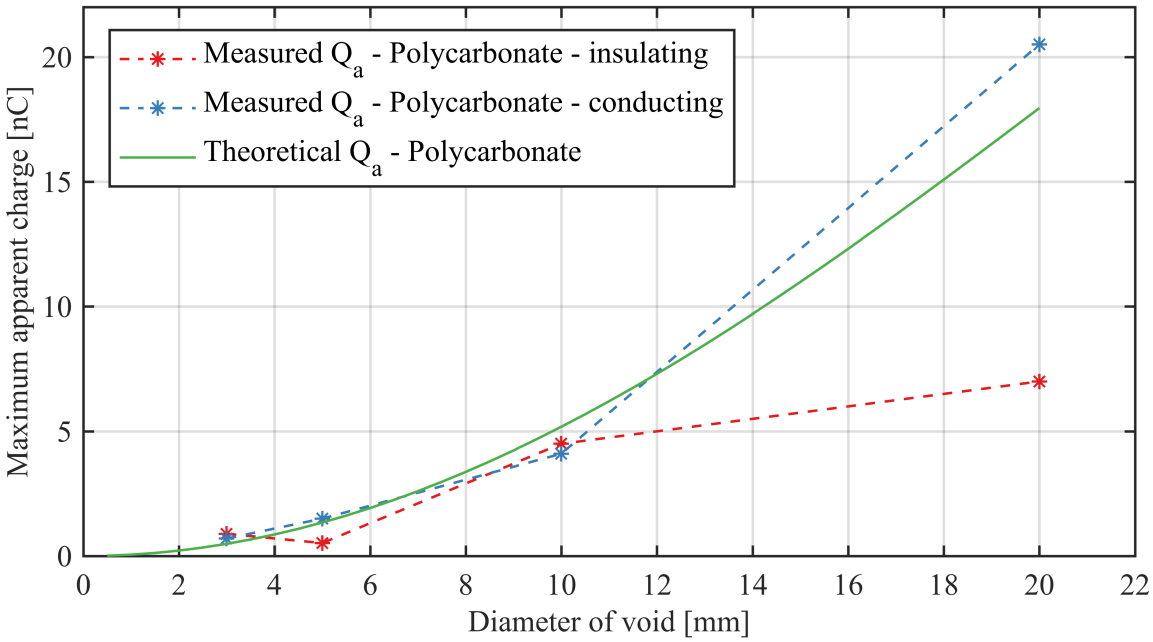

Figure 4.13: The discharge magnitude (the apparent charge) as a function of cavity diameter for polycarbonate. The theoretical graph is shown in solid green. The red dashed line shows the samples with insulating cavity surfaces, whereas the blue dashed line shows the results from the samples with conducting cavity surfaces. Applied voltage: 7.0 kV.

In the case of samples with insulating void surfaces, the experimental values correspond well with theoretical values for the 3 and 10 mm cavity. However, the discharge magnitude for the 20 mm cavity is less than 40 % of the theoretical discharge magnitude in a 20 mm cavity. The discharges in the 5 mm cavity is only 0.52 nC - 42 % lower than the 3 mm void and 60 % lower than the theoretical value.

In the case of the cavities with conducting surfaces, the experimental results correspond consistently very well with the theoretical graph. The 3 mm cavity and the 5 mm cavity match the theoretical graph perfectly. The 10 mm cavity has a 20 % lower apparent charge than the theoretical value, while the 20 mm cavity cause discharges that are on average 14 % larger

[1]Since the PDIV of the 5 mm void in samicatherm is higher than the test voltage, the PDIV was tested a second time by increasing the voltage above 7.0 kV. This measurement was not performed according to the test program in Figure 3.11 due to time restrictions, and therefore, the exact value of the PDIV for this sample is not directly comparable with the other samples.

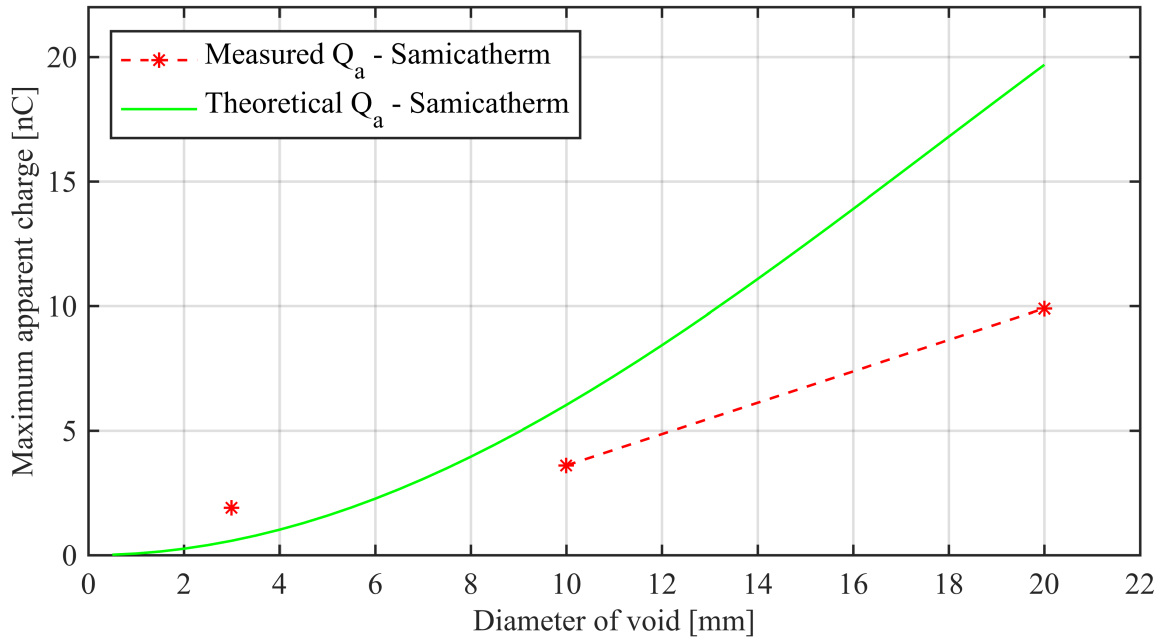

Figure 4.14: The discharge magnitude (the apparent charge) as a function of cavity diameter for samicatherm. The theoretical graph is shown in solid green. The dashed red line shows the measured apparent charge. Applied voltage: 7.0 kV. There is no data point for the 5 mm void since the PDIV of this void was higher than the test voltage of 7.0 kV.

than the theoretical apparent charge, but overall the measured apparent charge is consistent with the theoretical model.

Figure 4.14 and Figure 4.15 show the PD magnitude of discharges in samicatherm and mica mat.

One important observation which confirms what the PRPD patterns indicated, is the fact that the magnitude of the discharges is not increasing with increasing diameter in the case of the mica mat samples. The PD magnitude of the 3 mm void in mica mat is approximately equal to the theoretical discharge magnitude from a 3 mm void, but when increasing the diameter further, the magnitude of the discharges stays rather constant. In fact, the PDs from the 20 mm void are about 22 % smaller than the PDs from the 3 mm cavity even though the surface area of the 20 mm void is 44 times larger than the surface area of the 3 mm cavity. This shows that the measured PD magnitude in voids embedded in mica mat is not following the theoretical model.

In the case of the samicatherm samples, the magnitude is increasing with increasing diameter. The trend is somewhat similar to the trend observed for polycarbonate with insulating surfaces. Still, the discharge magnitude is generally lower than the theoretical value, except from the 3 mm cavity for which the magnitude is more than 3 times larger than the theoretical value. The 10 mm cavity has a discharge magnitude that is 42 % smaller than the theoretical value and which corresponds to a theoretical void diameter of 7.5 mm. The same trend is observed for the 20 mm cavity: the discharge magnitude is only half of the theoretical value which translates to a theoretical cavity diameter of about 13 mm.

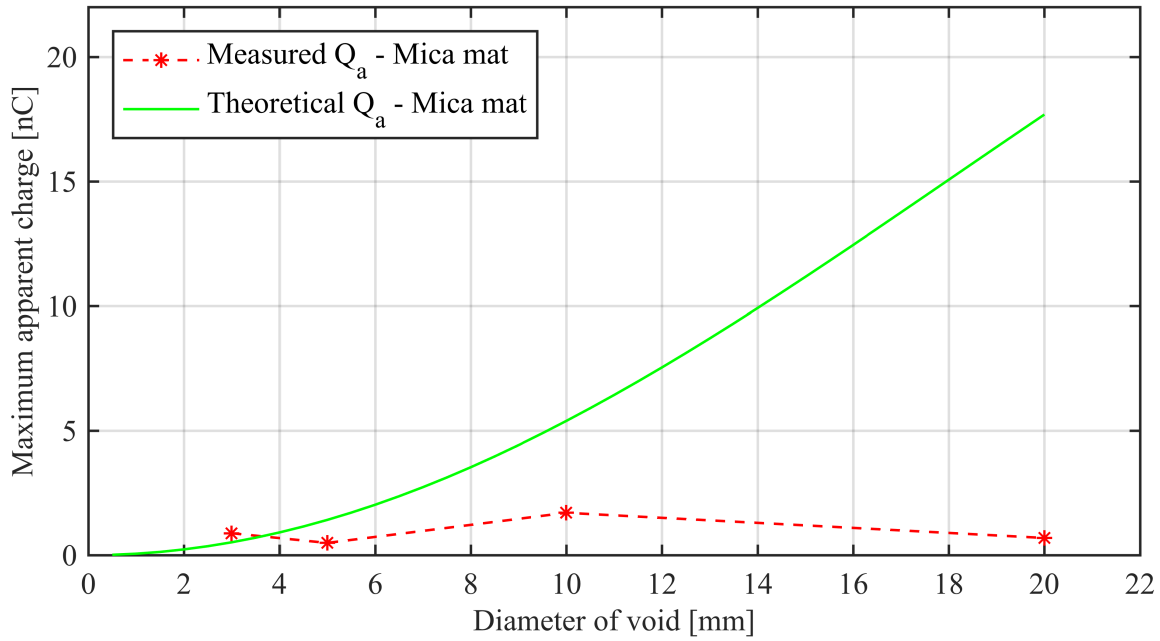

Figure 4.15: The discharge magnitude (the apparent charge) as a function of cavity diameter for mica mat. The theoretical graph is shown in solid green. The dashed red line shows the measured apparent charge. Applied voltage: 7.0 kV.

4.3.4 Discharge Frequency

The number of discharges, or the discharge frequency (in PD pulses/half-cycle), is shown for all sample types in Figure 4.16.

For the polycarbonate samples, it is observed that the discharge frequency is consistently higher for the samples with insulating cavity surfaces than the samples with conducting cavity surfaces. The discharge frequency of the voids with conducting surfaces generally agrees with the theoretical value. The exception is the 20 mm void which has a five times higher discharge frequency than the theoretical value.

The discharge frequency of the discharges from voids in samicatherm samples generally correspond well with the theoretical value. The discharge frequency ranges from 1.1 discharge per half cycle for the 10 mm void to 3.3 discharges for the 3 mm void and is not increasing with increasing diameter.

A very different trend is observed for the mica mat samples. First, there are more discharges in these samples than in any of the other sample types. Interestingly, the 3 mm void has a higher discharge frequency than both the 5 mm void and the 10 mm void. However, the 20 mm cavity has the highest discharge frequency of all the samples with 30 discharges per half-cycle.

Combining these results with the discharge magnitude, it is seen that discharges in cavities in the mica mat samples are high in numbers, but small in magnitude, whereas the discharges in the samicatherm samples are fewer but larger in magnitude.

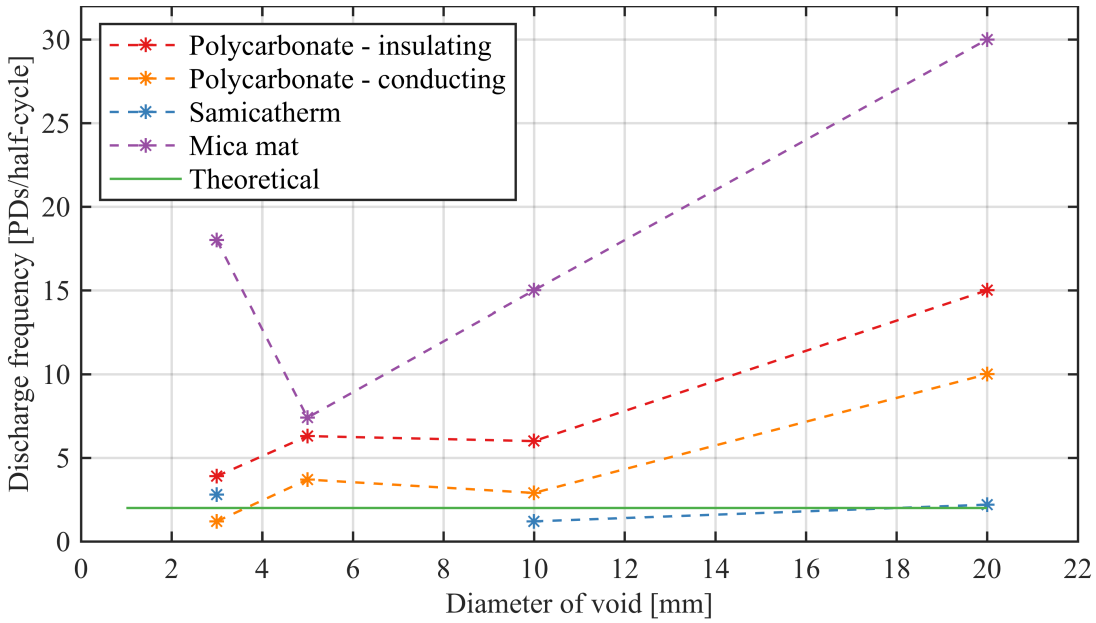

Figure 4.16: The discharge frequency as a function of void diameter for all sample types. The theoretical value, which is equal regardless of sample type, is shown in solid green. Applied voltage: 7.0 kV.

5 Discussion

5.1 Evaluation of Experimental Results with Respect to Theoretical Models

5.1.1 Inception Voltage and Extinction Voltage

According to Paschen's law, which assumes a homogeneous field and no fringe effects, the inception voltage is independent of the void diameter. However, the numerical simulations of the electric field in the voids clearly demonstrated that the field is not homogeneous and that there are significant fringe effects (see Figure 4.1 and 4.6 for the simulated electric field strength in the voids). Therefore, it was expected that the experimental results would not match the PDIV the theoretical model predicts.

The results showed that the measured PDIV was, in fact, dependent on the void diameter. More specifically, the PDIV decreased with increasing void diameter for all sample types except from samicatherm (see Figure 4.11 and 4.12). The decreasing trend in inception voltage with increasing void diameter agrees with observations made by Forssén and Edin [36].

The results can be explained by the differences in the enhancement of the electric field in the respective voids as revealed by the simulations of the electric field strength in the voids. The simulations show that the field enhancement is increasing with increasing cavity diameter, and a high electric field enhancement at a given applied voltage results in a low PDIV.

To further investigate the effect the field enhancement in the individual voids has on the theoretical inception voltage, the field enhancement has been incorporated into the theoretical model as follows:
Based on the calculations of the average field in the cavities (Figure 4.4, 4.8, J.1 and J.2), a normalized field enhancement factor has been calculated for the voids (see appendix K). Then this factor has been multiplied with the theoretical inception voltage, giving a modified theoretical model, in which the actual field enhancement of the voids has been incorporated.

In Figure 5.1, the measured inception voltage for polycarbonate with conducting surfaces is shown together with the PDIV from the original theoretical as well as the modified model. The graphs show that the modified model is consistent with the measured inception voltage for all four voids. These results demonstrate that it is necessary to incorporate the field enhancement of the individual voids when predicting the inception voltage of disk-shaped

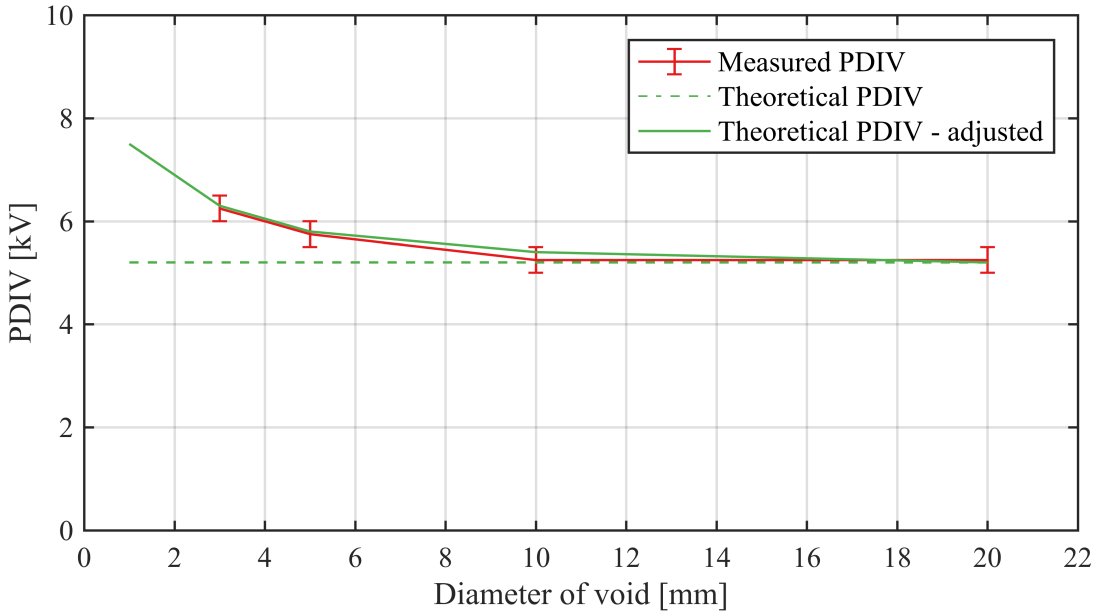

Figure 5.1: Inception voltage of the polycarbonate samples (with conducting void surfaces) as a function of void diameter. The measured values are indicated in the red graph with error bars (0.5 kV uncertainty as explained in 3.4.2). The green dashed graph shows the theoretical PDIV according to Paschen's law, whereas the theoretical PDIV after adjusting for the actual field enhancement in the voids is shown in solid green.

voids with varying diameters.

The polycarbonate samples with conducting surfaces are the samples that most closely resemble the insulation system as modeled by the abc model. Therefore, it is expected that the PD parameters for this sample type follow the theoretical model better than the samples without conducting surfaces. This will be proved to be the case.

As already seen, the measured inception voltage of the polycarbonate samples with conducting void surfaces matches the theoretical model perfectly when adjusting for the actual field enhancement. When it comes to the polycarbonate samples with *insulating* void surfaces, it is observed that the modified theoretical model fits better with the measured PDIV than the original theoretical model (Figure 5.2).

After including the field enhancement, it is now only the smallest (1 mm) and the largest (20 mm) void that do not match the theoretical value. The 1 mm void still has a PDIV that is at least 2.4 kV higher than the theoretical value, whereas the PDIV of the 20 mm void is about 1 kV lower than the theoretical value. This might be explained by differences in electron availability in the two voids. In voids bounded by an insulating material, volume generation of electrons play an important role [21]. A larger void volume yields a higher probability of a start electron occurring since the production rate of electrons is proportional to the effective volume of the gas in the void [21]. Therefore, the low PDIV of the 20 mm cavity can be due to very short PD inception delay because of a high availability of start electrons. And likewise, the high PDIV of the 1 mm cavity might be due to a lack of start electrons and consequently

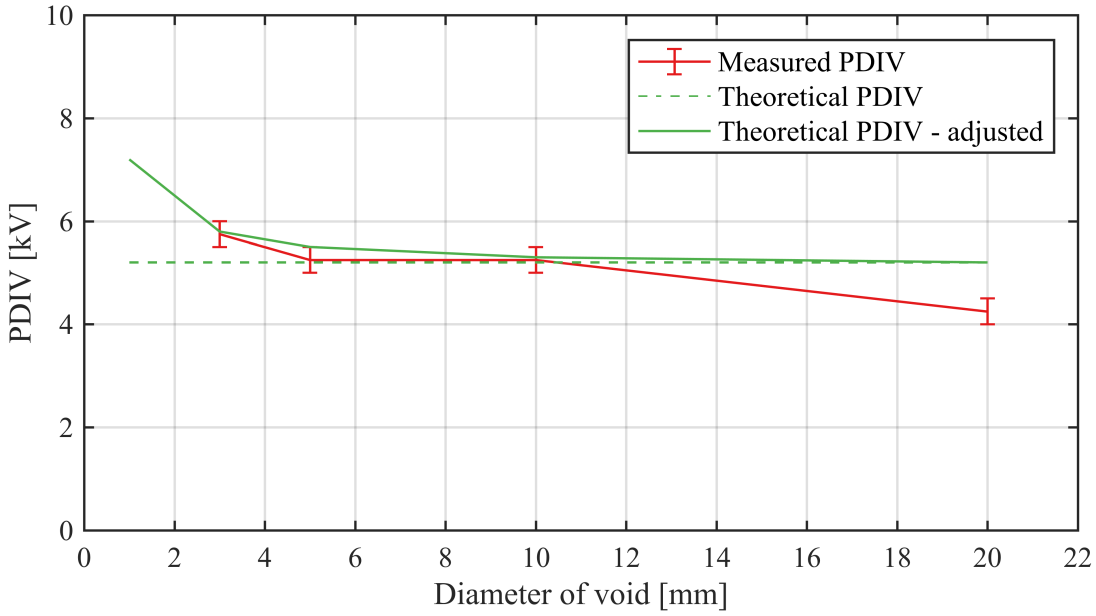

Figure 5.2: Inception voltage of the polycarbonate samples (with insulating void surfaces) as a function of void diameter. The measured values are indicated in the red graph with error bars (0.5 kV uncertainty as explained in 3.4.2). The green dashed graph shows the theoretical PDIV according to Paschen's law, whereas the theoretical PDIV after adjusting for the actual field enhancement in the voids is shown in solid green.

a long inception delay.

The PDIV of samicatherm samples was significantly higher than the inception voltage for the other samples (see Figure 5.3).

This is especially true for the larger cavities (10 mm and 20 mm) which have a PDIV that is respectively 27 % and 63 % higher than the corresponding polycarbonate samples. To investigate possible reasons for this, the thickness of the samicatherm sheets was measured again and they were actually found to be 1.2 mm instead of 1.0 mm. According to the analytical expression of Paschen's law (Equation 2.6), the breakdown voltage of a void with a height of 1.2 mm is 5.3 kV compared to 4.6 kV for a void with a height of 1.0 mm. The theoretical inception voltage is then 5.5 kV instead of 4.8 kV. This might help explain why the PDIV of the samicatherm samples is generally higher than the PDIV of the other samples.

However, when comparing the results with a modified model that takes into account both the increased thickness of the sheets and the field enhancement, the measured PDIV is still not consistent with the theoretical model.

A possible reason might be statistical variation. The stochastic nature of PD can play a large in contributing to the randomness of the inception voltage. and since only one sample was tested, it can be expected that some results deviate from the general trend.

The mica mat samples were the only samples used in this project that have been used as generator bar insulation. The material has been aged by partial discharge activity over the course of 35 years and the PDIV proved to be both lower than the theoretical PDIV and the

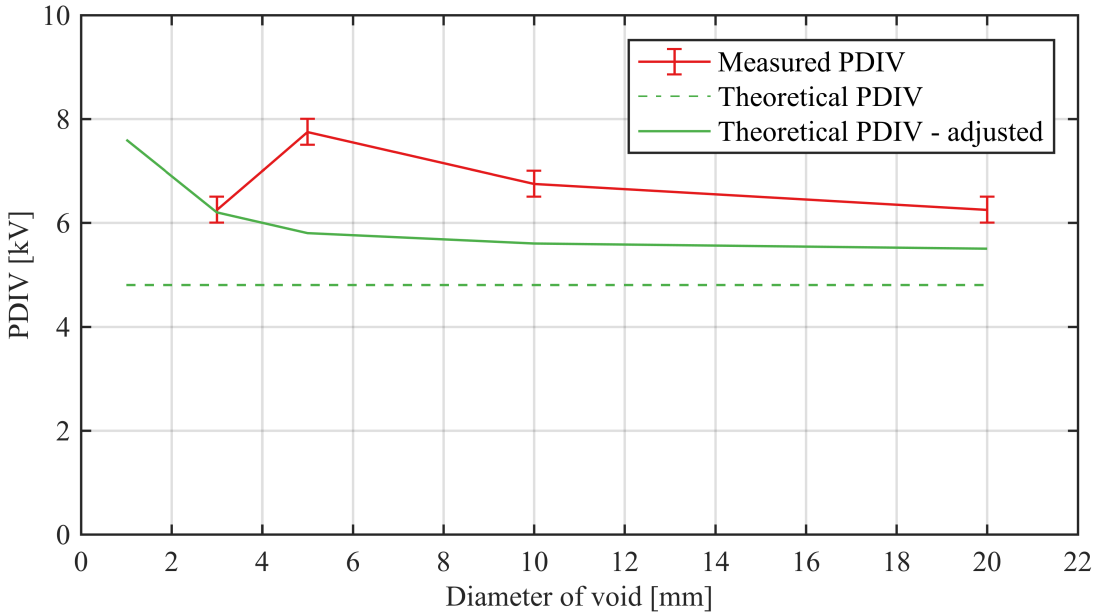

Figure 5.3: Inception voltage of samicatherm samples as a function of void diameter. The measured values are indicated in the red graph with error bars (0.5 kV uncertainty as explained in 3.4.2). The green dashed graph shows the theoretical PDIV according to Paschen's law, whereas the theoretical PDIV after adjusting for the actual field enhancement in the voids is shown in solid green.

PDIV of the other samples (see Figure 5.4).

This is thought to be a result of the aging the sample has been exposed to. Physical and chemical degradation of the material by erosion, bombardment of electrons, forming of pits and chemical dissociation of the material and creation of by-products generally results in more discharge sources in the material and also an overall lower dielectric strength. This can result in a reduced inception voltage compared to virgin materials.

In addition, the splitting of the insulation into three sheets and the making of the voids caused delaminations and tearing of the mica layers. Due to the brittle nature of the insulation, these samples also have rougher void surfaces, and especially rougher void edges. This can cause areas of higher electric field than the simulated field, which can explain why the inception voltage is lower than the theoretical value.

To summarize, the inception voltage is generally decreasing with increasing void size due to a lower field enhancement in larger voids. In addition, the theoretical model, when modified to account for the actual field enhancement in the individual voids, shows a perfect fit with the measured PDIV of the voids with conducting surfaces. The fit is also fairly good for the polycarbonate samples with insulating surfaces. However, the theory does not match the measured PDIV of the samicatherm samples or the mica mat samples. The stochastic nature of partial discharges (e.g. the availability of start electrons) and statistic variation, in addition to the actual physical condition of the sample (roughness, delaminations, general degradation, etc.) can explain these deviations between the measured and the theoretical inception voltage.

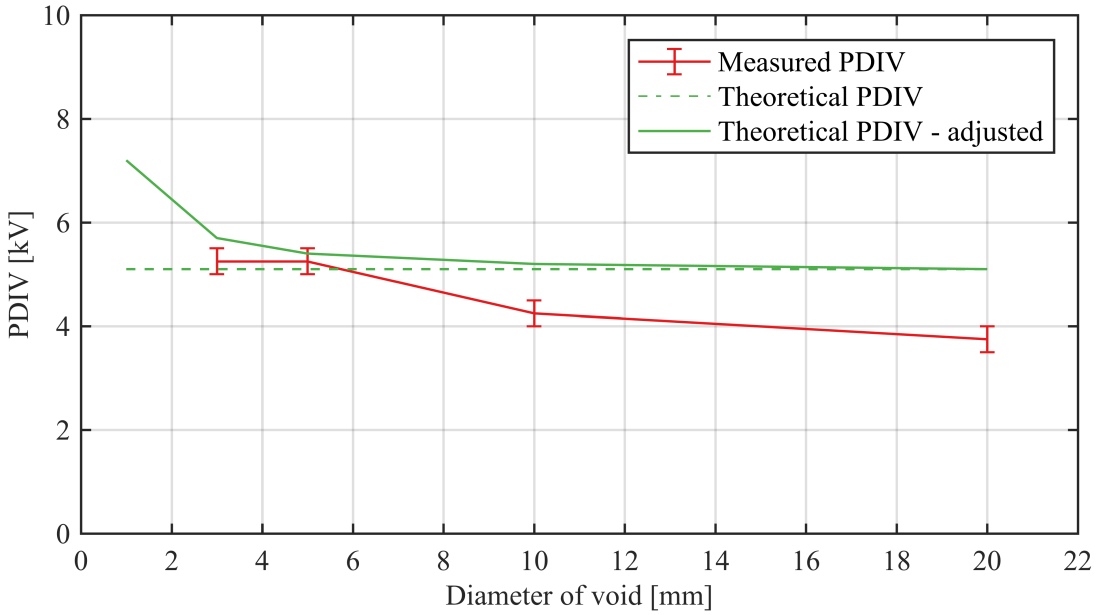

Figure 5.4: Inception voltage of mica mat samples as a function of void diameter. The measured values are indicated in the red graph with error bars (0.5 kV uncertainty as explained in 3.4.2). The green dashed graph shows the theoretical PDIV according to Paschen's law, whereas the theoretical PDIV after adjusting for the actual field enhancement in the voids is shown in solid green.

5.1.2 Magnitude of Discharges

Wu et al. have found that the PD magnitude is associated with the active discharge area, meaning the area of the void surfaces that is charged during a discharge, and that in the case of conducting void surfaces, the discharge area is always equal to the void surface area [37].

The experimental results show that the discharge magnitude follows the theoretical model when the void surfaces are conducting (see Figure 4.13). This demonstrates that the discharge area for each void size is equal to the surface area of that particular void as stated by Wu et al. A summary of discharge magnitude of all the samples is found in Figure 5.5.

In the case of polycarbonate with insulating void surfaces, the discharge magnitude does not follow the theoretical model as well as the samples with conducting surfaces. However, the discharge magnitude is still generally increasing with increasing diameter, with the exception of the 5 mm void.

The deviation from the theoretical discharge magnitude is seen to increase with increasing diameter. While the 10 mm void is fairly consistent with the theoretical model, the discharge magnitude of the 20 mm void only compares to a theoretical void size of about 11 mm. This shows that for the largest void, the discharge area is about 30 % of the total available void surface area. This is believed to be caused by the low conductivity of the void surfaces which limits the migration of the charges and therefore limits the active discharge area and hence also the discharge magnitude.

In the case of the samicatherm samples, the discharge magnitude is also seen to generally increase with increasing void size. However, the same trend as for the polycarbonate sam-

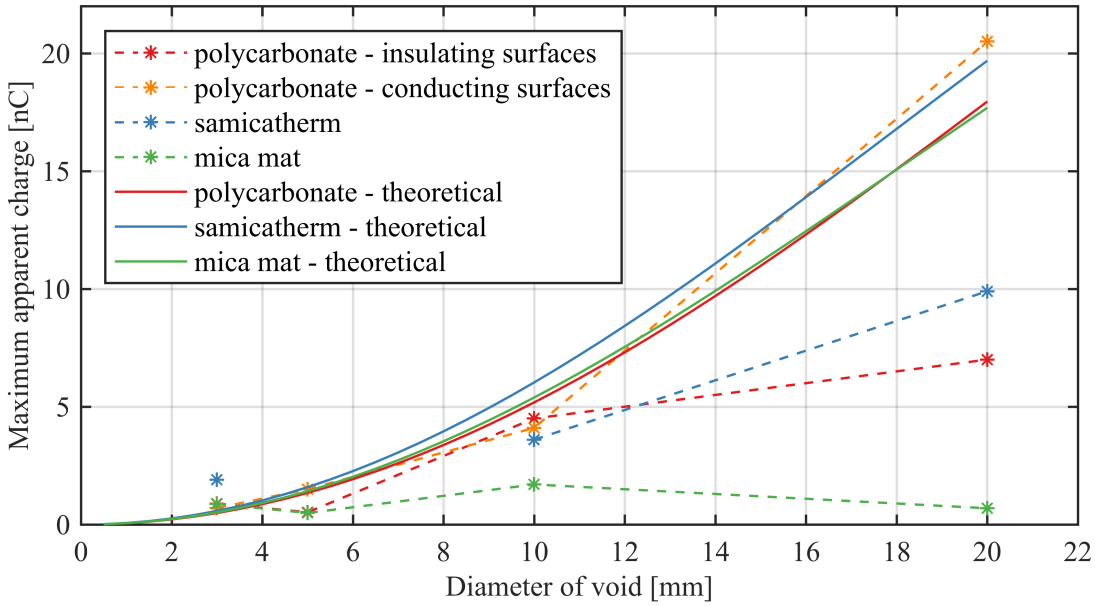

Figure 5.5: Summary of the apparent charge for all the four different sample types (dashed lines) in addition to the theoretical apparent charge (solid lines).

ples with insulating void surfaces is seen: the discharge magnitude is increasing at a lower rate compared to the theoretical model, causing the discharge magnitude, especially for the 10 mm and 20 mm void to be lower than the theoretical value. Again, this shows that the active area during a discharge is lower than the available surface area. Same as for the voids in polycarbonate, this might be related to the low conductivity of the void surface which limits the discharge area. It is interesting to observe, however, that the discharge magnitude from the 3 mm void is three times larger than the theoretical discharge magnitude for a 3 mm void embedded in samicatherm. One possible explanation is that a lack of start electrons cause a statistical time lag which delays the discharge so that it occurs at a higher field strength, which therefore results in a large magnitude.

When it comes to the measurements on the generator insulation samples (mica mat), the discharge magnitude is not increasing with increasing void size (see Figure 4.15). This indicates that in actual generator insulation, the active discharge area is not increasing with increasing void surface area; it is staying rather constant regardless of the available surface area.

These results do have some support in the findings of earlier research concerning the current pulses of partial discharges in disk-shaped voids in PET. The results indicated that voids with diameters up to 3 mm, behaved like voids with conducting surfaces, whereas *this was not the case for the larger voids* [38] and that the entire surface area of a 3 mm void therefore is active during a PD event [37]. Relating this back to the discharge magnitude in the mica mat samples, it can suggest that the discharge magnitude in the 3 mm void is limited by the available surface area, whereas the discharge magnitude of the larger voids is limited by factors like the surface conductivity and the surface condition in general.

The mica mat samples are the only sample type that exhibits a constant discharge magnitude regardless of the void size. This can be a result of the differences in the surface conditions of these samples compared to the specially designed laboratory samples. Due to the aging of the material, and the damage caused by the splitting of the mica laminates when creating the voids, the void surfaces have a higher surface roughness than the rest of the sample types. It might be that a higher surface roughness and generally a more uneven surface can limit the discharge magnitude. Regardless of the reason, the experimental results clearly show that the discharge magnitude is not increasing with increasing void diameter, and that the theoretical model fails to describe the discharge magnitude in voids in actual generator insulation.

To summarize, in samples with conducting void surface areas, the discharge area is equal to the void surface area and the discharge magnitude is therefore increasing with increasing void size as according to the theoretical model. However, when the void surface is insulating, the low conductivity is limiting the charge migration during a discharge, and thus limiting the discharge area. In the case of smooth void surfaces (polycarbonate and samicatherm), the discharge magnitude is still generally monotonously increasing with increasing diameter, but the magnitude is lower than the theoretical PD magnitude, especially for voids with a diameter larger than 10 mm. Lastly, in the case of actual generator insulation, the discharge magnitude is not increasing with increasing diameter, and the theoretical model fails to predict the PD magnitude.

5.1.3 Discharge Frequency

The results (Figure 4.16) showed that the discharge frequency is generally higher than the theoretical discharge frequency of 2 discharges per voltage cycle. However, all the samicatherm samples show a good consistency with the theoretical value. Same with the three smallest aluminum covered voids of 3, 5 and 10 mm. The PD frequency of the polycarbonate with insulating voids is consistently between 1.5 and 2 times higher than the corresponding samples with conducting surfaces. Moreover, the mica mat samples have the highest number of discharges for any void size. There is also a general trend that the discharge frequency is increasing with increasing void size.

When analyzing the discharge frequency with a focus on discharge mechanisms that can explain the results, it is highly important to see the results in the light of the applied voltage. Since the field enhancement of the voids is dependent on the void size, the specific voltage at which the discharge frequency is measured will not correspond to the same electric field strength in the cavities.

If adjusting the theoretical discharge frequency according to the actual inception voltage of the samples, the discharge frequency is still equal to two discharges per voltage half-cycle at an applied voltage of 7.0 kV. The only exceptions are the two measurements with the lowest

PDIV (mica mat 10 and 20 mm) for which the theoretical PDIV at 7.0 kV will be 3 discharges per voltage half-cycle. Therefore, the theoretical model can still not explain the trends in the measured discharge frequency.

Another possible explanation for the high discharge frequency, is the occurrence of parallel discharges, i.e. the discharges are occurring at several different places in the void.

Wu et al. have investigated the charge distribution in disk-shaped voids and found that a higher applied voltage can give a higher number of charge spots in one single void compared to a lower applied voltage [39] i.e. the number of charge spots per area increases with increasing voltage. They also observed that an increase in the number of charge spots on the void surface resulted in a higher discharge frequency. Only one void diameter was tested in this research, and therefore, increasing the voltage is equivalent to increasing the field strength in the void.

Earlier in this chapter, it has been seen that the electric field strength in the voids depends on the void diameter. And therefore, under the application of the same voltage magnitude, the field strength will be higher in the larger voids. Thus, the number of charge spots can be higher in the larger voids. This can be a possible explanation why the discharge frequency is generally increasing with increasing void diameter.

Even so, it is not only a higher field that can cause more charge spots and therefore a larger number of discharges. A large void surface area might in itself give room for more charge spots and thus more discharges [36]. This hypothesis is supported by microscopy analysis of the aluminum coating. Figure 5.6 shows one of the aluminum layers of the 20 mm void after exposure to PD activity. Abrasion/erosion of the aluminum is evident around parts of the edge of the aluminum as well as in the center. The aluminum coating of the 3 mm void, however, mainly shows abrasion due to PD around the edge of the void (see Figure 5.7). These observations strongly suggest that there has been PD activity around the edge of the void in the 3 mm void, whereas in the 20 mm void there has been PD activity both around the edge and in the center of the void. This can help explain why the 20 mm void has a higher discharge frequency.

Microscopy analysis of the polycarbonate samples with insulating void surfaces show, similarly to the aluminum covered samples, signs of strong PD activity along the perimeter of the void (see Figure L.11). This can be explained by the higher field enhancement in these areas. In addition, however, signs of PD activity in form of erosion of the void surface were detected across the entire surface area of the void (see Figure 5.8). This can explain why the polycarbonate samples with insulating void surfaces have a consistently higher discharge frequency compared to the samples with aluminum: The aluminum samples mainly show PD abrasion around the edge of the void and some abrasion in the center of the void, whereas the polycarbonate samples with insulating surfaces also show evidence of PD activity across the rest of the void surface area.

See appendix L for a more thorough microscopy analysis of the samples.

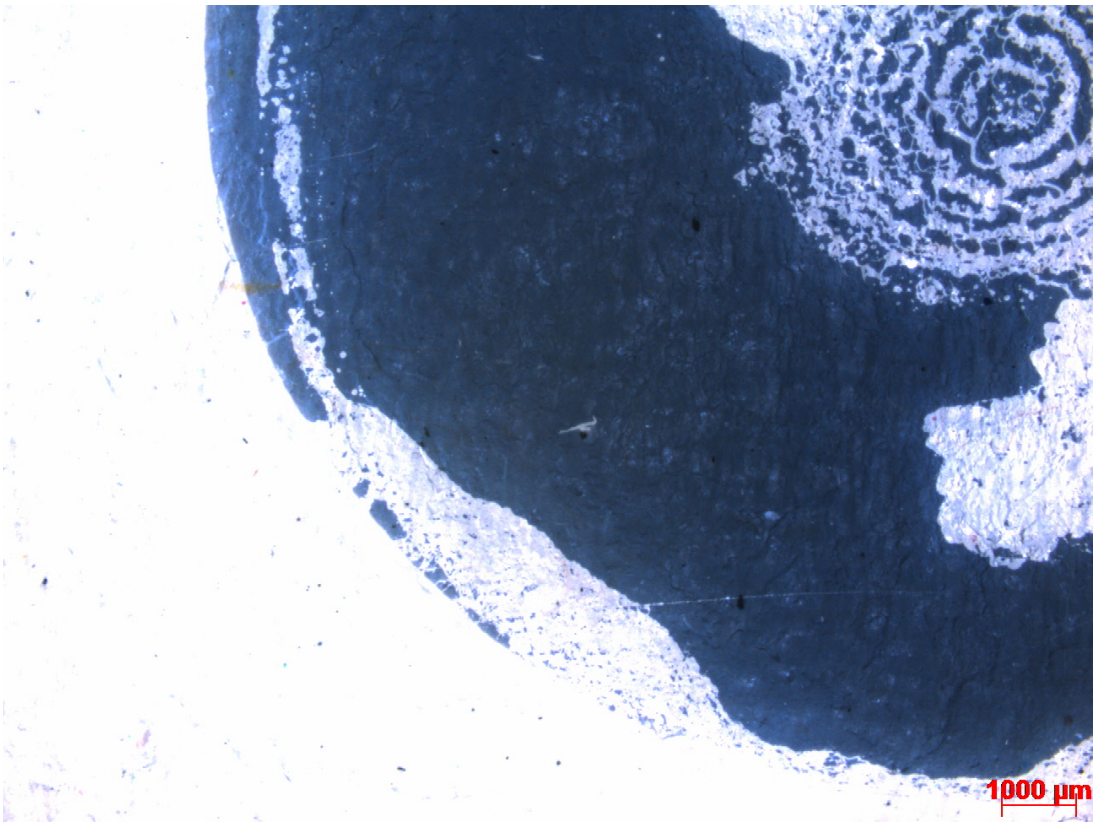

Figure 5.6: Aluminum layer of the 20 mm void (top sheet) after exposure to PD. The scale is shown in the bottom right corner of the picture. The picture shows about a quarter of the total area of the aluminum.

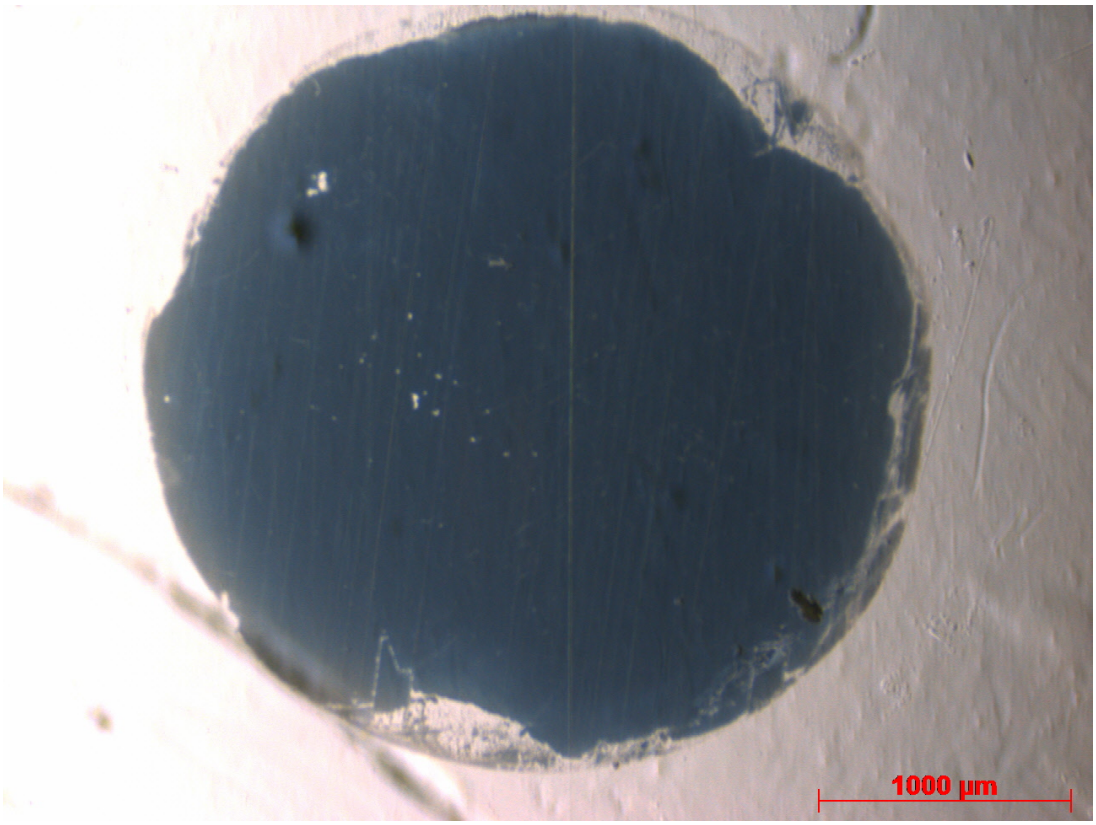

Figure 5.7: Aluminum layer of the 3 mm void (bottom sheet) after exposure to PD. The scale is shown in the bottom right corner of the picture.

The samicatherm samples have a consistently low discharge frequency which is not increasing with increasing void diameter, and which therefore corresponds well with the theoretical discharge frequency. This can be explained by the fact that the PDIV for these samples is not decreasing with increasing diameter. This means that the electric field strength in all the voids is just above the critical field strength (the streamer inception criterion) which causes a low number of discharges.

An interesting observation is that the 20 mm void does not seem to exhibit parallel discharges since the discharge frequency is similar to that of the 3 mm void and their respective inception voltages are also equal. This can indicate that right above the inception voltage there is only one active discharge spot, causing the discharge frequency to be consistent with the theoretical value.

Even though the PDIV of the mica mat samples is generally lower than the PDIV of other samples, the high number of discharges might also partly be due to the aging of the material. Aging of the generator insulation can lead to more delaminations, small voids and a general degradation of the material which can give rise to more discharge sources and a higher number of partial discharges.

To summarize, the trend in discharge frequency is likely caused by the differences in inception voltage for the different samples which generally cause an increase in discharge fre-

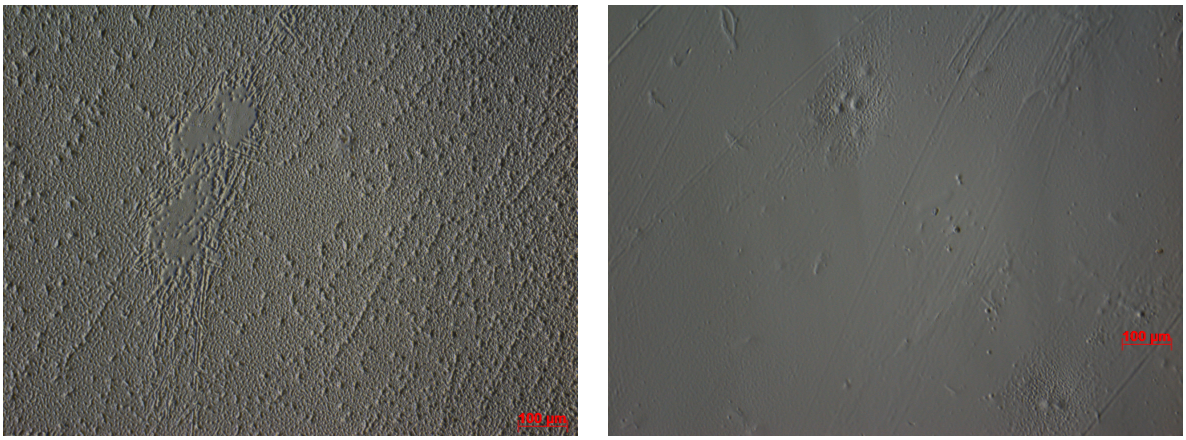

(a) Middle of the void. (b) Outside of the void.

Figure 5.8: Two different areas of the polycarbonate sheet. Figure 5.8a shows the surface of the sample inside the void, whereas Figure 5.8b shows the sample in an area that has been outside the void and therefore not been exposed to PD.

quency with increasing void diameter. In addition to the differences in inception voltage, a larger void diameter can also give room for more discharges as confirmed by microscopy analysis of the samples.

The higher discharge frequency in polycarbonate samples with insulating surfaces compared to the corresponding polycarbonate samples with conducting surfaces, is principally due to discharges occurring across the entire void surface area, not only along the edge of the cavity. In addition, the entire void surface is active during a discharge when the surfaces are conducting, and thereby limiting the number of parallel discharges.

5.2 Possibilities and Limitations Regarding PD Measurements as a Diagnostic Tool

5.2.1 Detectability of Critical Voids and Sensitivity of PD Measurements

Two questions will be addressed in this section: First, is the PD method successful in detecting the voids? And if that is the case, can the PD method assess the size of the defect?

Results showed that even in specially designed, PD free laboratory samples, the 1 mm void could not be detected. This is likely caused by the low field enhancement and possibly a deficiency of start electrons which cause the PDIV of PDs in the void to be higher than the maximum test voltage. However, one should not completely rule out the possibility that the apparent charge of PDs from a 1 mm void is smaller than the PD threshold value of 30 pC and that there are discharges occurring, only that they are too small to be detected. In any case, the result is the same: A void with a diameter of 1 mm is not possible to detect with the chosen PD approach.

Nevertheless, in samples made of smooth polycarbonate sheets, voids with diameters of

minimum 3 mm are detectable. If the void surfaces are conducting, the size of the voids can also be assessed since the apparent charge follows the predictions of the theoretical a^*bc model. In the case of insulating void surfaces, the relative void size can, to a degree, be decided since the charge magnitude is generally increasing with increasing void size. However, it is not possible to accurately assess the absolute size of the voids.

The situation is not so simple when the samples are not as smooth as the polycarbonate sheets. The samicatherm sheets do not have a completely smooth surface and therefore there is some PD activity when measuring on samicatherm samples without a cavity that results from small voids between the sample sheets. These discharges have a discharge magnitude and discharge frequency similar to PDs resulting from a 3 mm void. See Figure 5.9 for a comparison of the reference measurement and the measurement on the 3 mm void in samicatherm. This shows that it is not possible to conclusively identify a void with a diameter of 3 mm in a sample type that is not inherently PD free.

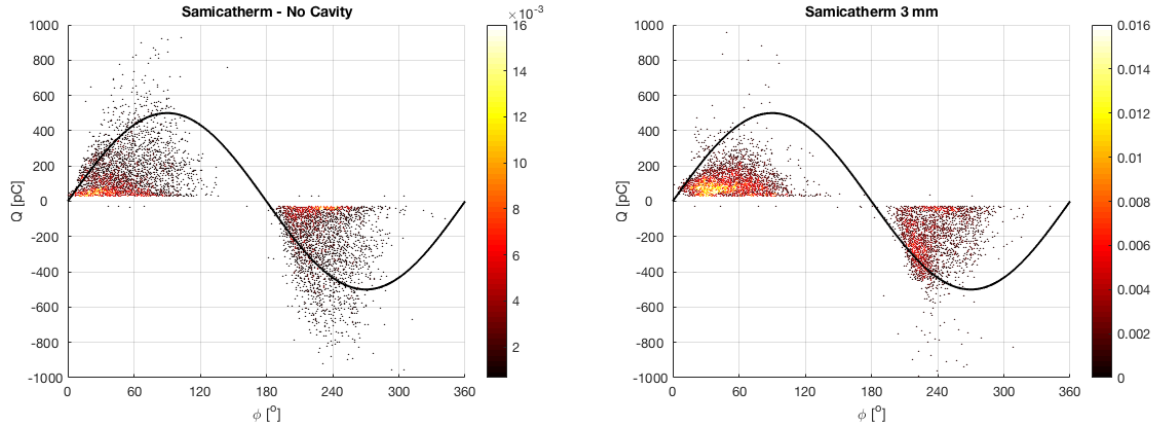

(a) Reference measurement.

(b) Measurement of 3 mm void.

Figure 5.9: The discharge magnitude of the discharges in Figure 5.9a is 1.5 nC and the discharge frequency is 2.7 discharges per half-cycle of the applied voltage. The discharge magnitude of the discharges in Figure 5.9b is 1.9 nC and the discharge frequency is 2.8 discharges per half-cycle.

The detectability of the 5 mm void is also rather poor since the PDIV deviates significantly from the theoretical value and therefore is higher than the test voltage in the developed test program. To be able to detect this void, a test program with a higher maximum voltage has to be used. Therefore, by using the test program developed as a part of this project, this void could not be detected.

Voids smaller than 10 mm are therefore not possible to identify with a high certainty using the chosen detection method and test program. Voids of 10 mm or larger are possible to detect, and it is also possible to conclude, based on the discharge activity, that the 20 mm void is larger than the 10 mm void.

The reference measurements on the insulation samples that were performed before the voids were created, showed a discharge magnitude that in two of the four reference measurements was larger than the discharge magnitude resulting from the constructed voids. None

of the voids showed a significantly higher discharge magnitude than the discharges inherent in the insulation.

The discharge frequency is generally higher after introducing a void. However, the 5 mm void does not cause considerable more discharges than the reference measurement. Therefore, one has to be careful with concluding that a void is detected solely based on the number of discharges.

Since the PDs resulting from the voids are not larger than the discharges inherent in the samples, and the discharge frequency is not consistently higher, it is not possible to distinguish the PD activity from the voids from the reference measurements and thus detect the voids with a high certainty.

As for assessing the relative size of the voids in generator insulation samples, the PD approach is not successful. The discharge magnitude is not increasing with increasing void size in the case of the mica mat samples. In fact, the 3 mm void had larger discharges than the 20 mm void. In addition, the number of discharges is not monotonously increasing with void size. The 3 mm void has a larger discharge frequency than both the 5 mm void and the 10 mm void. Only the 20 mm void had a larger discharge frequency.

Based on these results, neither the discharge magnitude nor the number of discharges can give unambiguous information about the size of the internal voids. The measurements cannot conclusively distinguish a 20 mm void from a 3 mm void even though the 20 mm void has a 44 times larger surface area than the 3 mm void.

Particularly low inception voltages may, however, indicate the presence of large voids since only the 20 mm void shows a significantly lower PDIV than the reference measurements and the theoretical value (more than 1 kV lower). However, the stochastic nature of partial discharges makes it difficult to conclude with this based on one single measurement. This observation might just as well be a result of statistic variation.

In conclusion, detecting smaller voids than 10 mm is only possible if the test sample is inherently PD free as the case is with the polycarbonate samples. Then, the detection method can identify voids as small as 3 mm. In the case of conducting void surfaces, the PD approach can also assess the size of the voids. However, it is still possible to assess the relative size of the voids when the void surfaces are insulating.

If there are inherently some PD activity in the samples, as is the case with samicatherm, only the two largest voids (10 and 20 mm) are possible to detect. The PD approach can also give information about the relative size of these two voids.

In real generator insulation samples which inherently have a high level of PD activity, the PD approach is not successful in providing information which makes it possible to assess the size of the internal voids. In addition, the measurements performed in this thesis work, indicate that the PD approach is unsuccessful at even detecting any of the voids with a high certainty.

As indicated, the sensitivity of the PD measurements when measuring on real generator

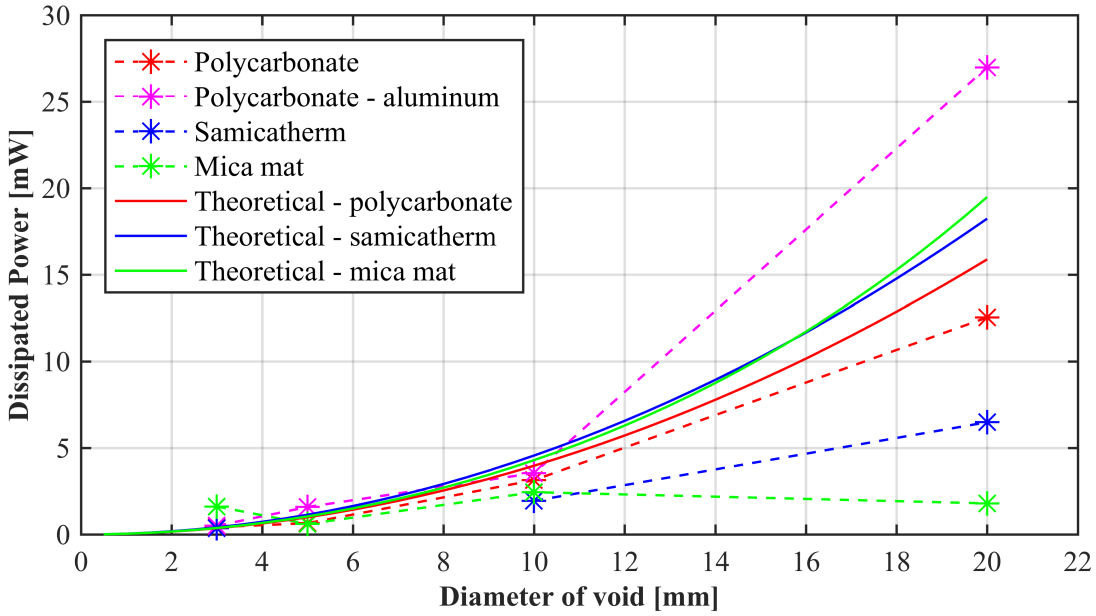

Figure 5.10: The dissipated energy caused by PD activity for the different samples as a function of cavity diameter. The theoretical graphs according to the abc model are indicated by solid lines, whereas the dissipated energy calculated based on the measured PD activity is shown in dashed lines. Test voltage is 7.0 kV and the frequency is 50 Hz.

insulation samples is poor. When performing PD measurements as a condition assessment method of generator bar insulation, the test objects are usually a lot larger than the small samples used in this thesis work. A larger test object will result in a lower sensitivity. The PD approach used in this thesis work will therefore likely not be successful in detecting critical voids if measuring on larger insulation systems. Therefore, it might be necessary to complement the electrical PD measurements with for examples acoustic detection of discharges to successfully detect critical voids. Another diagnostic tool which might be suitable for testing on insulation which inherently has a high content of voids, is measuring the tip-up dissipation factor. This method can be used to assess the total volume of voids within an insulation system [40].

5.2.2 Ability of PD Measurements to Assess Insulation Damage

The dissipated energy (Equation 2.21) caused by the discharges in the voids might give an indication of the potential damage the discharges can inflict on the surrounding insulation material. This parameter combines the number of discharges and the discharge magnitude into one single parameter. The dissipated energy per second (dissipated power) at a voltage frequency of 50 Hz for the different sample types as well as the theoretical dissipated energy is shown in Figure 5.10.

The dissipated energy is generally increasing with increasing void size in the case of the specially designed laboratory samples. However, the results show that in the case of the samples made of actual generator insulation, the total dissipated energy is not increasing with increasing void diameter. This means that the dissipated energy is higher per surface

area in the smaller voids. The implications of this have to be investigated further, but these results might suggest that the degradation rate due to PD activity in voids might not increase with increasing void size. However, the results obtained about the PD activity in voids in this thesis work are far from enough to be able to conclude on the severity of voids of different sizes. Nevertheless, it is an observation that can be interesting to investigate further.

6 Conclusion

The main aim of this thesis work was to investigate the PD activity in air-filled voids and to clarify how important PD parameters relate to the void size and the discharge mechanisms in the voids. Another important part of the thesis was to compare the experimental results with a much used existing theoretical model for internal partial discharges: the abc model.

Different test samples with embedded disk-shaped voids of different diameters have been constructed with this purpose in mind. The test samples range from specially made laboratory samples with aluminum-covered void surfaces, which closely resemble the representation of the insulation system the theoretical model is based on, to samples made of actual, aged generator bar insulation.

Based on the results and discussions in this thesis, the following conclusions can be drawn:

- The PD activity in specially designed laboratory samples with conducting void surfaces is consistent with the theoretical model when adjusting for the electric field distribution in the individual voids. The theoretical model is, however, unsuccessful at describing the PD activity in actual generator insulation samples.

- The inception voltage is generally decreasing with increasing void diameter due to higher field enhancement in larger voids. The samples made of generator insulation have the lowest inception voltages which might be a result of the aging of the material.

- The discharge magnitude is increasing with increasing void size for the specially made laboratory samples. However, the discharge magnitude in generator insulation is constant regardless of void size. PDs from samples with conducting void surfaces have a larger magnitude than in the case of insulating void surfaces.

- The discharge frequency is generally increasing with increasing void surface area, and conducting void surfaces result in a lower discharge frequency than insulating void surfaces. Deviations from the theoretical model can be explained by the occurrence of parallel discharges which the theoretical model does not account for. The highest discharge frequency is observed for the generator insulation samples, which can be due to the aging of the material.

One important aspect of this master thesis was to examine the possibilities and limitations regarding partial discharge measurements as a diagnostic tool. The ability of the PD approach to detect and assess voids in insulation materials can be summarized as follows:

- For samples that are inherently PD free, voids with a diameter of 3 mm and larger were detectable. However, the PD measurements were not successful at detecting a 1 mm void. In the case of conducting void surfaces, the size of the voids was also possible to assess. In the case of insulating void surfaces, it was generally only possible to assess the relative size of the voids.
- For laboratory designed samples that were inherently not completely PD free, only voids with a diameter of 10 mm or larger were conclusively possible to detect. The relative size of these two voids could also be determined.
- In the case of aged generator insulation samples, the PD approach is not successful in conclusively detecting the voids since it is not possible, with a high certainty, to distinguish the PD activity in the voids from the PD activity due to general aging of the insulation.

The results indicate that there are challenges related to the theoretical model for internal discharges. The more similar the samples are to real generator insulation, the less successful the theoretical model is in describing the PD activity in the void. In addition, the poor detectability and sensitivity in the case of measuring on real generator bar insulation samples, point to important limitations regarding the PD approach.

There are some important limitations to this work. Due to limited time, measurements were only done once for each void size for each of the four sample types. The conclusions are thus based on a limited number of measurements, and the results might therefore be sensitive to statistic variation. To increase the robustness of the conclusions, it is advisable to increase the sample population as well as the number of measurements performed on each sample.

7 | Further Work

In addition to generally increase the number of measurements and the sample population, there are a number of possibilities to how the work can be extended:

- In this thesis, only variations in void diameter has been investigated. In future work, it would be highly interesting to investigate how the PD parameters depend on the void height and shape of the cavity in general (spherical, oblong etc.). It would also be relevant to investigate the effect of void location and surface conditions (electrode bounded or insulation bounded).

- The aluminum that was applied to the samples showed signs of erosion/abrasion under PD exposure. Therefore, the time and the maximum voltage level of the test program had to be limited to avoid too long exposure of PD. Test showed that after more than about 5 minutes to PD activity, the aluminum had disappeared completely. To increase the withstand of the aluminum to PD activity, it would be beneficial either use aluminum paint or tape which is thicker and more robust than the thin layer of aluminum that was applied by vacuum evaporation. It would then be interesting to investigate the number of discharges and the discharge magnitude compared to the samples with abraded aluminum.

- In this thesis work, the focus has been on measurable PD parameters like inception voltage, discharge magnitude and discharge frequency. In further work, it would be interesting to make use of signal interpretation in the form of statistical analysis of PRPD patterns. Analyzing the distribution of discharge magnitude can give more information about the discharge mechanisms in the voids. For example, Weibull distribution can be used to identify different PD sources.

- Measuring partial discharges in voids at different applied voltage frequencies can give important information about the discharge activity and discharge mechanisms in the voids. It can also be interesting to perform the measurements at different temperatures since the temperature of the generator bar insulation varies with the current load.

Bibliography

[1] CIGRÉ Working Group A1.10, "Survey of Hydrogenerator Failures," 2009.

[2] T. M. Sneve, "Aldersfordeling for komponenter i kraftsystemet," NVE, Tech. Rep., 2005.

[3] "IEEE Std 43-2013 (Revision of IEEE Std 43-2000) - IEEE Recommended Practice for Testing Insulation Resistance of Electric Machinery," 2013.

[4] "IEEE Std 56-2016 - IEEE Guide for Insulation Maintenance of Electric Machines," 2016.

[5] "IEEE Std 95-2002 - IEEE Recommended Practice for Insulation Testing of AC Electric Machinery (2300 V and Above) With High Direct Voltage," 2002.

[6] "IEEE Std 522-2004 (Revision of IEEE Std 522-1992) - IEEE Guide for Testing Turn Insulation of Form-Wound Stator Coils for Alternating-Current Electric Machines," 2004.

[7] "IEEE Std 286-2000 IEEE Recommended Practice for Measurement of Power Tip-Up of Electric Machinery Stator Coil Insulation," 2000.

[8] "IEEE Std 1434-2014 (Revision of IEEE Std 1434-2000) - IEEE Guide for the Measurement of Partial Discharges in AC Electric Machinery," 2014.

[9] G. C. Stone, "A perspective on online partial discharge monitoring for assessment of the condition of rotating machine stator winding insulation," *IEEE Electrical Insulation Magazine*, vol. 28, no. 5, pp. 8–13, 2012.

[10] R. Bodega, P. H. Morshuis, M. Lazzaroni, and F. J. Wester, "PD Recurrence in Cavities at Different Energizing Methods," *IEEE Transactions on Instrumentation and Measurement*, vol. 53, no. 2, pp. 251–258, 2004.

[11] C. Hudon and M. Bélec, "Partial discharge signal interpretation for generator diagnostics," *IEEE Transactions on Dielectrics and Electrical Insulation*, vol. 12, no. 2, pp. 297–319, 2005.

[12] M. Bélec, C. Hudon, C. Guddemi, and D. N. Nguyen, "A case study of condition-based maintenance of a 202-MVA hydro-generator," *Proceedings of 2008 International Conference on Condition Monitoring and Diagnosis*, pp. 163–166, 2007.

[13] T. G. Aakre, E. Ildstad, S. Hvidsten, and A. Nysveen, "Review of Partial Discharge and Dielectric Loss Tests for Hydropower Generator Bars," *Proceedings of the Nordic Insulation Symposium*, no. 25, 2017.

[14] K. Temmen, "Evaluation of Surface Changes in Flat Cavites Due To Aging By Means of Phase Angle Ressolved Partial Discharge Measurement," *J. Phys. D: Appl. Phys.*, vol. 33, p. 603, 2000.

[15] R. Skattenborg, "Condition Assessment of Hydro Generators," Unpublished, Tech. Rep., 2017.

[16] E. Ildstad, *TET4160 Insulating Materials for High Voltage Applications*, 1st ed. Trondheim: NTNU Norwegian University of Science and Technology, 2015.

[17] CIGRE TF 15.11/33.03.02, "KNOWLEDGE RULES FOR PARTIAL DISCHARGE DIAGNOSIS IN SERVICE," Cigré, Tech. Rep., 2003.

[18] E. Commission, "High-Voltage Test Techniques - Partial Discharge Measurements," IEC60270, Tech. Rep., 2000.

[19] E. Ildstad, "Theoretical background of ageing and breakdown mechanisms for extruded dielectrics," NTNU, Trondheim, Norway, 1995.

[20] F. H. Kreuger, *Industrial High Voltage*. Delft, The Nederlands: Delft University Press, 1991.

[21] L. Niemeyer, "A Generalized Approach to Partial Discharge Modeling," *IEEE Transactions on Dielectrics and Electrical Insulation*, vol. 2, no. 4, pp. 510–528, 1995.

[22] B. Fruth and L. Niemeyer, "The Importance of Statistical Characteristics of Partial Discharge Data," *IEEE Transactions on Electrical Insulation*, vol. 27, no. 1, pp. 60–69, 1992.

[23] H. D. Young, R. A. Freedman, and A. L. Lewis, *University Physics with Modern Physics*, 13th ed. Addison-Wesley, 2012.

[24] F. Gutfieisch and L. Niemeyer, "Measurement and Simulation of PD in Epoxy Voids," *IEEE Transactions on Dielectrics and Electrical Insulation*, vol. 2, no. 5, pp. 729–743, 1995.

[25] T. Tanaka, "INTERNAL PARTIAL DISCHARGE AND MATERIAL DEGRADATION," *IEEE Transactions on Electrical Insulation*, vol. EI-21, no. 6, pp. 899–905, 1986.

[26] I. Gallimberti, "The mechanism of the long spark formation," *Journal de Physique Colloques*, vol. 40, no. C7, pp. 193–250, 1979.

[27] S. Hvidsten, "Power Cables - Partial Discharge Measurements," Trondheim, 2017.

[28] E. Kuffel, W. Zaengl, and J. Kuffel, *High Voltage Engineering: Fundamentals*, 2nd ed. Newnes: Butterworth-Heinemann, 2000.

[29] J. Skaar, *Elektromagnetisme*. Trondheim: Akademika forlag, 2013.

[30] E. Lemke, "A Critical Review of Partial-Discharge Models," *IEEE Electrical Insulation Magazine*, vol. 28, no. 6, pp. 11–16, 2012.

[31] A. Gemant and W. Philippoff, "Die Funkenstrecke mit Vorkondensator," *Zeitschrift fur Technische Physik*, vol. vol 13, no. no. 9, pp. 425–430, 1932.

[32] F. H. Kreuger, *Partial Discharge Detection in High-Voltage Equipment*. Butterworth-Heinemann, 1989.

[33] General Electric Company, "Lexan 9030 Sheet."

[34] "Mica products for electrical insulation," 2018. [Online]. Available: https://www.vonroll.com/en/product-detail/samicatherm-366.28?id=product7480

[35] International Electrotechnical Commision, "IEC TS 60034-27," 2006.

[36] C. Forssén and H. Edin, "Partial Discharges in a Cavity at Variable Applied Frequency Part 1: Measurements," *IEEE Transactions on Dielectrics and Electrical Insulation*, vol. 15, no. 6, pp. 1601–1609, 2008.

[37] K. Wu, Y. Suzuoki, and L. A. Dissado, "The contribution of discharge area variation to partial discharge patterns in disc-voids," *Journal of Physics D: Applied Physics*, vol. 37, no. 13, pp. 1815–1823, 2004.

[38] K. Wu, T. Ijichi, T. Kato, Y. Suzuoki, F. Komori, and T. Okamoto, "Contribution of Surface Conductivity to the Current Forms of Partial Discharges in Voids," *IEEE Transactions on Dielectrics and Electrical Insulation*, vol. 12, no. 6, pp. 1115–1124, 2005.

[39] K. Wu, C. Pan, Y. Meng, and Y. Cheng, "Dynamic Behavior of Surface Charge Distribution during Partial Discharge Sequences," *Dielectrics and Electrical Insulation, IEEE Transactions on*, vol. 20, no. 2, pp. 612–619, 2013.

[40] M. Farahani, H. Borsi, E. Gockenbach, and M. Kaufhold, "Partial Discharge and Dielectric Response Behaviour of Insulation Systems for High Voltage Rotating Machines under Electrical Stress," *IEEE Annual Report Conference on Electrical Insulation and Dielectric Phenomena*, pp. 271–274, 2004.

[41] "Lecture Notes from ELK-30 Condition Assessment of High Voltage Equipment," NTNU, Trondheim, 2017.

[42] P. H. Morshuis, "Partial Discharge Mechanisms," Ph.D. dissertation, Delft University of Technology, 1993.

[43] ——, "Degradation of Solid Dielectrics due to Internal Partial Discharge: Some thoughts on progress made and where to go now," *IEEE Transactions on Dielectrics and Electrical Insulation*, vol. 12, no. 5, pp. 905–913, 2005.

A | Discussion of the Area of the Aluminum Layer

One question that was raised and discussed was how large an area compared to the void area that should be covered in aluminum. Three options were considered:

1. Diameter of aluminum = diameter of void
2. Diameter of aluminum = diameter of void + 2 mm
3. Diameter of aluminum » diameter of void

Of the three, the first one ended up being the preferred choice. This was decided after careful consideration of several factors. First, the specimens with aluminum are supposed to be comparable with specimens without aluminum, therefore, it is favorable that the conditions in the void with and without aluminum are similar i.e. same electric field distribution. Based on COMSOL simulation, the 1. option gave a 49-82 % higher maximum electric field when compared to the situation without aluminum. However, option 2 gave an 8 % higher field for the largest void (20 mm), down to 0.3 % lower field for the smallest void (1 mm). The third option was ruled out since when the diameter of aluminum became much larger than the void diameter, the floating potential that the aluminum represents shielded the void and caused a much lower electric field compared to the field in the void without aluminum; it was also lower than the breakdown strength of air.

The second deciding factor is that the effective available discharge area should be similar to the situation without aluminum. In the case of conducting surfaces, the discharge area will always be the whole surface and therefore, theoretically all the discharges will have the same PD magnitude [38]. Wu et al. [38] also showed that for different void sizes, but with a constant area covered in aluminum, the PD magnitude did not vary significantly between the tests on the different void sizes. This indicates that the PD magnitude is mostly decided by the conducting surface area and not the void size. Since the aim with this project is to investigate different parameters as a function of void size, these indications therefore make strong arguments in favor of choosing alternative 1 where the aluminum surface is equal to the void area.

Because of the high field enhancement in the cavity for alternative 1, it was decided to compare experiments with alternative 1 and 2 to see if any pronounced differences would

indicate a major drawback against alternative 1. Based on the results from these tests, alternative 1 was indeed chosen as the preferred option.

B | Vacuum Evaporator for Application of Aluminum Coating

A picture of the vacuum evaporator is seen in Figure B.1. The interior of the bell jar is shown in Figure B.2 with the specimens and the wire basket source indicated. A detailed picture of the wire basket source is found in Figure B.3. An information chart which shows the operation of the valves of the vacuum evaporator is shown in Figure B.4.

To limit the area of the aluminum to the cavity surface area, and to shield the rest of the sample, steel plates with holes of diameters matching the diameters of the voids were placed underneath the polycarbonate plate in the stand during the application process. An illustration of the mechanism which holds the samples in place and limits the area that is covered in aluminum is shown in Figure B.5.

A summary of the operation of the vacuum evaporator follows:

First, the rotary pump must be turned on and cooling in the form of water must be turned on. Then, the pressure around the oil diffusion pump must be reduced by opening the valve to the rotary pump.

Then, the bell jar can be opened and the samples and the aluminum pellet are placed. Then, the bell jar is adjusted and locked in place.

After about half an hour when the pressure of the diffusion pump is "low enough", the pressure of the bell jar can slowly be reduced by alternating between opening the valve to the rotary pump and the diffusion pump. This must be continued until the indication lamp turns green.

Then, the current can be increased slowly up to 40 A. When the light in the bell jar turns from yellow to white, the current can be turned off.

The test samples now have to be cooled for about an hour to avoid oxidation of the aluminum when opening the bell jar. After removing the samples and closing the bell jar again, the diffusion pump should be turned off and be let alone for 20 minutes to cool down. Then the pressure of the bell jar should be reduced before the water cooling and the rotatory pump is turned off. At the end of the operations, all valves must be closed the equipment must be turned off.

Figure B.1: The vacuum evaporator while in operation. The bell jar is protected by a plastic and metal shield.

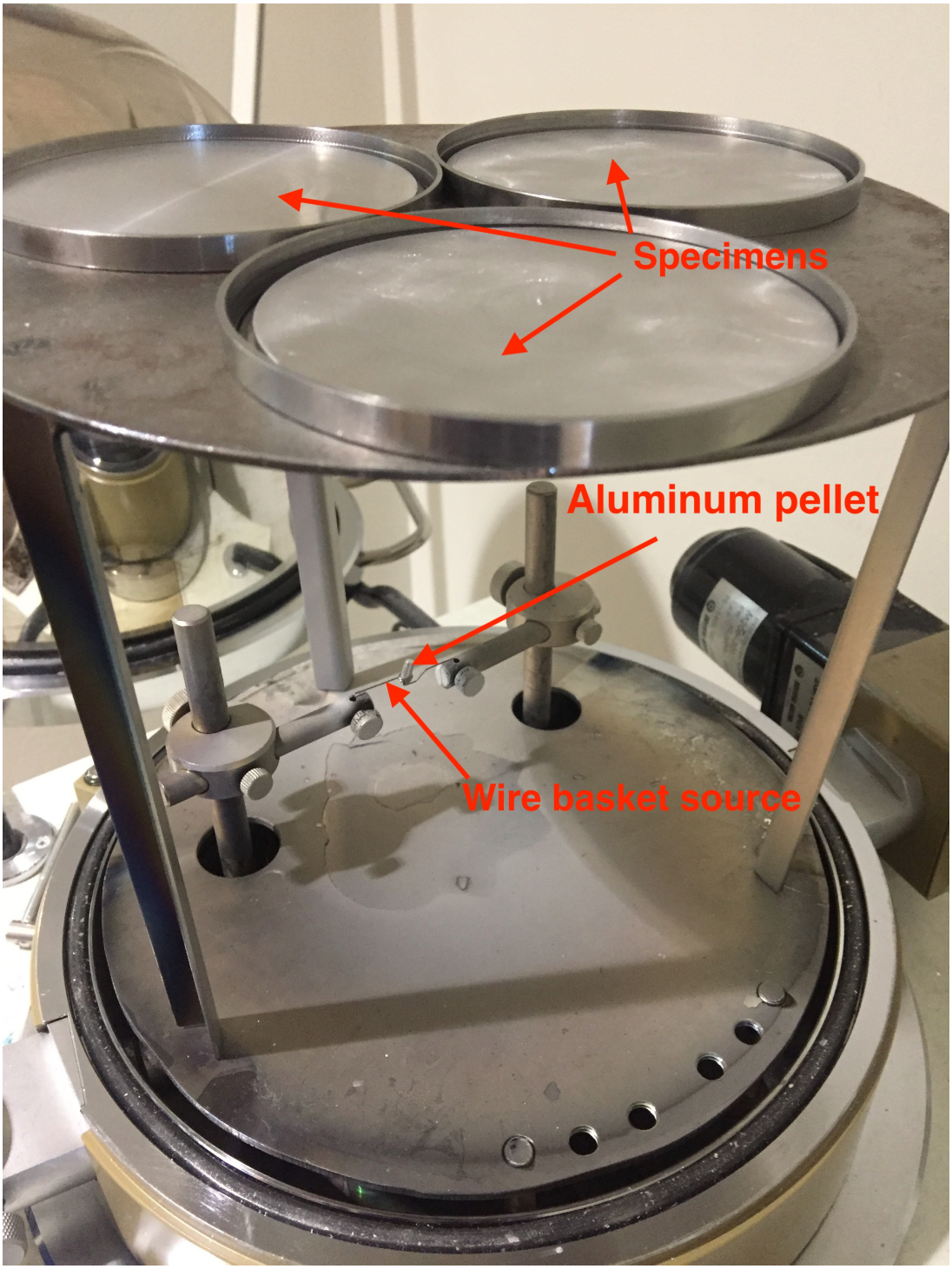

Figure B.2: Inside the bell jar. The wire with the aluminum pellet and the specimens (covered with steel plates to keep them in place) are indicated in the figure.

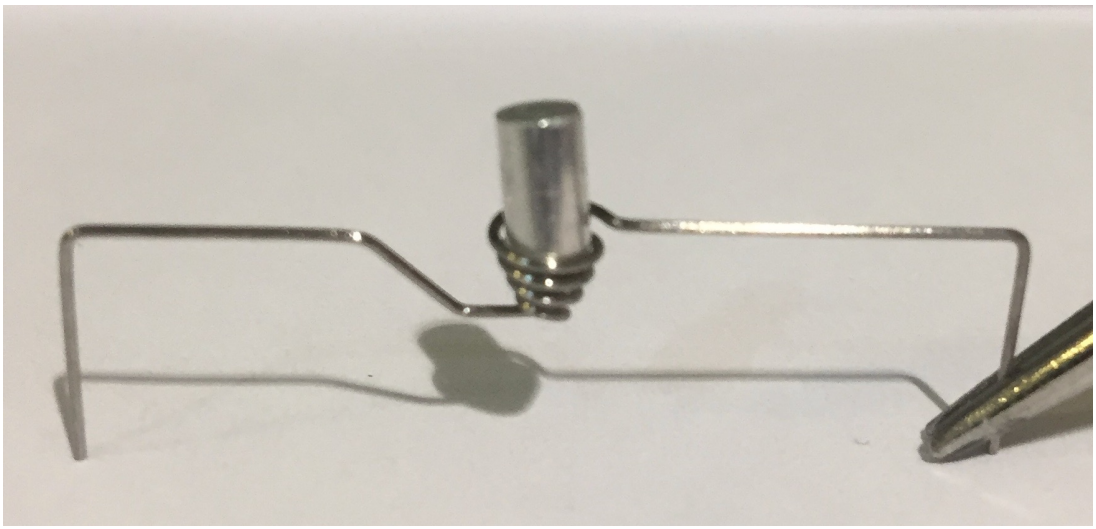

Figure B.3: The wire basket source with the aluminum pellet placed in the basket.

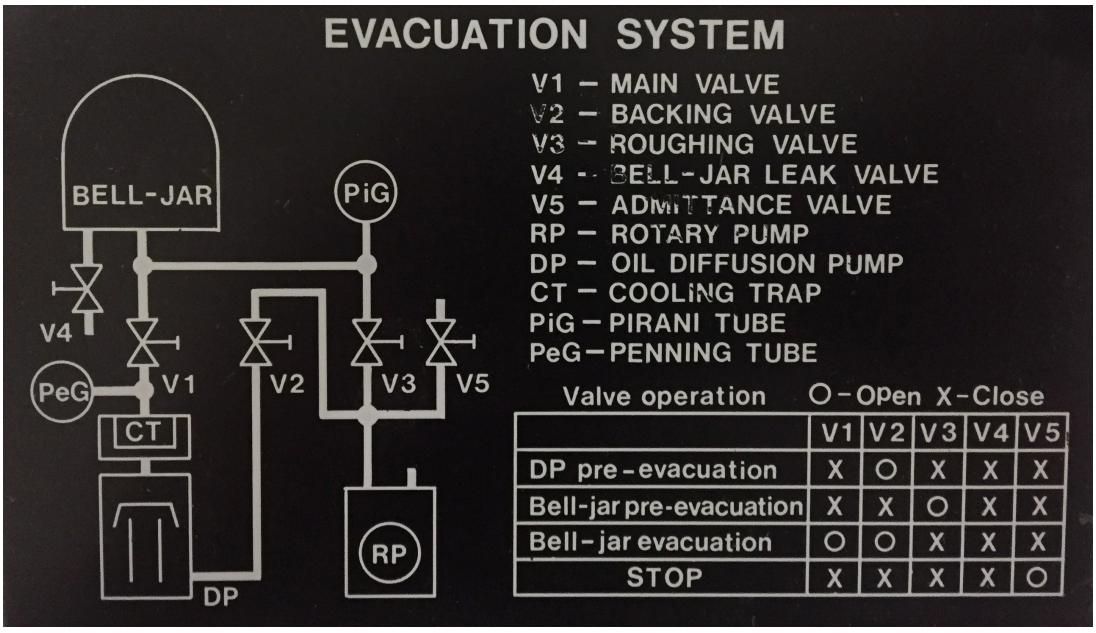

Figure B.4: Schematics of the different elements of the vacuum evaporator and instructions on the valve operations.

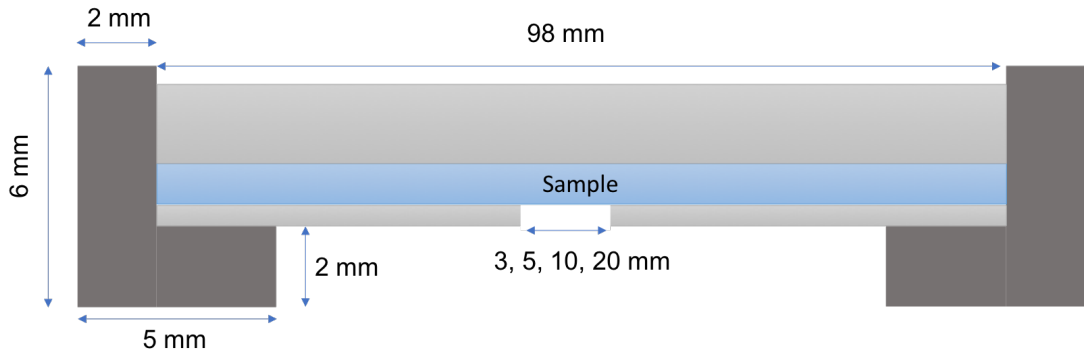

Figure B.5: Cross-section of the sample setup in the vacuum evaporator. The illustration shows the holder (dark grey) which holds the sample in place, the steel plate which covers the parts of the sample that should not be covered in aluminum (light grey), the thicker steel plate which presses the sample and the bottom steel plate together (light grey), and the sample (blue). Proportions are not correct.

C | Capacitance and Relative Permittivity

The relative permittivity of polycarbonate, samicatherm and mica mat as a function of frequency is shown in Figure C.1.

The different measurements of the capacitance which lead to the values of ϵ_r for polycarbonate are shown in Figure C.2. As one can see, the capacitance of the test setup with a sample of 1 mm thickness is not 3 times larger than the capacitance of the setup with a 3 mm thick sample. This is due to the stray capacitance.

The area which the electric field is confined to is only unambiguously defined when the guard is present and therefore, the material constant ϵ_r for polycarbonate has been calculated based on the measurement "polycarbonate new guard" in Figure C.2. When the guard is removed (causing fringe effects - spreading of the electrical field), the capacitance increases. When using an electrode molded in epoxy, the capacitance increases further as can be seen reflected in the green and yellow lines in the graph of Figure C.2. This is due to the additional storage of electrical energy in the epoxy mold.

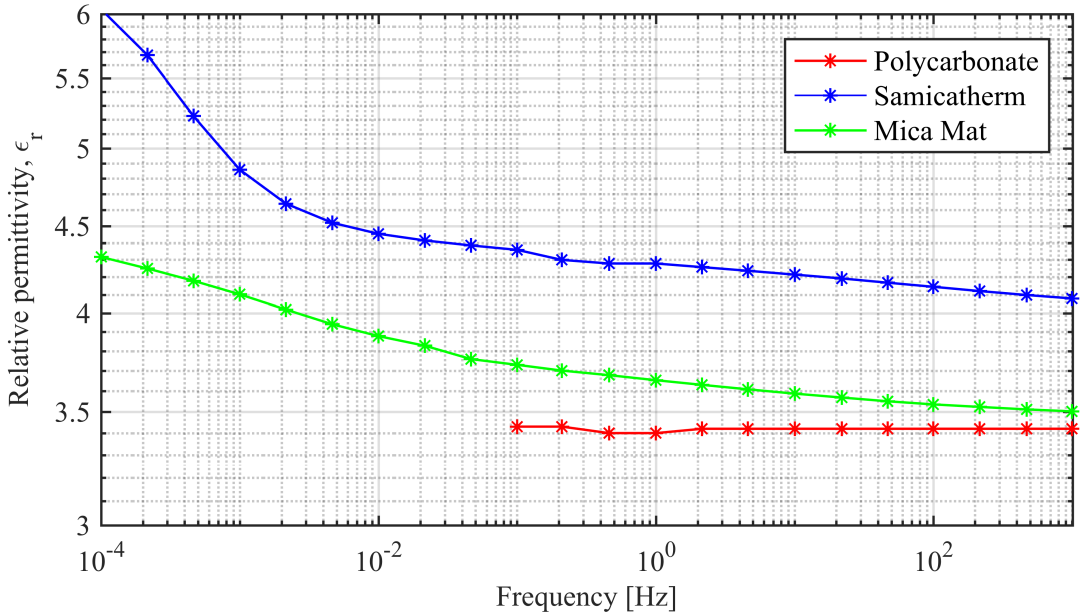

Figure C.1: The relative permittivity of the three different materials used in this project as a function of frequency. To save time, the lowest frequency that was used when testing polycarbonate was 1 mHz. The two other materials were measured earlier as a part of the Ph.D. work of Torstein Grav Aakre.

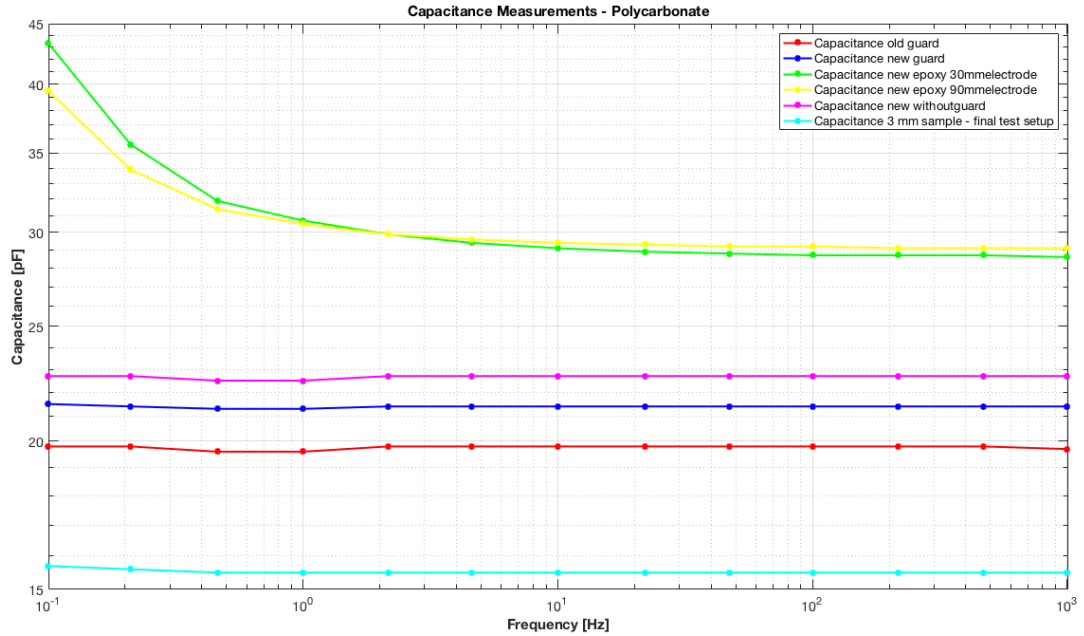

Figure C.2: Capacitance of different test setups and different polycarbonate samples. Two different polycarbonate sheets were measured: one "old" sheet which was not cleaned and had scratches, and a "new" sheet which came in plastic wrapping and had not been used before. Then the tests were performed with and without guard and with two different electrodes: One electrode without epoxy and one molded in epoxy. Lastly, one test was performed with the electrode molded in epoxy and with the "ground" electrode used in the experiments in this project as seen in figure 3.8. The "cyan" graph is the resulting capacitance of the finished test setup, identical to the one used for the PD measurements. The measurement "Capacitance new guard" was used to calculate the relative permittivity which can be seen in Figure C.3.

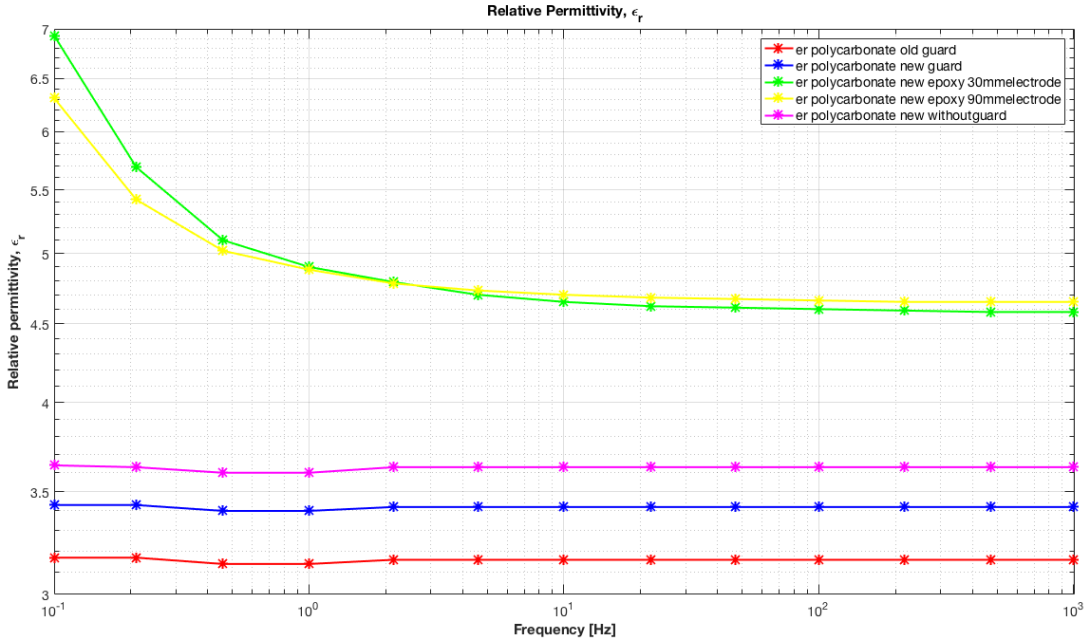

Figure C.3: Resulting relative permittivity as a function of frequency from measurements of capacitance.

D | List of Equipment

Table D.1: Equipment used as part of the thesis work.

Equipment	Specifications	SINTEF (S) or Elkraft NTNU (N) reg. number
Data Acqusition unit	OMICRON MPD 600	H02-0196-01 (N)
Power sypply	OMICRON MPP 600	H02-0196-09 (N)
Measuring impedance unit	OMICRON CPL 542	H02-0196-06 (N)
Control unit	OMICRON MCU 502	H02-0196 (N)
High voltage amplifier	Trek Model 20/20B	B03-0271 (N)
Digital to analog converter	National Instruments NI USB 6216	P08 0505 (N)
Computer	Dell Latitude E6430	P07-1858 (N)
Temperature gauge	Keysight 34972A LXI Data	G05-0207 (N)
Insulation diagnostic analyzer	IDAX 206 200V	P01-0108 (S)
Drying oven	Termaks	P02-0222 (S)
Low pass filter		
Coupling capacitor	3.4 nC	
Start battery	Biltema 12 V, 74 Ah	
Battery charger	Elektro mekanisk industri AS ESL 600	B02-0363 (N)
Kitchen oven		
Vacuum evaporator	Jeol JEE-4X	EFI P01-0042 (N)
Microscope	ZEIZZ SteREO Discovery.V2	P03-0260 (S)

E | OMICRON Interface and Settings

The OMICRON software interface is seen in Figure E.1. A presentation of the different panes of the OMICRON interface follows:

1. Settings Area: Controls the charge integration settings, display settings, detection settings and gating options, calibration settings, and controls the histogram and stream recordings.
2. Large Scope View Area: Shows the test voltage and the phase-resolved histogram.
3. Small Scope View Area: Shows the time domain of the PD pulses. Other views, like the FFT of the PD pulse can also be shown here.

In the following list, essential settings used in this project are presented.

- The charge integration settings are set to time domain with defined limits of [-100 ns, 100 ns] which corresponds to the width of a PD pulse at the zero crossing. The shape of the pulse is independent of the physical discharge and is determined by the circuit parameters [41]. This justifies choosing time domain over frequency domain, which was initially done to reduce reflections.
- To completely filter away reflections, the dead time was increased from 6.25 μs to 45 μs. A control test was performed to make sure this did not filter away actual discharges. The number of discharges was 0.9 % lower with 45 μs compared to 6.25 μs which justifies increasing the dead time.
- The noise level was determined by reducing the threshold value, which showed a noise band up to about 30 pC. The threshold value was therefore set to 30 pC to avoid detecting noise. If some of the noise is larger than 30 pC, it can be gated in OMICRON after PD measurements.
- Data streams of the discharges were recorded. These streams include where on the phase the discharge occurs, the voltage at that instant, the time, and the apparent charge - making it possible to replay the measurements and export the data to MATLAB compatible files for further processing.

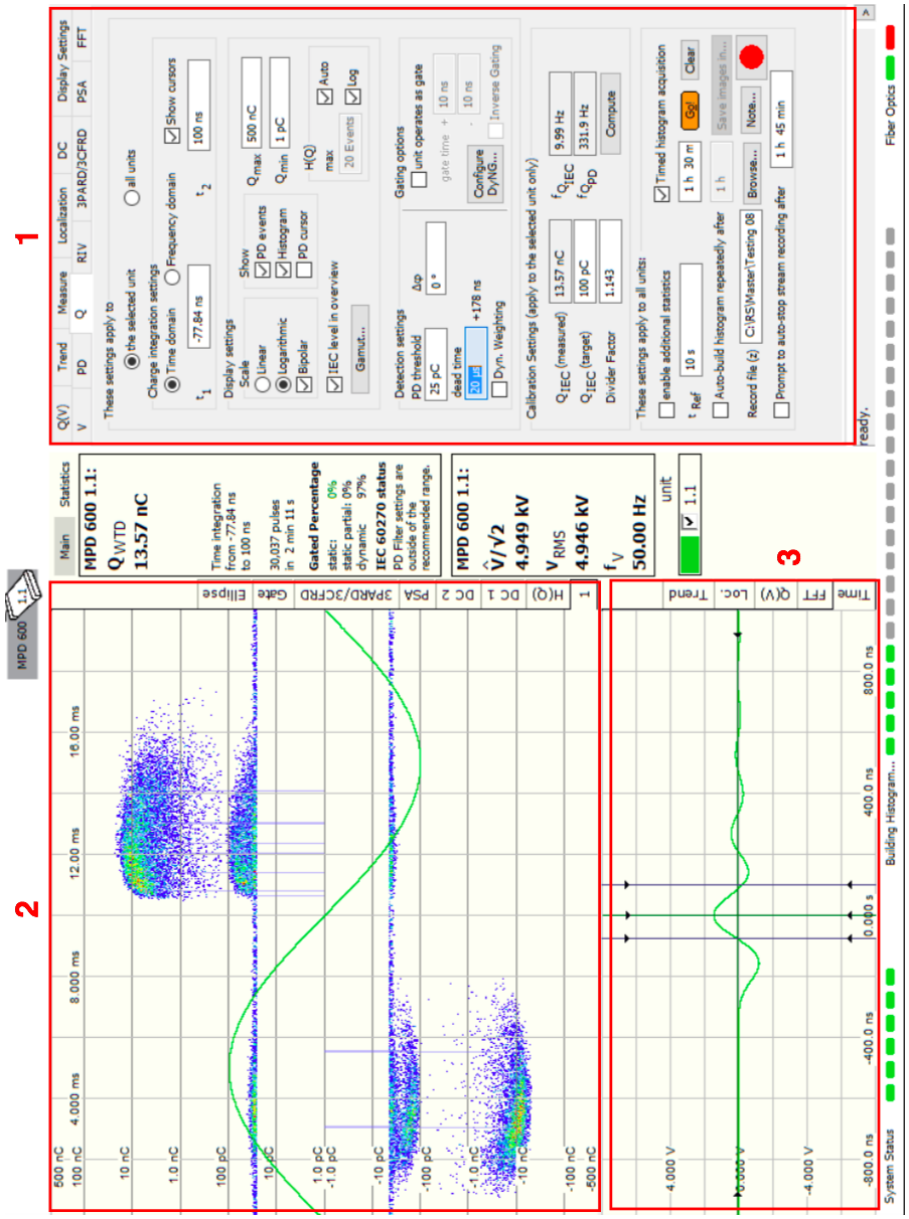

Figure E.1: The computer interface of OMICRON. This is the MPD600 product.

F | Designing the Test Program for PD Measurements

F.1 The Test Voltage

The maximum voltage, and the test voltage at which the apparent charge and the number of discharges per half-cycle are extracted, is 7.0 kV. This voltage level was chosen because it was necessary to pick a test voltage that is higher than the highest PDIV of all the samples, and initial PD measurements showed that some specimens had a PDIV of up to 6.5 kV. It was also discussed if the test voltage should be 0.5 kV + PDIV for each individual sample, but this option was discarded. The reason for this is that the PDIV is measured with an accuracy of ± 0.5 kV and choosing 0.5 kV above this relative uncertain PDIV would just introduce one more uncertain factor. Choosing a voltage level that was a certain percentage of the PDIV above the PDIV, was also considered, but that would require a lot of manual adjustment of the voltage and it would also introduce the need for deciding the PDIV at the time of the measurements, which can be difficult. Therefore, to increase the consistency of the measurements and the simplicity of performing the experiments, the same program with the same test voltage was chosen for analysis for all of the samples. The consequences of this choice have to be taken into consideration when analyzing the results. For example, it is expected that the samples with a lower PDIV will experience a higher number of discharges per half cycle at 7.0 kV than the samples with a PDIV closer to 7.0 kV.

F.2 Time Interval at each Voltage Level

The decision to keep the voltage constant for 30 seconds at each voltage level was done on the basis of trying to limit the time the sample is exposed to PD. Especially with the samples that are covered in aluminum, exposure to PD was shown to erode the aluminum coating. The duration of the measurement at the test voltage, 7.0 kV, was set to 1 min to be able to extract a full 30 seconds of measurements for further data processing and analyzing. Each time the voltage is changed, it takes a few seconds for it to stabilize at the new voltage level. Therefore, by increasing the time to 1 min and extracting the data from the middle 30 seconds, effects from voltage adjustments can be avoided.

F.3 Voltage Steps

The last parameter which had to be decided was the size of the voltage steps or the voltage increments. When analyzing and comparing the PDIV of different test samples, it is favorable to have a high precision of the value of PDIV. Therefore, it is beneficial to use small voltage increments for each step. However, very small increments would increase the duration of the test program and therefore also the duration of PD exposure. Consequently, a compromise was made between high accuracy and short duration of PD exposure and 0.5 kV was chosen as a suitable increment.

F.4 Test Program for Investigating Voltage Frequency Dependence and Temperature Dependence

A different test program was also used in this project, but due to time constraints, there was not enough time to analyze the results from these in-depth measurements. However, for further work, the test program that was used is presented here:

The test programs that are described in the past sections, were made to analyze the basic parameters at 50 Hz and at room temperature. However, by measuring PD at different voltage frequencies and temperatures, more information about the mechanisms that govern the discharge activity in the voids can be extracted. Therefore, further measurements were done to investigate what effects varying voltage frequency and varying temperature may have on the measurable parameters. The full test program iterates over five values of the temperature and over ten different frequencies ranging from 0.01 Hz to 100 Hz for each temperature. For each frequency and temperature, the program runs a PDIV/PDEV program similar to that of Figure 3.10.

This program lasts for about 24 hours and is developed and used as a part of the Ph.D. work of the co-advisor of this thesis work. This program is made in LabVIEW and it is not seen as a part of this thesis work to learn the technicalities of making a LabVIEW program. In addition, it is beneficiary if the results from this work are comparable to that of the Ph.D. work. Therefore, the test program was utilized in more or less its original form.

G | MATLAB Script

G.1 Abc Model - Theoretical Values

```
clear all
clc

e = 8.85e-12;
cavity_height = 1e-3; % 1 mm
sample_height = 3e-3; % 3 mm
cavity_diam = 0:0.0005:0.020; % Diameter of the cavity
electrode_diam = 30e-3; % 30 mm
Us0 = 4600; % Ignition voltage: 4.6 kV
Ur0 = 0; % Remanent voltage: assumed zero
U = 7000; % test voltage (RMS)

%%---------POLYCARBONATE--------------%%
er_poly = 3.4; % relative permittivity
Ca_poly = (er_poly*e*(pi()/4)*(electrode_diam^2-cavity_diam.^2))./sample_height;
Cb_poly = (er_poly*e*(pi()/4).*cavity_diam.^2)./(sample_height-cavity_height);
Cc_poly = (e*(pi()/4).*cavity_diam.^2)./cavity_height;
Cd_poly = 8.4*10^(-12); % Stray capacitance
Ca_poly_eff = Ca_poly + Cd_poly;
C_tot_poly = Ca_poly_eff + Cb_poly.*Cc_poly./(Cb_poly+Cc_poly);

Ui_poly = ((Cb_poly+Cc_poly)./Cb_poly)*Us0/sqrt(2);

Qa_poly = (Cb_poly./(Ca_poly_eff+Cb_poly))*(Us0-Ur0).* ...
    (Ca_poly_eff + (Cb_poly.*Cc_poly)./(Cb_poly+Cc_poly));
Qa_poly_simple = Cb_poly*(Us0-Ur0);
Qa_error_poly = ((Qa_poly_simple-Qa_poly)./Qa_poly)*100;

n_poly = 2*((Cb_poly./(Cb_poly+Cc_poly))*sqrt(2)*U)/(Us0);
```

Figure G.1: The script for calculating the theoretical values of the capacitances in the abc model: the inception voltage, the apparent charge and the number of discharges per voltage half-cycle at test voltage 7.0 kV. This script shows the calculation of these parameters for polycarbonate. To calculate the same values for samicatherm and mica mat, the relative permittivity and the stray capacitance has to be changed according to Table 3.2 and Table 4.3 respectively.

G.2 Import of Data from COMSOL

```
1
2     %Importing the PD parameters from OMICRON
3     %The folder from which the data should be taken from is defined by the user
4     %as input.
5
6 -   clc
7 -   clear all
8
9     %Uncomment the following line if trendplot.m is needed:
10    %trendplot
11
12 -  file = input('What folder should the data be taken from? (Copy the path to the folder): ','s');
13    %Digitized, pre-processed PD parameters
14
15    %Voltage sampled every 48 microsecond
16 -  [t_v, V] = importVdata(file, 'unit1.1');
17
18    %The apparent charge of every PD event and the time of occurance
19 -  [t_q, Q] = importQdata(file, 'unit1.1');
20
21    %Phase position for every PD event [0,1] where the number represent the
22    %percentage of the voltage cycle.
23 -  PH = importPHdata(file, 'unit1.1');
24
25    %Phase of each PD event in degrees
26 -  phase_deg = PH*360;
27
28 -  clearvars file
```

Figure G.2: The script that imports PD data to MATLAB. The specific scripts that import the voltage data, the apparent charge of the PDs and the phase value of the PDs are shown in the following figures.

```
1     function [v_tm, v] = importVdata(folder, vUnit)
2     %Voltage sampled every 48 micro-second
3 -   fileName = sprintf('%s/%s.V', folder, vUnit);
4
5 -   file = fopen(fileName, 'rb');
6
7 -   if file == -1
8 -      msg = sprintf('file %s could not be opened', fileName);
9 -      error(msg);
10 -  end
11
12 -  fseek(file, 0, 'bof');
13 -  v = fread(file, inf, 'float32');
14 -  v_tm = 48e-6 * (0:size(v, 1) - 1);
15 -  end
```

Figure G.3

```
function [q_tm, q] = importQdata(folder, qUnit)
%Q_apparent and time for every PD event
fileName = sprintf('%s/%s.Q', folder, qUnit);

file = fopen(fileName, 'rb');

if file == -1
   msg = sprintf('file %s could not be opened', fileName);
   error(msg);
end

fseek(file, 0, 'bof');
q = fread(file, inf, 'float32', 8);
fseek(file, 4, 'bof');
q_tm = fread(file, inf, 'float64', 4);
end
```

Figure G.4

```
function phase = importPHdata(folder, qUnit)
%Phase position for every PD event. Range: [0,1] (pos. at voltage cycle)
fileName = sprintf('%s/%s.PH', folder, qUnit);

file = fopen(fileName, 'rb');

if file == -1
   msg = sprintf('file %s could not be opened', fileName);
   error(msg);
end

fseek(file, 0, 'bof');
phase = fread(file, inf, 'float64');
end
```

Figure G.5

G.3 Data Processing

```
function PRPD_plot(PH, Q, ttl)
fprintf('-------------- PRPD-plot --------------\n')
lb_ub = input('Y-aksens grenseverdi (i absoluttverdi), Q_max [pC]: ');
label_interval = input('Antall pC mellom hver label p? y-aksen: ');

[N1,C1] = hist3([Q PH],[200 360]);
qN1 = C1{1};
phiN1 = C1{2};

figure(2), ...

    c = zeros(1,length(Q));
for i = 1:length(Q)
   % a = Finn n?rmeste index q i qN1
   [~, a] = min(abs(qN1 - Q(i)));
   % b = Finn n?rmeste index PHI i PHIN1
   [~, b] = min(abs(phiN1 - PH(i)));
   c(i) = N1(a,b);
end

%Linearly spaced vector with 1e3 points between 0 and 2*pi:
t = linspace(0,2*pi,1e3);

    %scatter((PH-0.167)*360,Q*1e12,3,c,'filled')
    scatter(PH*360,Q*1e12,3,c/(30*50),'filled')
    xlim([0 360])
    hold on
    plot(t*180/pi,(lb_ub/2)*sin(t),'k','Linewidth',2)
    hold off

    xlim([0 360])
    ylim(lb_ub*[-1 1])
    set(gca,'XTick',0:60:360)
    set(gca, 'YTick', -lb_ub:label_interval:lb_ub)
    set(gca, 'YTickLabel',-lb_ub:label_interval:lb_ub,'fontsize',13)

    grid

    xlabel('\phi [^o]','fontsize',13)
    ylabel('Q [pC]','fontsize',13)

    title(ttl)
    colorbar('EastOutside','FontSize',13)
    colormap('hot')
end
```

Figure G.6: The construction of PRPD plots.

H | COMSOL Model - Explanation

The model is made in the space dimension 2D axisymmetric. The physics that is selected to study the electrical potential and field in the model is the AC/DC Electrostatics (es). The solution is a stationary solution.

H.1 Geometry

The geometry of the model is seen in Figure. H.1. The geometry consists of rectangles representing the different parts of the model. A box of air is added to encapsulate the geometry.

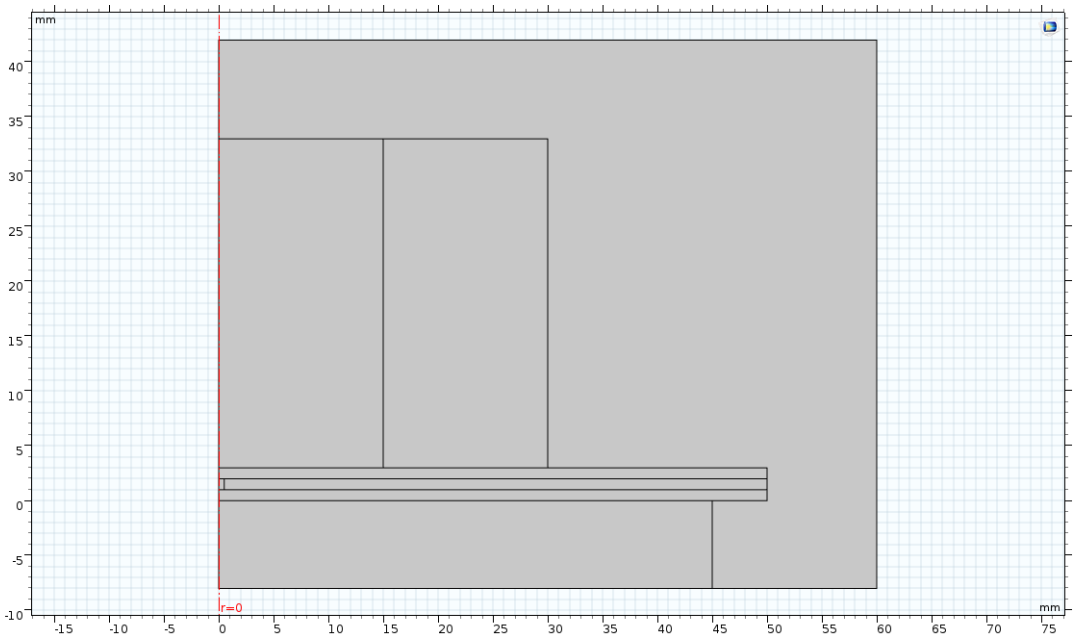

Figure H.1: The geometry of the model in the region r>0. The diameter of the cavity is here 1 mm. All dimensions are in millimeters. The axis of symmetry is the line r = 0.

H.2 Materials

For the stationary electrostatics study, the only material parameter needed is the relative permittivity. The two electrodes are made of copper which is a predefined material in COMSOL ($\epsilon_r = 1$). The cavity and the space around the model are made up of air ($\epsilon_r = 1$). The

material around the HV electrode is epoxy with $\epsilon_r = 4.2$. The plexiglas plates have a relative permittivity of 3.4. The model with the different materials emphasized is shown in Figure H.2.

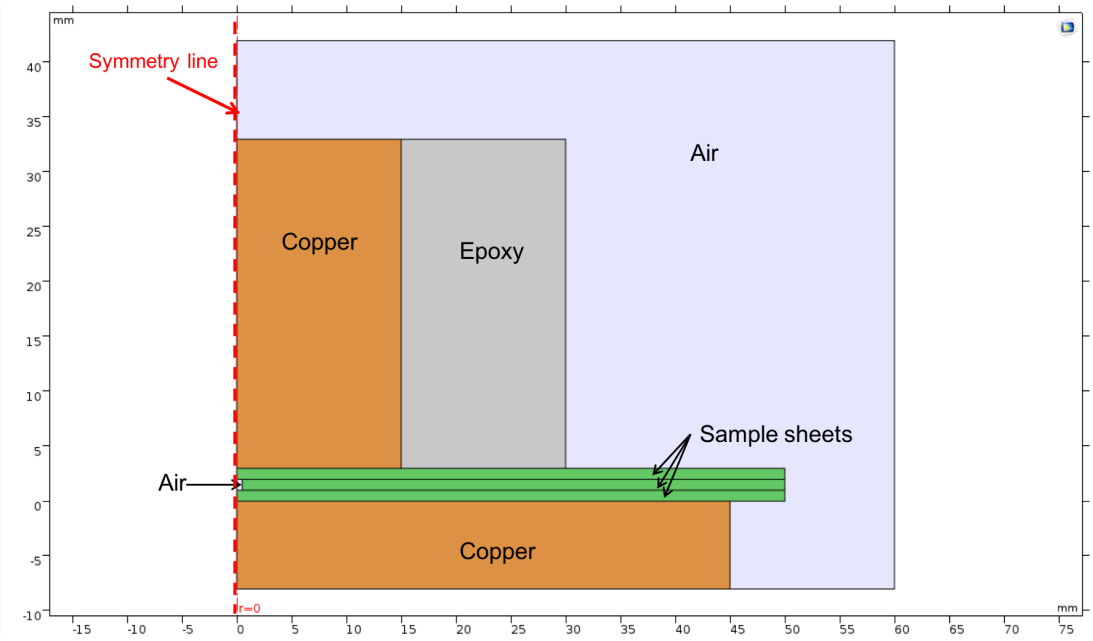

Figure H.2: The COMSOL model's different materials and their respective domains.

H.3 Physics - Electrostatics

Electrostatics is chosen as the relevant physics based on the aim of simulating the electric field and the electric potential. The temperature is set to 293.15 K (20 C), and the pressure is set to 1 atm.

Charge conservation is applied to all areas of the model as it is a fundamental law of physics. The two elements of charge conservation are in this context: 1) Gauss Law is fulfilled and 2) The vector field is conservative i.e. the line integral is independent on the path between the two points (differential form: E = - div V).

Zero charge is applied to all outer boundaries of the surrounding air, in other words, the normal component of the electric displacement field will have to be zero at these boundaries.

Initial values are set to 0 V of all domains in the model. Then the electric potential of the high voltage electrode is set to the peak value of the applied test voltage (7.0 kV) in this thesis work: $\sqrt{2} \cdot 7$ This voltage is chosen because it will represent the maximum momentary field strength the samples will be exposed to and this is an important parameter which can be related to the inception voltage of the samples. The domain of the ground electrode is then defined as ground potential (0 V).

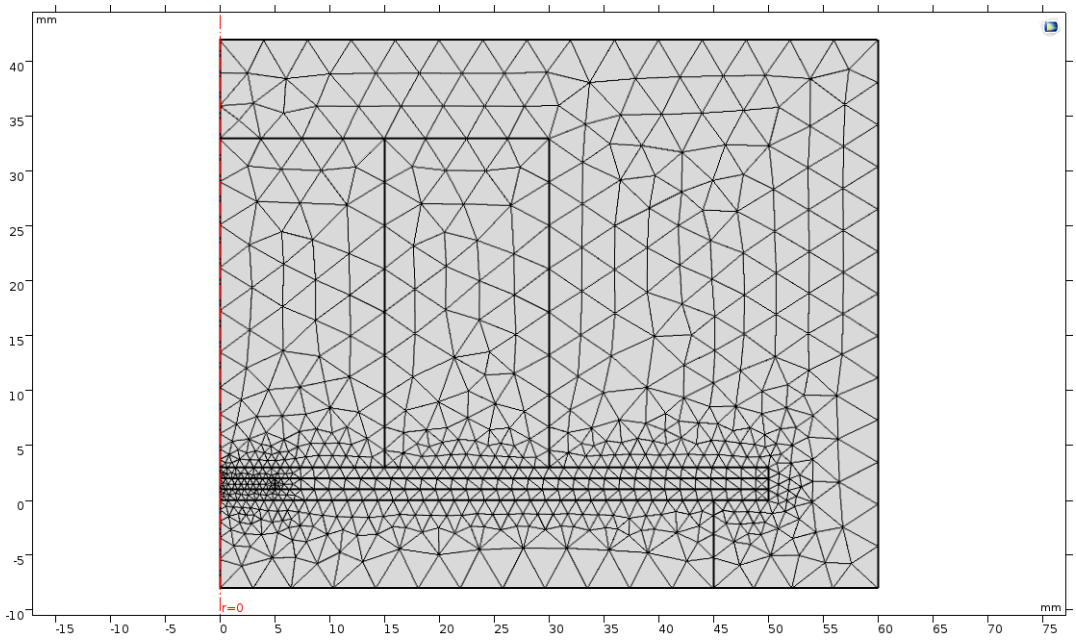

Figure H.3: The mesh of the model. The air-filled cavity is meshed extremely fine, while the rest of the model has a "normal" element size.

H.4 Mesh

The meshing is of the type "free triangular". All elements are thus triangles. The size differs between different domains and is manually defined. The cavity is meshed with an "extremely fine" mesh with the maximum element size reduced manually from 0.6 mm to 0.05 mm. The predefined mesh size was too coarse to result in a smooth graph of the electric field in the cavity. The remaining domains are automatically meshed based on the geometry of the domains with a "normal" mesh size i.e. edges and interfaces between domains are generally meshed finer than large areas of the same material. The resulting mesh of the model of the 10 mm cavity is shown in H.3.

H.5 Study and Results

A stationary study is chosen. Assumption: the permittivity has no complex term - the field follows the applied field perfectly. This simulation is a snapshot of the field during a short period when the voltage can be seen as constant. The results consist of different 2D plot groups with surface plots of the voltage and the electric field. The maximum, average and minimum value (and where it occurs) are also identified. Finally, the results show two line plots of the electric field along horizontal lines from the center of the cavity to the cavity edge (top and middle of the cavity).

I | Abc Model - Results

Table I.1: The capacitances in the abc model and the total capacitance of the samples.

		Capacitances [pF] - Abcd Model				
	Diameter of cavity	1 mm	3 mm	5 mm	10 mm	20 mm
a	Polycarbonate	7.1	7.0	6.9	6.3	3.9
	Samicatherm	8.7	8.7	8.5	7.8	4.9
	Mica mat	7.5	7.4	7.3	6.7	4.2
b	Polycarbonate	0.012	0.11	0.30	1.2	4.7
	Samicatherm	0.015	0.13	0.36	1.5	5.8
	Mica mat	0.013	0.11	0.31	1.3	5.0
c	Polycarbonate	0.0070	0.063	0.17	0.70	2.8
	Samicatherm	0.0070	0.063	0.17	0.70	2.8
	Mica mat	0.0070	0.063	0.17	0.70	2.8
d	Polycarbonate	8.4	8.4	8.4	8.4	8.4
	Samicatherm	8.9	8.9	8.9	8.9	8.9
	Mica mat	4.7	4.7	4.7	4.7	4.7
C_{tot}	Polycarbonate	15	15	15	15	14
	Samicatherm	18	18	14	13	12
	Mica mat	12	12	12	12	11

Table I.2 show that the approximation in Equation 2.15 yield an error ranging from 0.048 % for the 1 mm cavity and 34 % for the 20 mm cavity compared to using the exact formula. This shows that for especially the largest cavities used in this thesis work, the assumptions that the approximation is based on are not valid.

Table I.2: The relative error of the apparent charge calculated by using the approximation in Equation 2.15 compared to using Equation 2.14.

	Relative Error of q_a [%]				
Diameter of cavity	1 mm	3 mm	5 mm	10 mm	20 mm
Polycarbonate	0.048	1.43	1.2	4.9	21
Samicatherm	0.056	0.51	1.8	7.5	34
Mica mat	0.066	0.59	1.7	6.8	30

J Simulations of Samicatherm and Mica Mat

J.1 Maximum, Minimum and Average Field Strength

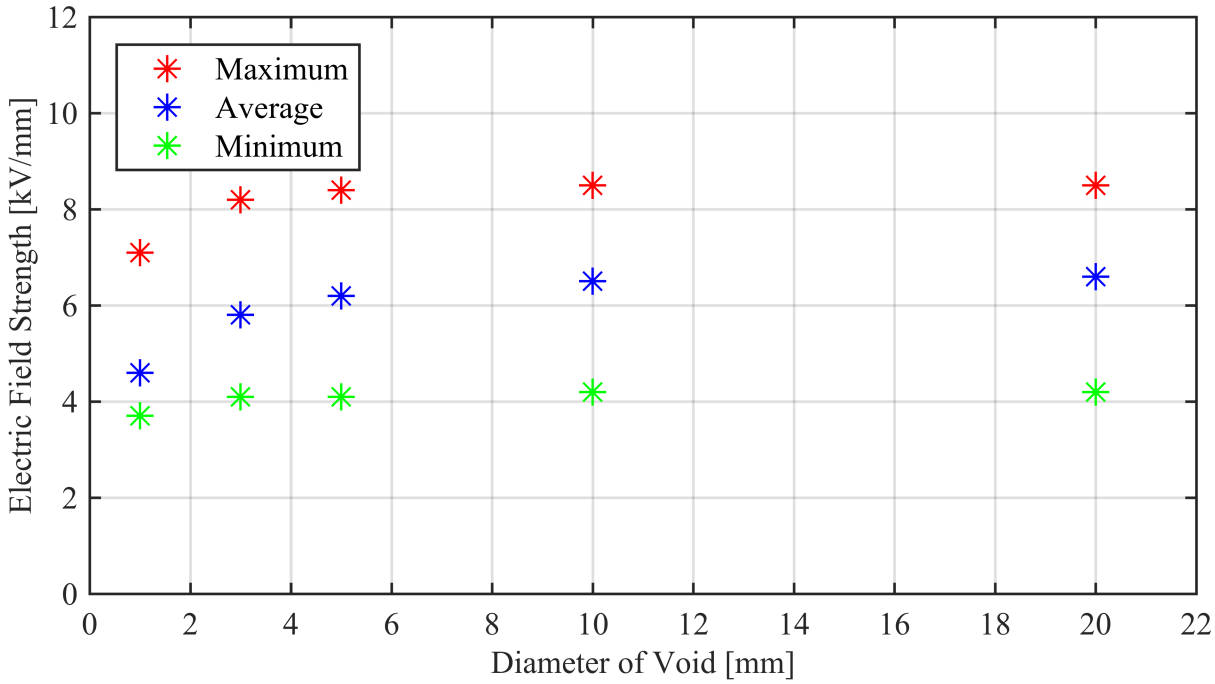

Figure J.1: The maximum, minimum and average electric field strength in the voids embedded in samicatherm.

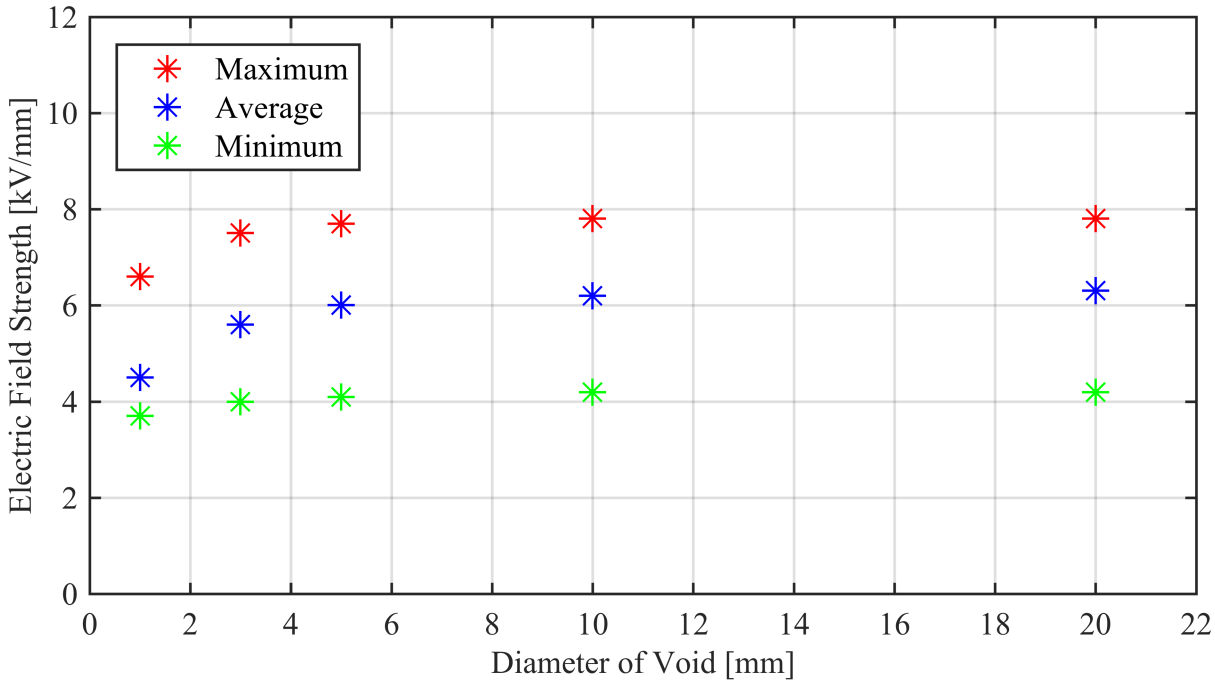

Figure J.2: The maximum, minimum and average electric field strength in the voids embedded in mica mat.

K | Field Enhancement Factor

Based on the simulations in COMSOL, the field in the respective voids has been found. The following field enhancement factor has been calculated based on the *average* field in the cavities. This is because the average field is not affected by the chosen mesh size which both the maximum field and the minimum field is dependent on.

One of the voids (here the 20 mm void since this void has the file enhancement that is closest to the theoretical field enhancement, ε_r) has been chosen as a reference and the field enhancement factor has been calculated by dividing the field of the respective cavities with the reference value. The modified inception voltage is then found by multiplying the original PDIV with the reciprocal of the field enhancement factor.

The calculations and the results for the four different sample types are shown Table K.1, K.2, K.3 and K.4.

Table K.1: The adjusted PDIV of polycarbonate with insulating void surfaces based on simulations of the field in the voids.

Diameter [mm]	Average field strength [kV/mm]	Base value (20 mm)	Enhancement factor	PDIV factor	Theoetical PDIV	Adjusted PDIV
1	4.4	6.2	0.72	1.39	5.2	7.2
3	5.5	6.2	0.89	1.12	5.2	5.8
5	5.8	6.2	0.95	1.05	5.2	5.5
10	6.1	6.2	0.99	1.01	5.2	5.3
20	6.2	6.2	1.00	1.00	5.2	5.2

Table K.2: The adjusted PDIV of polycarbonate with conducting void surfaces based on simulations of the field in the voids.

Diameter [mm]	Average field strength [kV/mm]	Base value (20 mm)	Enhancement factor	PDIV factor	Theoetical PDIV	Adjusted PDIV
1	4.1	5.9	0.69	1.44	5.2	7.5
3	4.9	5.9	0.83	1.20	5.2	6.3
5	5.3	5.9	0.90	1.11	5.2	5.8
10	5.7	5.9	0.97	1.04	5.2	5.4
20	5.9	5.9	1.00	1.00	5.2	5.2

Table K.3: The adjusted PDIV of samicatherm based on simulations of the field in the voids.

Diameter [mm]	Average field strength [kV/mm]	Base value (20 mm)	Enhancement factor	PDIV factor	Theoetical PDIV	Adjusted PDIV
1	4.6	6.6	0.69	1.44	4.8	6.9
3	5.8	6.6	0.88	1.14	4.8	5.5
5	6.2	6.6	0.94	1.06	4.8	5.1
10	6.5	6.6	0.98	1.02	4.8	4.9
20	6.6	6.6	1.00	1.00	4.8	4.8

Table K.4: The adjusted PDIV of mica mat based on simulations of the field in the voids.

Diameter [mm]	Average field strength [kV/mm]	Base value (20 mm)	Enhancement factor	PDIV factor	Theoetical PDIV	Adjusted PDIV
1	4.5	6.3	0.71	1.40	5.1	7.2
3	5.6	6.3	0.89	1.13	5.1	5.7
5	6.0	6.3	0.95	1.06	5.1	5.4
10	6.2	6.3	0.98	1.02	5.1	5.2
20	6.3	6.3	1.00	1.00	5.1	5.1

L | Microscopy Analysis of Samples

The samples were examined using a microscope after the PD measurements. Figure L.1 to L.8 show the resulting pictures of the aluminum coatings of the top and bottom sheet of samples with 3, 5, 10 and 20 mm voids.

A number of observations were made when analyzing the aluminum coatings. First, an obvious abrasion of the aluminum layers was observed. This abrasion is believed to be caused during the impact of the streamer channel on the aluminum surface due to high local temperature of the streamer channel and the bombardment of electrons. The abrasion was, on most samples, mainly located around the edge of the aluminum coating (see Figure L.2 and L.3). This is most likely due to the great field enhancement at the edge of the aluminum as seen in Figure 4.7 which initiates PD in these areas.

However, signs of PD activity are not only shown at the edges of the aluminum coating. For example, the top layer of the aluminum of the 10 mm void (Figure L.5) showed signs of abrasion in patterns resembling straight line segments, or chords, between two endpoints on the outer edge of the aluminum. The 20 mm top sheet (Figure L.7) showed fingerprint patterns of abraded aluminum in the center of the aluminum coating. The fingerprint pattern can be a result of the PD is moving across the cavity since it has no favorable starting point at the surface of the cavity. This is supported by earlier research performed on similar virgin cavities with no asperities on the void surface [42]. The 3 mm top sheet (Figure L.1) showed a pattern resembling a lightning strike. This is assumed to be caused by the impact of the streamer channel and then the migration of the charges on the surface.

It was also observed an asymmetry between the top and bottom sheets in the degree of abrasion. The top sheets generally exhibit more erosion of the aluminum than the bottom samples which show signs of erosion, but only in smaller, individual dots (see L.4, L.8 and L.6). This asymmetry is interesting since the PD activity shows no sign of asymmetry for the samples covered in aluminum. Both the apparent charge and the number of discharges is symmetrical between the two voltage half-cycles.

Scattered across the aluminum surface, observations of crystals were made (see Figure L.4). Crystals have been observed after some hundreds of hours of PD activity [43] and they are a sign of high PD activity over time. Even though the aluminum coated samples were only exposed to PD activity for a few minutes in total, it can be that the PD activity in certain locations has been high enough to form crystals in that particular spot.

In summary, the aluminum shows abrasion in several areas of the coating, but it is most

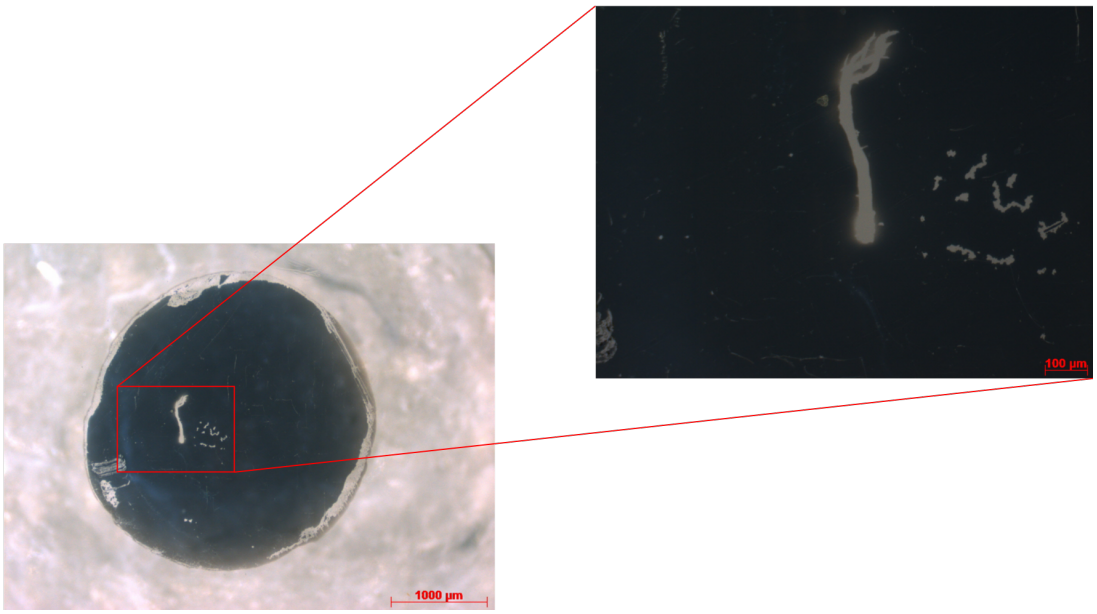

Figure L.1: Aluminum layer of the 3 mm void (top sheet) after exposure to PD. The scale is shown in the bottom right corner of the picture.

evident along the perimeter of the coating, meaning around the edge of the void. Since there are several distinct areas that are abraded, this indicates that PD activity is not limited to one specific area. PD activity can therefore occur at the same time in different areas of the void. This result is supported by earlier research conducted by Wu et al. [39].

As for the samples without aluminum are shown in Figure L.9 - L.13. Figure L.9 shows that there is a milk-colored by-product on the void surface which indicates PD activity. When magnifying the picture further (Figure L.10), the PD activity is seen to be extra strong around the perimeter of the void where there is a marked erosion of the polycarbonate as well as crystal formation. A picture of the void edge is seen in Figure L.11 and crystals can be observed here too. In addition, the edge is seen to not be perfectly smooth. This will give rise to strong field enhancement at the tips of the asperities (and later also on the tips of the crystals) that can initiate PD.

In contrast to the aluminum covered samples, PDs seems to occur on the entire surface area (Figure L.12) where by-products and erosion of the polycarbonate surface can be observed evenly across the surface. Again, this can be due to the even field enhancement across the cavity and therefore there is no preferable starting point for the discharges [42]. For comparison, a picture of the polycarbonate surface outside of the void area has been included (Figure L.13). Here, there is no clear sign of erosion of the surface and no by-products were observed.

In summary, the samples without aluminum show a discharge activity that is generally evenly spread across the entire area of the void. However, the microscopy analysis indicates an increased PD activity around the perimeter of the void. This might be due to the higher field enhancement by the void edge.

The edge of the 20 mm void in a sample made of polycarbonate is shown in Figure L.11.

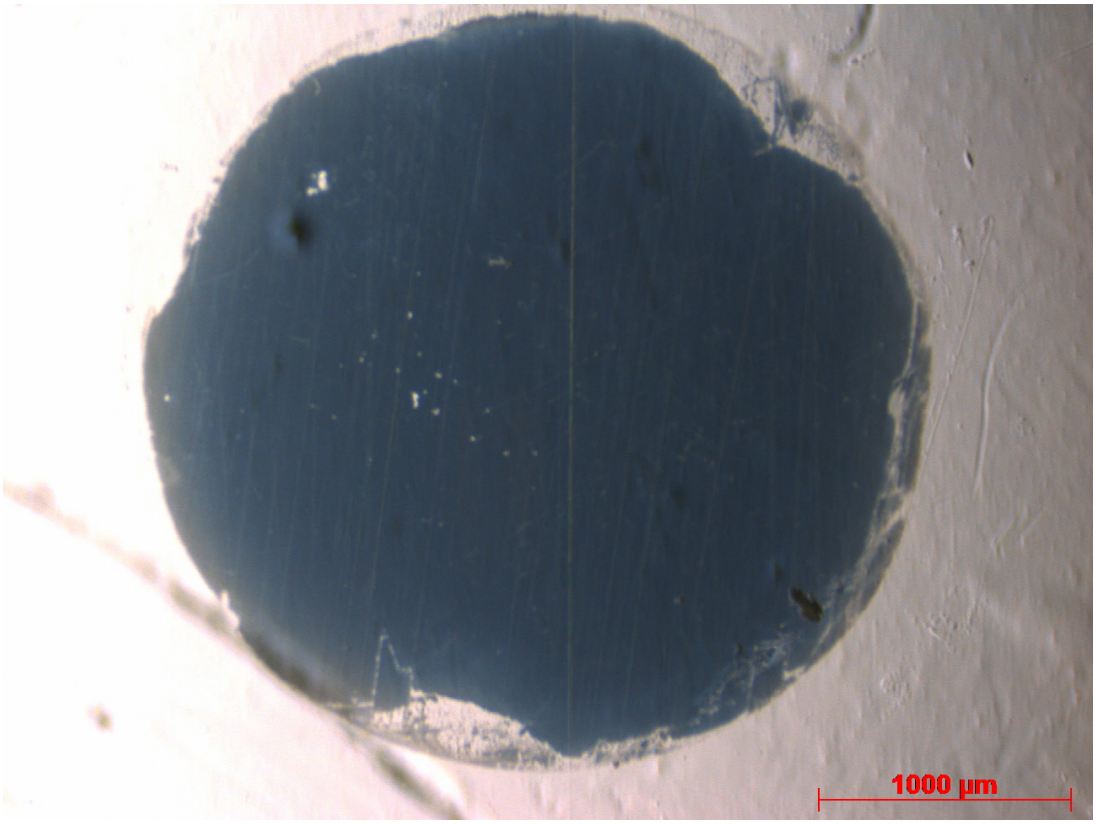

Figure L.2: Aluminum layer of the 3 mm cavity (bottom sheet) after exposure to PD. The scale is shown in the bottom right corner of the picture.

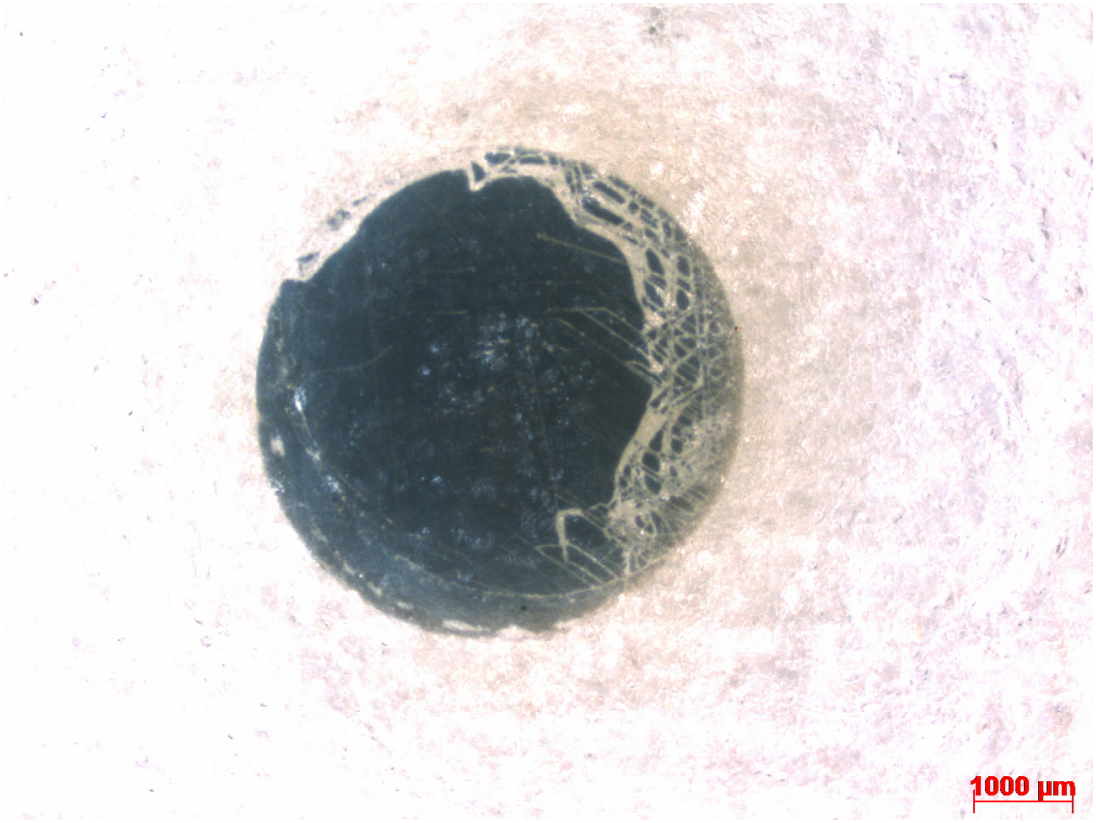

Figure L.3: Aluminum layer of the 5 mm void (top sheet) after exposure to PD. The scale is shown in the bottom right corner of the picture.

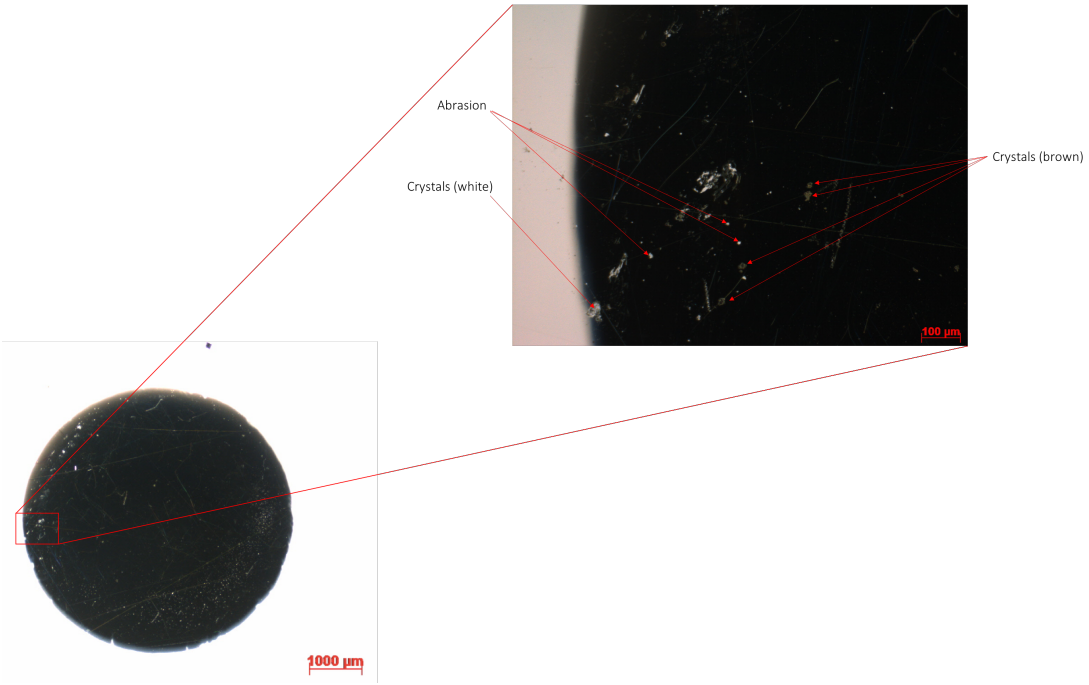

Figure L.4: Aluminum layer of the 5 mm void (bottom sheet) after exposure to PD. The scale is shown in the bottom right corner of the picture. Crystals were observed on the surface of the aluminum as indicated in the Figure. Some were white whereas others had a brown/beige color. The rest of the "white dots" in the picture show abrasion of the aluminum coating due to PD activity.

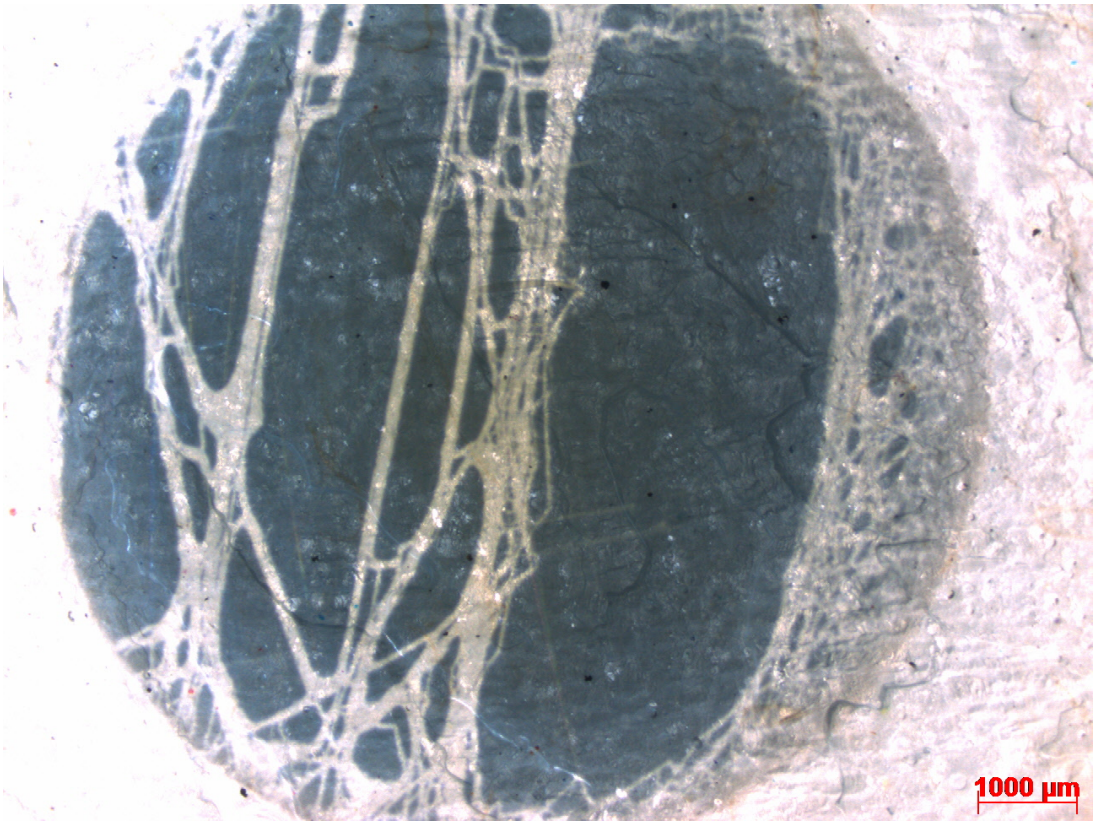

Figure L.5: Aluminum layer of the 10 mm void (top sheet) after exposure to PD. The scale is shown in the bottom right corner of the picture.

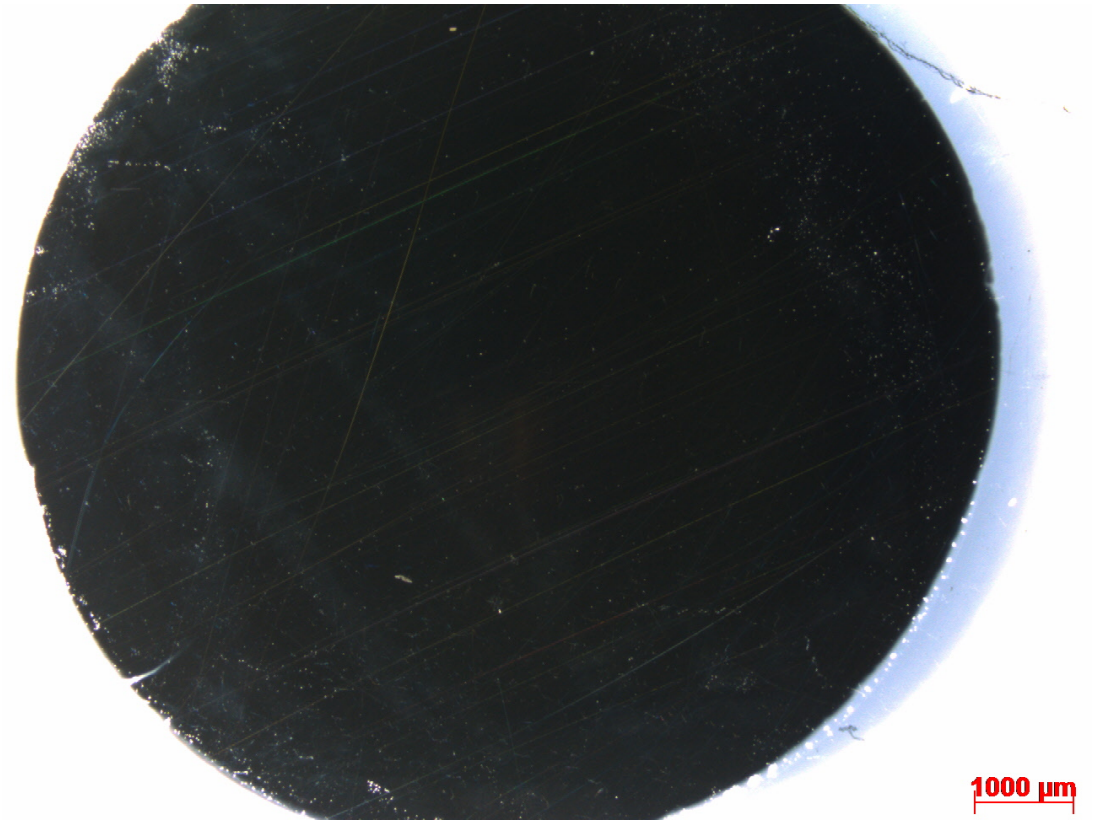

Figure L.6: Aluminum layer of the 10 mm void (bottom sheet) after exposure to PD. The scale is shown in the bottom right corner of the picture.

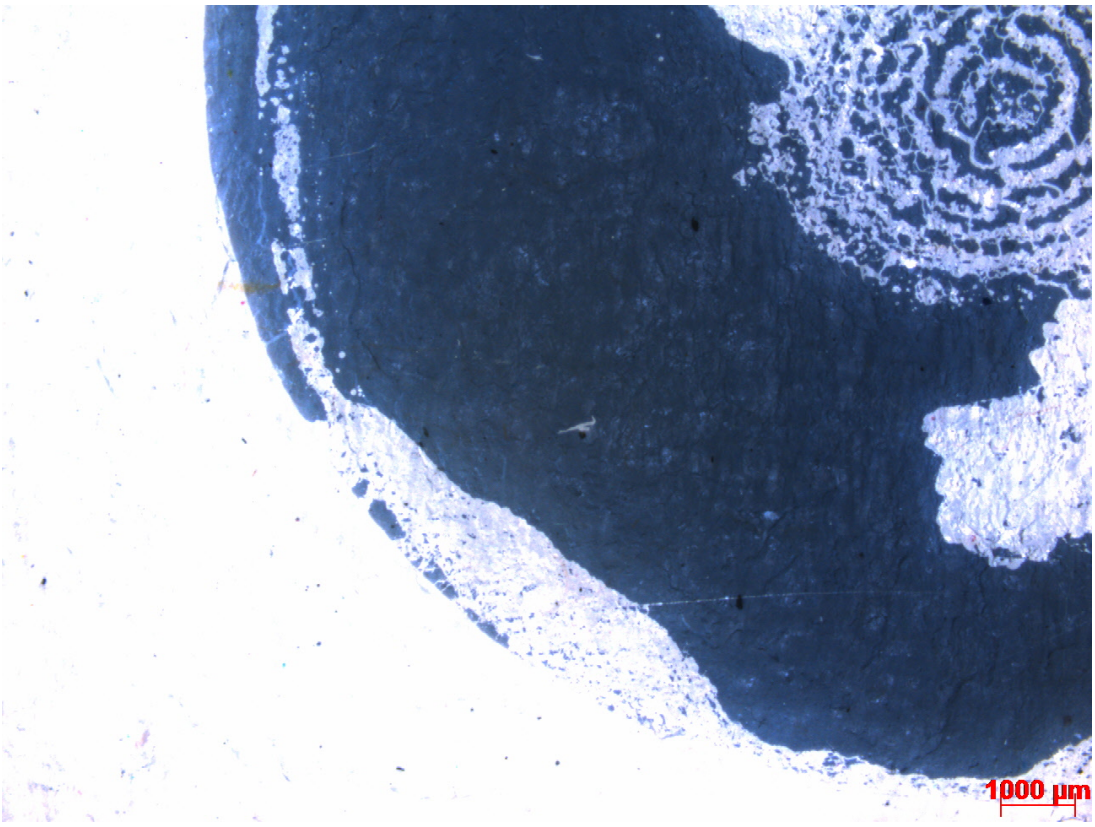

Figure L.7: Aluminum layer of the 20 mm void (top sheet) after exposure to PD. The scale is shown in the bottom right corner of the picture.

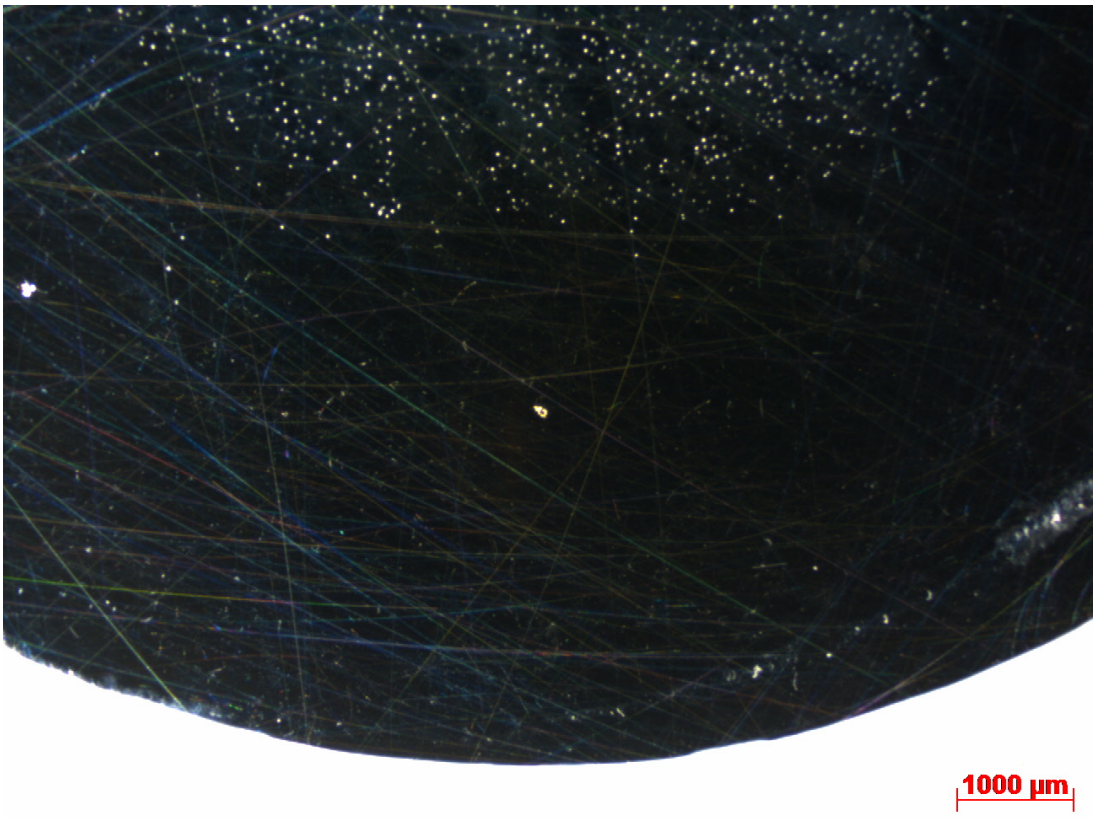

Figure L.8: Aluminum layer of the 20 mm void (bottom sheet) after exposure to PD. The scale is shown in the bottom right corner of the picture.

This picture shows that the edge is slightly uneven which causes an electric field enhancement to very likely be higher than the maximum simulated field enhancement since the simulation assumes perfectly smooth cavity walls. However, the cavity edge of the mica mat samples was a lot more uneven than the polycarbonate sample because of the brittleness of the mica flakes. This might cause a substantially lower inception voltage than the theoretical PDIV for a particular void.

Figure L.9: The bottom sheet of the polycarbonate sample with a 20 mm void after PD testing. The picture shows about a quarter of the perimeter of the void. In the figure, the area above this line is the area that has been the bottom surface of the void, while the area under the line has been outside of the void (area of no PD).

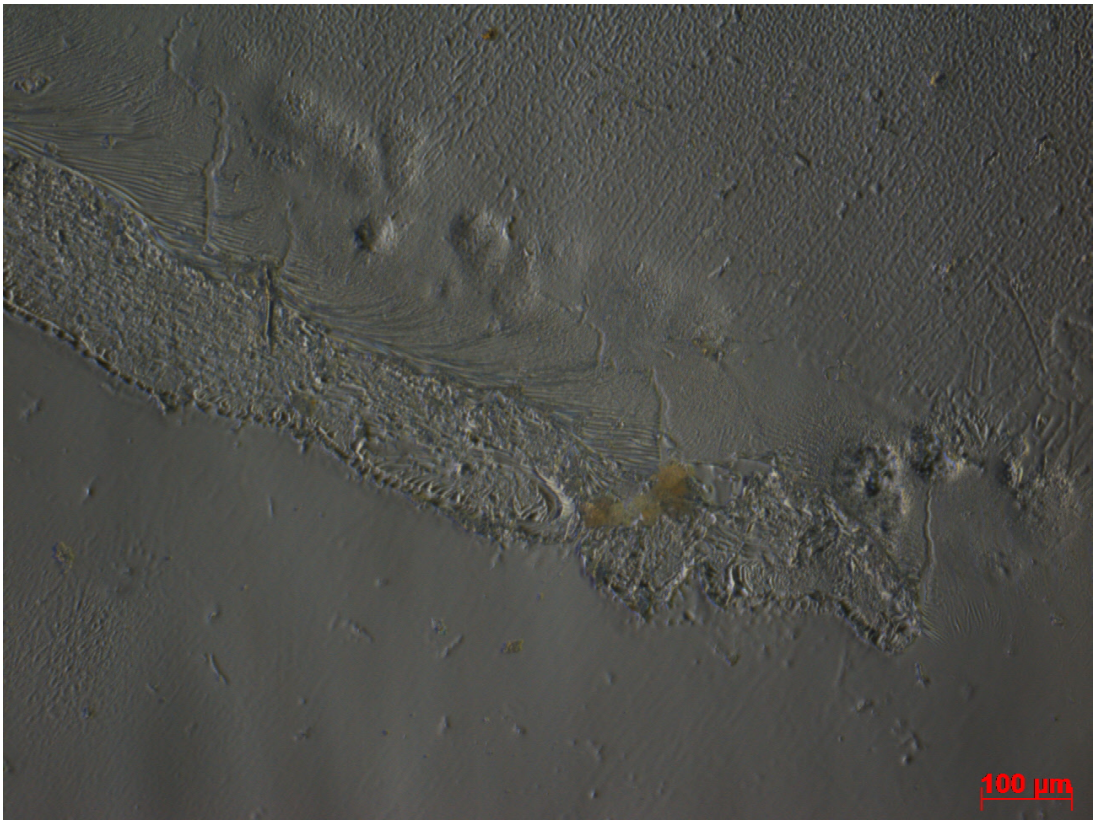

Figure L.10: The figure shows the bottom sheet of the polycarbonate sample at the edge of where the void has been.

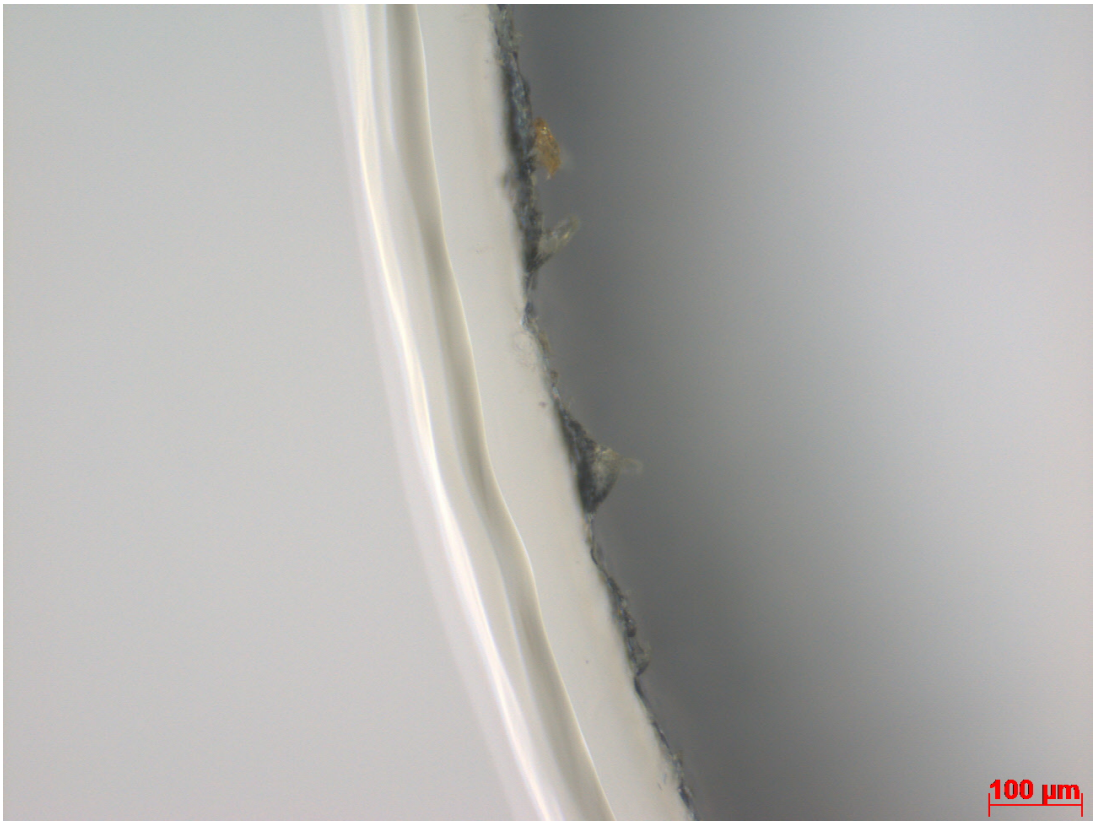

Figure L.11: The figure shows the edge of the 20 mm void in polycarbonate.

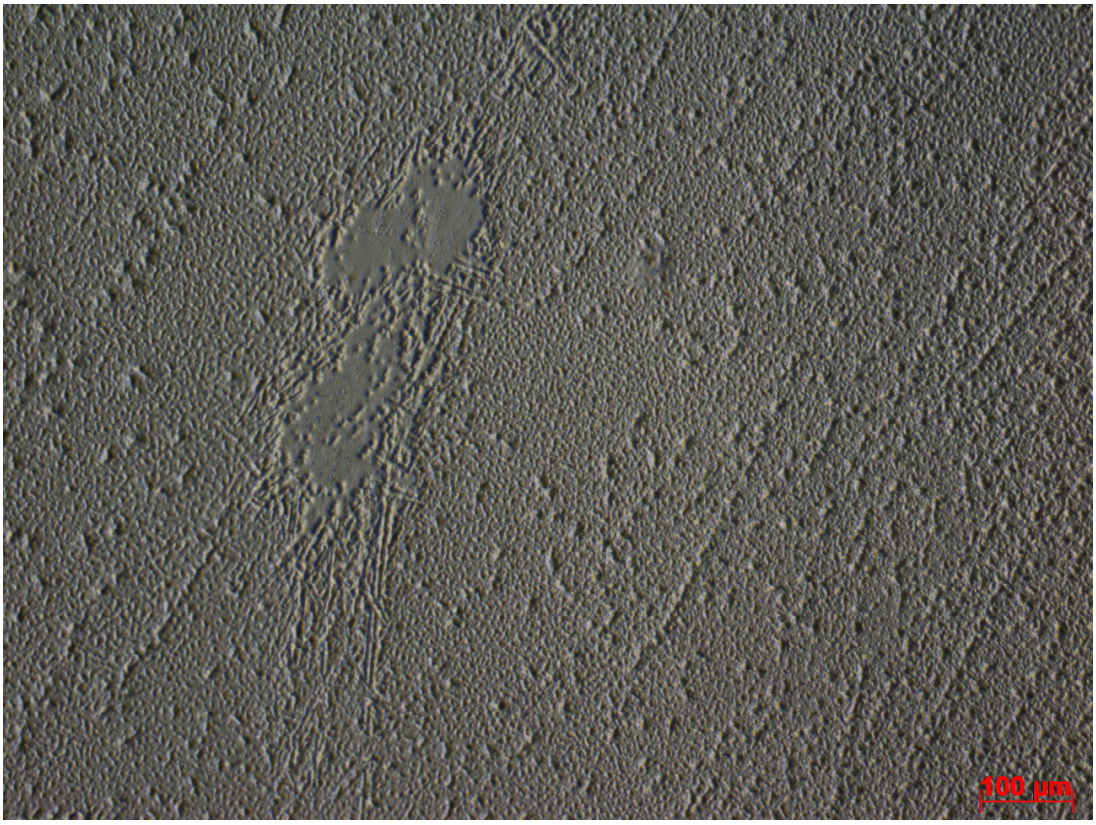

Figure L.12: The figure shows an area of the bottom sheet of the polycarbonate sample that has been exposed to PD activity.

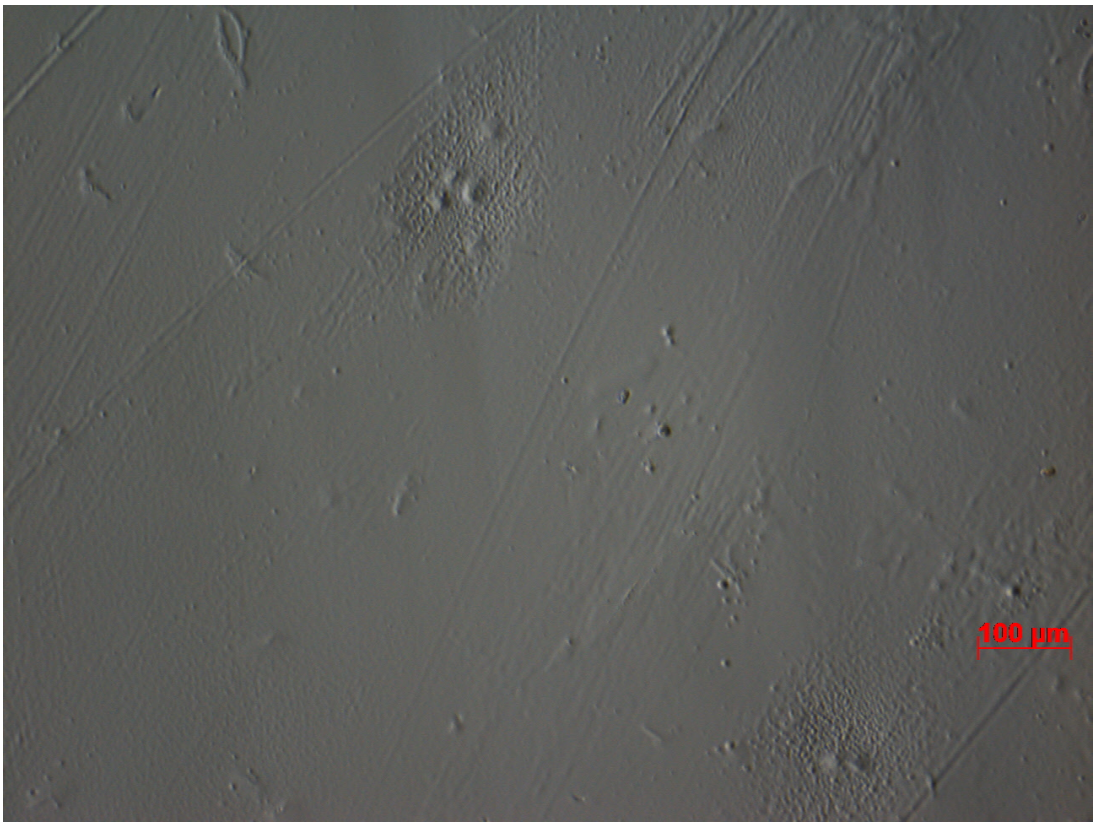

Figure L.13: The figure shows an area of the bottom sheet of the polycarbonate sample that has not been exposed to PD activity.